Investigation of aviation's contribution to tropospheric NO_x - O_3 presence

Paulam Partha Pratim Saha

Delft University of Technology

TU Delft

Investigation of aviation's contribution to tropospheric NO_x - O_3 presence

by

Paulam Partha Pratim Saha

Student Name	Student Number
Paulam P.P. Saha	5008840

Supervisor:	Prof. Dr. Volker Grewe
Institutions:	Delft University of Technology
Place:	Faculty of Aerospace Engineering, Delft
Project Duration:	May, 2021 - July, 2022

TU Delft

Preface

First and foremost, I would like to thank my supervisor Prof. Dr. Volker Grewe for giving me this wonderful opportunity to explore and expand my knowledge base in the amazing & vital research domain of climate change, as part of my Master Thesis research work at TU Delft. Without his continuous support and guidance, the project would not have been successfully realised.

This research opportunity was offered to me at a time when I was tackling perhaps the worst possible time of my life to date, owing to which I suffered extreme mental health problems, not to mention the challenge of working entirely alone from home, leading to additional issues with my motivation and working efficiency. This gives me more reason to thank my supervisor, since he not only offered me academic support, but also the much needed moral assurance that I always had someone to contact, should I face any problem.

I also take a moment to thank my beloved university & the entirety of its staff for having me here at this great institution, where I learnt a lot of virtues and life lessons, which would continue to guide me all throughout my life ahead. TU Delft is now an integral part of my life and I could not have imagined my life otherwise, had I not come here for pursuing my post-graduate studies.

Furthermore, I would like to make a special mention of my girlfriend Priyanka, who has stood by my side throughout the entire journey of working for my Masters degree, as my strongest support pillar my best friend who made me believe in my goal and kept me striving forth inspite of all the drawbacks. I would also like to extend feelings of gratitude to my friends Swarnadeep, Arnab, Sadaf Naman, without whom I wouldn't have been able to keep myself mentally healthy through one of the toughest phases of my life and come out stronger as a person. Any acknowledgement of my achievements could never end without a mention of my parents, without whom I wouldn't have ever realized the dream of moving to the Netherlands in the first place. I owe my life all of its achievements to them; thank you Ma and Baba. Thank you all you amazing people for believing in me!

Paulam Partha Pratim Saha
Delft, July 2022

Abstract

As global air traffic has continued to grow over the past two decades, it has effectively led to a sharp increase in the emissions. These aircraft emissions contribute to global warming through the 'greenhouse gas effect'. Apart from CO_2 and H_2O, NO_x is the next major aviation-emitted species which significantly contributes to climate change through its atmospheric chemistry leading to the formation of O_3, which in itself is another major greenhouse gas. Since global air traffic is a major source of tropospheric NO_x, this thesis analyzed the contribution of aviation to tropospheric mixing ratios of NO_x and O_3. The analyses was performed on 2 major aspects: (A) to identify and understand the seasonal & zonal patterns with respect to aviation's contribution to tropospheric VMR of NO_x and O_3, and (B) to comprehend the differences between Perturbation & Tagging methodologies in estimating aviation's contribution to tropospheric VMR of NO_x and O_3. In addition to NO_x and O_3, background availability of radicals OH and HO_2 was also analyzed, since OH and HO_2 are vital to the NO_x-O_3 chemistry.

The global climate-chemistry model EMAC (European Centre for Medium-Range Weather Forecasts – Hamburg (ECHAM)/MESSy Atmospheric Chemistry) was used, whereby the simulations were performed in quasi-chemistry transport model (QCTM) mode. The analyses presented an interesting overview of aviation's contribution to tropospheric NO_x and O_3. Throughout all the seasons, Western Europe and the USA emerged as aviation NO_x hotspots. Tropical regions were found to have higher atmospheric oxidation capacity owing to a higher presence of OH radicals, as compared to the polar regions. HO_2 radicals too depicted a trend similar to that of OH. The Western coasts of South America and Africa along with the Indian subcontinent were identified as hotspots for these O_3 precursors.

Aviation's contribution to tropospheric O_3 mixing ratio accumulated over tropical regions and mid-latitudes. A belt region covering North-Western China, Middle East & Africa, along with that of the West Coast of USA were aviation O_3 hotspots. Seasonal study in the Northern Hemisphere revealed that Summer & Fall registered the highest (mass) contribution of aviation to NO_x. Whereas for the Southern Hemisphere, Summer was the season with the lowest (mass) contribution from aviation to NO_x, leading to an equivalent low O_3 accumulation. From the seasonal patterns of background OH and HO_2, it was concluded that a chemical transformation of aviation-induced NO_x into O_3 is a function of the atmospheric availability of OH and HO_2 radicals (or, atmospheric oxidation capacity).

The thesis further analyzed the differences between Perturbation & Tagging methodologies, from the perspective of aviation's contribution to atmospheric mixing ratios of NO_x and O_3. The results for aviation NO_x implied that aviation NO_x emission & resulting mixing ratio in the atmosphere follow an almost linear relationship, thereby contributing only marginally to the non-linear characteristic of aviation NO_x-O_3 chemistry. As for the aviation O_3 mixing ratios, significant differences ranging from 15% to around 60% were calculated between Perturbation & Tagging's results. These differences were traced back to the Perturbation method underestimating aviation's O_3 production rate in the Northern Hemisphere, while overestimating the corresponding values in the Southern Hemisphere. Also the differences in O_3 production rate kept on increasing towards mid-latitudes and polar regions for the Northern Hemisphere, thus justifying the corresponding calculated trend for O_3 VMR. The inter-hemispherical differences in Perturbation and Tagging's estimates of O_3 were found to be caused by the NO_x emission level. A seasonal comparison pointed out that the differences between Perturbation and Tagging methods' estimations for tropospheric O_3 rose to its highest levels in Winter.

The thesis concluded that the differences (w.r.t. Tagging) in Perturbation method's estimation of aviation's contribution to tropospheric O_3 mixing ratios were due to the NO_x emission level and the methodological differences in estimating atmosphere's oxidation capacity.

Contents

Nomenclature

Abbreviations

Abbreviation	Definition
CCM	Climate-chemistry model
CO_2	Carbon dioxide
CO	Carbon monoxide
CH_4	Methane
DU	Dobson Unit
HO_2	Hydroperoxyl
H_2O	water vapor
MMR	Mass Mixing Ratio
$NMHC$	Non-methane hydrocarbons
NO_x	Nitrogen oxides
km	kilometre(s)
OH	Hydroxyl
O_2	Oxygen
O_3	Ozone
PAN	Peroxy Acetyl Nitrate
$ppbv$	parts per billion by volume
$pptv$	parts per trillion by volume
RF	Radiative forcing
Tg	Teragram
UV	Ultra-violet
VMR	Volume Mixing Ratio

Symbols

Symbol	Definition	Unit
M	Molar mass	[g/mol]
m	Mass	[kg]

List of Figures

List of Tables

1

Introduction

Aviation has emerged as one of the world's important modes of transportation owing to its advantages of safety, comfort and efficiency. But with the tremendous growth of aviation over the past two decades, emissions such as CO_2, NO_x and soot have registered a rise of upto 27% in the period 2013-2018 alone as compared to 1970-2012 [D. S. Lee *et al.* 2021]. These aircraft emissions alter the chemical composition of the atmosphere and consequentially, contribute to global warming by trapping the infrared (IR) radiation arising from the Earth's surface (also known as the 'greenhouse gas effect').

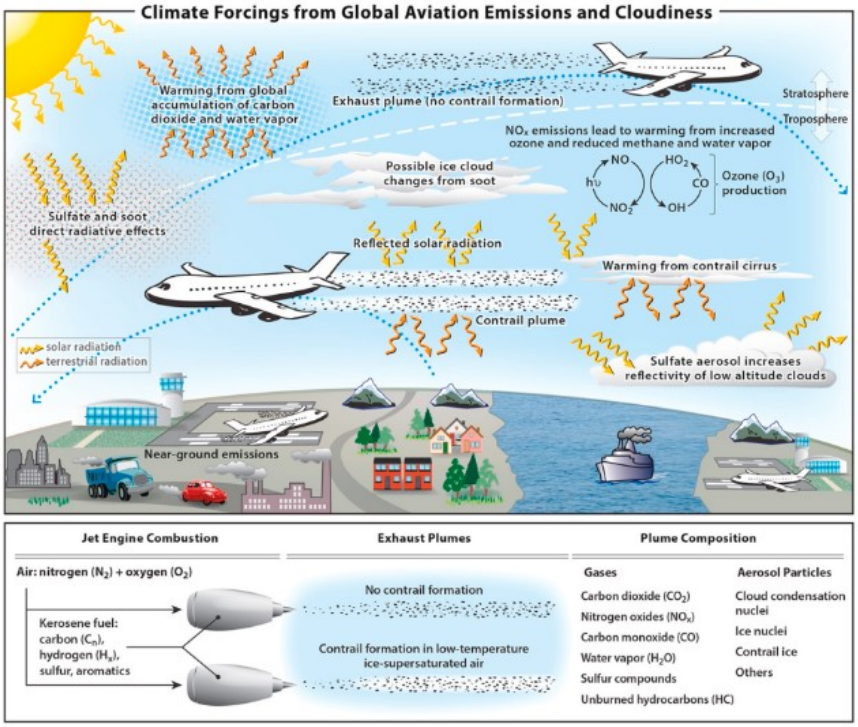

Figure 1.1: Overview of the Earth's climate system being affected by emissions of CO_2, H_2O, NO_x, and aerosols, and from contrail-cirrus cloudiness. CO_2, H_2O, NO_x & contrail-cirrus induce an overall positive RF effect (warming), whereas the presence of sulphate aerosols has a negative RF (cooling) effect on the Earth [D. S. Lee *et al.* 2021].

The report published by Intergovernmental Panel on Climate Change (IPCC) (titled 'Aviation and the Global Atmosphere') [IPCC 1999] extensively evaluated the impacts of global air traffic on climate change through the use of the climate metric 'radiative forcing' (RF) [Prather *et al.* 1999]. RF (units: watts per square metre, or, W/m^2) is a measure of the change in Earth-atmosphere energy budget (measured at the top of the atmosphere) relative to statistics of the year 1750 (by convention in IPCC

usage), which occurs due to changes in the chemical composition of the atmosphere. So, if RF is positive for any particular chemical compound, it implies that at the tropopause, more energy (radiation) is incoming than outgoing from the Earth's atmosphere due to the corresponding chemical compound, and consequently the Earth is heating up. And in case RF is negative due to a particular chemical compound, the implication is that the concerned chemical compound's presence in the Earth's atmosphere is having a cooling effect on the Earth.

The several processes directly/indirectly linked to aviation & their corresponding RF trends are listed as follows [D. S. Lee *et al.* 2009]:

- Emission of CO_2: positive RF
- Emission of NO_x: positive RF
- Emission of H_2O: positive RF
- Formation of persistent contrails: positive RF
- Aviation-induced cloudiness (AIC): potentially positive RF
- Emission of sulphate particles: negative RF
- Emission of soot particles: positive RF

As compared to the impact of aviation CO_2 emissions, estimating the impacts of non-CO_2 effects has always proved to be particularly challenging IPCC 1999. The primary (quantified) non-CO_2 effects result from the emissions of NO_x, along with H_2O and soot both of which can lead to the formation of contrails. Furthermore, there are also aerosols emitted from aircraft jet exhaust, which are small particles composed of soot (black carbon/organic carbon) and sulfur (S) and nitrogen (N) compounds. The largest positive (warming) climate forcings next to that of CO_2 are those from contrail cirrus and from NO_x-driven changes [D. S. Lee *et al.* 2009]. D. S. Lee *et al.* 2009 estimated that in the year 2005 alone, radiative forcing due to CO_2 emissions from the aviation sector amounted to 1.59% of total anthropogenic $CO2$ RF and when the non-CO_2 effects were added, the aviation contribution rose significantly to about 5% of the overall net anthropogenic RF. The values presented in table 1.1 correspond to the latest study conducted by D. S. Lee *et al.* 2021 for the year 2018.

	RF ($mW\ m^{-2}$)	Sensitivity to emissions
Contrail cirrus	111.4	1.82 x $10^9 mWm^{-2}km^{-1}$
CO_2	34.3	-
Short-term O_3 increase	36.0	$25.1 \pm 7.3 mWm^{-2}(Tg(N)yr^{-1})^{-1}$
Long-term O_3 decrease	-9.0	$-7.9 \pm 2.9 mWm^{-2}(Tg(N)yr^{-1})^{-1}$
CH_4 decrease	-17.9	$-15.8 \pm 5.9 mWm^{-2}(Tg(N)yr^{-1})^{-1}$
Stratospheric water vapor decrease	-2.7	$-2.4 \pm 0.9 mWm^{-2}(Tg(N)yr^{-1})^{-1}$
Net NO_x	8.2	$1.0 \pm 6.6 mWm^{-2}(Tg(N)yr^{-1})^{-1}$
Stratospheric H_2O increase	2.0	$0.0052 \pm 0.0026 mWm^{-2}(Tg(H_2O)yr^{-1})^{-1}$
Soot (aerosol-radiation)	0.94	$100.7 \pm 165.5 mWm^{-2}(Tg(BC)yr^{-1})^{-1}$
Sulfate (aerosol-radiation)	-7.4	$-19.9 \pm 16.0 mWm^{-2}(Tg(SO_2)yr^{-1})^{-1}$
Net RF (only non-CO_2 terms)	114.8	-
Net aviation RF	149.1	-

Table 1.1: Estimates for aviation RF components in the year 2018 [D. S. Lee *et al.* 2021].

Owing to the fact that global air traffic is a major source of NO_x in the troposphere [IPCC 1999; Brasseur *et al.* 1998; Sausen *et al.* 2005] and the NO_x chemistry due to aviation emissions is a significant source of global warming (refer to Table 1.1), this thesis investigates aviation's contribution to atmospheric presence of NO_x and O_3. Previous research has pointed out that the chemistry between NO_x emissions and O_3 concentration is non-linear [Liu *et al.* 1987; Lin *et al.* 1988; J. U. Grooß *et al.* 1998]. This implies that O_3 concentration in the atmosphere does not always increase linearly with the increasing emissions of NO_x, with O_3 concentrations even decreasing at very high NO_x emission levels [Dahlmann *et al.* 2011]. This non-linearity makes it difficult to evaluate aviation's contributions to atmospheric concentrations of NO_x and O_3.

In order to understand the behaviour of non-linear atmospheric O_3 chemistry due to aviation emissions only, the emitted species NO_x and O_3 will be studied for seasonal and zonal patterns. To examine these patterns, climate-chemistry simulation results will be analysed across 4 seasons: Spring, Summer, Fall & Winter. Currently, there exist 2 methods to evaluate any particular emission source's contribution to the atmospheric concentration of chemical species such as NO_x and O_3: Tagging (Source apportionment) and Perturbation (Source sensitivity). Tagging method traces the fate of an emission from a particular source within a single simulation, and thereby estimates the source's individual contribution to atmospheric concentration of a chemical species. Whereas perturbation method works with 2 simulations: one with all the emission sources and another with one source's emissions decreased partially or switched off. A subtraction of the latter from the former helps to form an estimate of that one source's pollutant contributions. Difference in the source contribution estimations from Tagging and Perturbation methods indicate the presence of a non-linearity in the atmospheric chemistry [Grewe *et al.* 2012; Koo *et al.* 2009].

The study of NO_x-O_3 chemistry is prone to uncertainties owing to simplifications of the chemical reaction chain [Lin *et al.* 1988]. But recent studies have yet successfully predicted the chemical species' contributions from aviation and their impacts with 90% confidence [D. Lee *et al.* 2010]. This research will therefore contribute to a better understanding of the Tagging and Perturbation methods, and to the understanding of NO_x-O_3 chemistry.

The research questions formulated in order to attain the objective of the thesis, are outlined in Chapter 3. The setup of the CCM and the simulations which are used for the purpose of analyzing the contribution of aviation to tropospheric mixing ratios of NO_x and O_3, are explained in Chapter 4. The climate chemistry simulation results are analysed and thoroughly discussed in Chapter 5, offering an insight into the (a) seasonal and zonal variations in aviation's contribution to NO_x and O_3 VMR in the troposphere, and (b) differences between Perturbation & Tagging methods in evaluating aviation's contribution to tropospheric NO_x and O_3 VMR. Following this, Chapter 6 presents some uncertainties which could arise in climate-chemistry research work such as that done in this thesis. To conclude, Chapter 7 outlines the key points and conclusions from the analyses of the climate-chemistry simulations and presents brief points of discussion.

2

NO_x - O_3 chemistry

This section presents the theoretical knowledge required to comprehend the research work presented in the following chapters. Firstly, an introduction to the chemistry leading to O_3 production is discussed in Section 2.1. Along with this, the non-linear characteristic of the NO_x-O_3 chemistry is discussed in Section 2.2. Following this, Section 2.3 elaborates on the concepts of Tagging and Perturbation methodologies. Previous research [Grewe *et al.* 2012] is used as a reference to discuss the differences among these two aforementioned methodologies. Lastly, a previous analysis of aviation's NO_x emissions and the subsequent impact on atmospheric O_3 chemistry [M. O. Köhler *et al.* 2008] is discussed in Section 2.4.

2.1. Introduction to O_3 chemistry

In the troposphere, the incoming UV radiation from the Sun does not possess enough energy to directly dissociate the atmospheric O_2 and produce O_3. An investigation was made by Lin *et al.* 1988 into the existence of a high O_3 concentration in the urban atmosphere, which ultimately led to the suggestion that peroxy radicals, the likes of HO_2 and RO_2 (R denoting organic radicals), might be responsible for the oxidation of NO to NO_2. Although some NO_2 is emitted directly into the atmosphere by combustion processes [Lenner 1987], most of it is formed as a product of oxidation of NO. This oxidation of NO to NO_2 is initiated in turn by the oxidation of non-methane hydrocarbons, through one of the most reactive chemical species in the troposphere: OH radical. The hydroxyl (OH) radical plays a vital role in atmospheric chemistry owing to its characteristic of high reactivity with organic compounds as well as inorganic compounds.

Alkyl peroxy (RO_2) and hydroperoxy (HO_2) free radicals are generated by the oxidation of NMHC in the atmosphere, which then oxidize NO to NO_2, and a substantial fraction of the time the OH radical is regenerated to persist this reaction chain. NO_2 then eventually undergoes photolysis to produce O_3. These photo-chemical processes involving the oxidation of NMHC to produce the peroxy radicals, eventually ending up in the formation of O_3, are extremely complex [Seinfeld 1989; Finlayson-Pitts and Pitts 1997]. As a simplification to the research methodology within this study, a simplified tropospheric O_3 production reaction chain has been assumed as shown below, summing up all the theory above:

$$NMHC + OH \rightleftarrows R + H_2O \tag{2.1}$$
$$R + O_2 + M \rightleftarrows RO_2 + M \tag{2.2}$$
$$RO_2 + NO \rightleftarrows RO + NO_2 \tag{2.3}$$
$$RO + O_2 \rightleftarrows HO_2 + carb \tag{2.4}$$
$$HO_2 + NO \rightarrow NO_2 + OH \tag{2.5}$$
$$NO_2 + h\nu \rightarrow NO + O \tag{2.6}$$
$$O + O_2 \rightarrow O_3, \tag{2.7}$$

where $carb$ stands for carbonyl compounds. Carbonyls further oxidise & produce additional O_3.

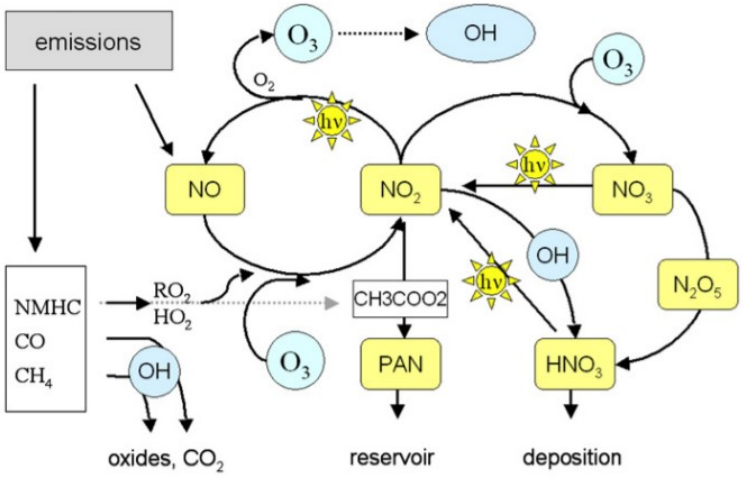

Figure 2.1: Basic processes involved in tropospheric O_3 chemistry [Uherek *et al.* 2010].

This O_3 production scheme establishes that both NMHC and NO_x (NO + NO_2) are precursors of O_3. It also shows that OH and HO_2 are not directly responsible for O_3 formation, but they act as essential catalysts in the process.

In case where there is shortage or absence of hydrocarbons, in order to facilitate the ozone production, HO_2 can be produced through the following reactions:

$$O_3 + hv(\lambda \leq 320nm) \rightarrow O + O_2 \tag{2.8}$$
$$O + H_2O \rightarrow 2OH \tag{2.9}$$
$$OH + CO \rightarrow CO_2 + H \tag{2.10}$$
$$H + O_2 + M \rightarrow HO_2 + M, \tag{2.11}$$

after which reactions (2.5) to (2.7) lead to production of O_3. So studying these series of reactions shows that CO can also act as an O_3 precursor.

As for the mechanisms responsible for tropospheric O_3 loss, the following destruction cycle is significant [J. U. Grooß *et al.* 1998; D. Lee *et al.* 2010]:

$$O_3 + OH \rightarrow HO_2 + O_2 \tag{2.12}$$
$$O_3 + HO_2 \rightarrow OH + 2O_2 \tag{2.13}$$

Reactions (2.12) and (2.13) show that OH and HO_2 present in the atmosphere not only are responsible for O_3 formation from atmospheric NO_x, but also act as pathways for the loss of O_3.

2.2. Non-linearity of NO_x-O_3 chemistry

Owing to the fact that the destruction rates of NO_x, and that of OH, HO_2 depend strongly on the concentrations of NMHC and NO_x, O_3 production does not observe a linear growth with respect to the increase in concentration of O_3 precursors. In certain circumstances O_3 production decreases as the atmospheric concentration of NO_x increases [Lin *et al.* 1988], which is why the NO_x - O_3 chemistry is said to be non-linear.

Liu *et al.* 1987 defined 'O_3 production efficiency' as the number of O_3 molecules produced per molecule of precursor. It was found that the non-linearity of this O_3 production efficiency is quite significant in a rural and clean background atmosphere as compared to a more urban/polluted one, and that this non-linearity may have a pronounced impact on the estimations of regional and global O_3 concentrations.

In the troposphere, the competition between reactions (2.3), (2.4) and (2.5), coupled with the loss of NO_x, effectively decides the amount of O_3 being produced per molecule of NO_x. Therefore it is essential to have a clear understanding of odd hydrogen (OH and HO_2) along with NO_x. The major pathway for the loss of NO_x during the daytime is:

$$OH + NO_2 + M \rightarrow HNO_3 + M \tag{2.14}$$

NO_x may also be lost at nighttime as a consequence of reactions involving NO_3 and N_2O_5 [Ehhalt and Drummond 1982; Platt *et al.* 1984; Noxon 1983]. Photo-chemical sinks for odd hydrogen include (equation 2.14) and recombination reactions of the peroxy radicals

$$HO_2 + HO_2 \rightarrow H_2O_2 + O_2$$
$$HO_2 + RO_2 \rightarrow ROOH + O_2$$

followed by the reaction of OH with the peroxide. The interplay of the catalytic cycle and the reactions amounting to loss of radicals, is what determines the production of O_3 with respect to its precursors' losses. The relative importance of the catalytic cycle versus that of the radical loss reactions (resulting in losses of precursors and odd hydrogen), leads to the O_3 production not being a linear function of the concentrations of its precursors.

The non-linearity of the ozone production efficiency obtained by Liu *et al.* 1987 has been depicted in figure 2.2.

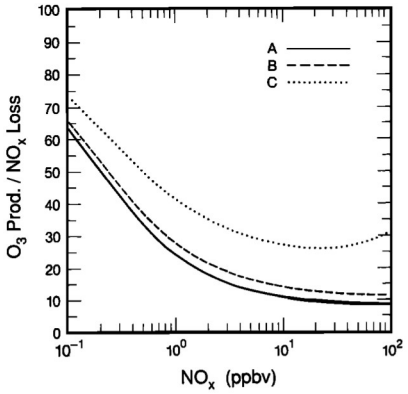

Figure 2.2: O_3 production efficiency [mol/mol] calculated by using absolute O_3 production for different compositions of NMHC [Lin *et al.* 1988].

In their study, Lin *et al.* 1988 used 3 different models composed of different NMHC compositions: (A) the composition observed at Niwot Ridge, Colorado [Liu *et al.* 1987]; (B) the composition of a representative anthropogenic emission used by a regional acid deposition model [Acid Deposition Modeling Project (ADMP), 1987]; and (C) the so-called "default Empirical Kinetic Modeling Approach (EKMA)" composition [M. Dodge 1977; M. C. Dodge 1977]. Examination of the three profiles in figure 2.2 shows that the non-linearity of the ozone production efficiency decreases as NMHC become more reactive (thereby producing more peroxyl radicals) when the efficiency is defined by using absolute O_3 production. As an example, at NO_x = 0.1 ppbv, the O_3 production efficiency for three different NMHC compositions vary within 20% of each other, whereas further up the NO_x scale at 100 ppbv, the ozone production efficiency for case-C is about 4 times greater than that of case-A. This is reflected in the concentrations of OH and the sum of all peroxy radicals (HO_2 + RO_2), as seen in figure 2.3.

It was concluded by Lin *et al.* 1988 that higher presence of NMHC in the atmosphere leads to a higher concentration of HO_2 + RO_2, thereby augmenting the O_3 production. The increase in HO_2 + RO_2 reduces the non-linearity by enhancing O_3 production at high concentrations of NO_x (and NMHC). The non-linearity is reduced even further by the decrease of NO_x loss due to reduced availability of OH.

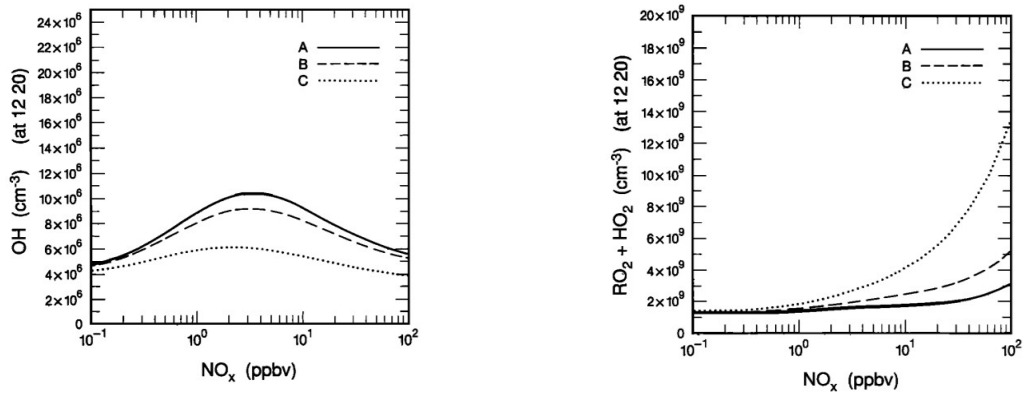

Figure 2.3: Production of OH and peroxyl radicals (RO_2 + HO_2) at different NO_x concentrations, for three different NMHC compositions [Lin *et al.* 1988].

2.3. Methodologies to evaluate emission source contributions to pollutants' concentrations

In order to evaluate the contribution of any particular source/activity to the concentration of a pollutant (such as CO_2, NO_x), two major types of approaches have always been used to support air quality decision making:

- Source apportionment approach (more popularly known as "Tagging approach")
- Sensitivity analysis (also known by the term "Perturbation approach")

The tagging approach is an accounting system, which follows reaction pathways and traces the fate of an emission from a particular source within a single simulation [Grewe *et al.* 2012; Grewe 2013; Clappier *et al.* 2017]. Therefore, aviation's contribution to the atmospheric concentrations of NO_x and subsequently O_3 is inherently defined as the fraction (or component) of current total NO_x and total O_3 mixing ratios which are attributable to aircraft emissions. The methodology of tagged species is designed to attribute atmospheric chemical species' concentrations to the individual contributions from several emission sources. This approach tags each emission source and quantifies its contribution to the concentration or mixing ratio of chemical species such as NO_x and O_3.

The primary and simplest perturbation method approach estimates the change in a chemical species' atmospheric concentration by performing and subtracting two simulations, one with all the emission sources 'activated' (no change in their original emissions' data) and the second being the one without a specific emission source (the one which is to be analysed/is the source of interest) [Blanchard 1999; Yarwood *et al.* 2007], or its emissions reduced by a fixed amount. This then helps to find the particular emission source's contribution to the atmospheric concentration of a particular chemical species. In scenarios involving non-linear chemistry such as the $NO_x - O_3$ one, the concentration change resulting from a set of emission sources' contributions changed together is no longer equivalent to the sum of the concentration changes resulting from these sources' contributions individually [Clappier *et al.* 2017].

Here, a vital point to be noted is that the perturbation (or sensitivity analysis) approach often requires identical meteorology (identical weather conditions) across all its simulations (one without any emission source manipulation and subsequent simulations with the source contribution reductions) to enhance the signal-to-noise ratio enabling a robust signal.

Before understanding the theory behind the methodologies [Grewe *et al.* 2010] used in the thesis analyses, the reader must note that for the theoretical elaboration presented in sections 2.3.1 and 2.3.2 below, all emissions are described by a number of sectors ('n': e.g. air traffic, road traffic, biomass burning, etc.), which are denoted with $i = 1, ..., n$. Each sector emits their respective chemical species

(such as X and Y), which are denoted as $E_{X,i}$ and $E_{Y,i}$, such that

$$\sum_{i=1}^{n} E_{X,i} = E_X, and \tag{2.15}$$

$$\sum_{i=1}^{n} E_{Y,i} = E_Y \tag{2.16}$$

2.3.1. Source apportionment (or "Tagging") approach

This section defines the contributions of individual emission sources (or sectors) to the concentrations of individual chemical species through the analyses of reaction pathways. Every species is decomposed into n sub-species, which define the concentration contributed by an individual sector to the regarded species.

Here, the sub-species considered for the explanation are X_i, Y_i and Z_i. Their concentrations X_i, Y_i and Z_i are those parts of the concentrations X, Y and Z which are attributed to sector i.

The sub-species are subjected to the following mathematical relations: first according to equations 2.15 and 2.16

$$\sum_{i=1}^{n} X_i = X \tag{2.17}$$

$$\sum_{i=1}^{n} Y_i = Y \tag{2.18}$$

$$\sum_{i=1}^{n} Z_i = Z \tag{2.19}$$

For the second mathematical relation, consider atmospheric chemical reactions of the following type

$$X + Y \rightarrow Z + X + Y \tag{2.20}$$

$$X + Z \rightarrow X \tag{2.21}$$

$$Y + Z \rightarrow Y, \tag{2.22}$$

where species Z is produced through a reaction involving X and Y, and is then further destroyed by reaction with either X or Y. The reaction rates of reactions (2.20), (2.21) and (2.22) are P_{XY}, D_X and D_Y. This atmospheric chemical system can be described by

$$\dot{X} = E_X - \tau_X^{-1} \tag{2.23}$$

$$\dot{Y} = E_Y - \tau_Y^{-1} \tag{2.24}$$

$$\dot{Z} = P_{XY} XY - D_X XZ - D_Y YZ, \tag{2.25}$$

where τ_X and τ_Y are constant lifetimes of species X and Y. Reaction 2.20 represents the production of O_3 through reaction 2.5), owing to the fact that this reaction is the limiting step in the atmospheric production scheme of O_3 through reactions (2.5) to (2.7). Reactions 2.21 and 2.22 represent the loss mechanism of O_3 (reactions 2.12 and 2.13).

Now for the aforementioned second mathematical relation pertaining to the sub-species, these sub-species are assumed to follow the same reaction pathways, which is, e.g. for reactions 2.20, 2.21 and 2.22:

$$X_i + Y_j \rightarrow \frac{1}{2} Z_i + \frac{1}{2} Z_j + X_i + Y_j \tag{2.26}$$

$$X_i + Z_j \rightarrow X_i - \frac{1}{2} Z_i + \frac{1}{2} Z_j \tag{2.27}$$

$$Y_i + Z_i \rightarrow Y_i - \frac{1}{2} Y_i + \frac{1}{2} Y_j, \tag{2.28}$$

For the Z-production reaction 2.26, a molecule X_i (a molecule X emitted by source i) and a molecule Y_j (a molecule Y emitted by source j) are considered. The product is one molecule Z. Both emission sources i and j are attributed equal importance in this production reaction, thereby resulting in the products denoted as $\frac{1}{2}Z_i$ and $\frac{1}{2}Z_j$. In the case that a molecule X_i reacts with Y_i, the product is Z_i. For the loss mechanism of Z (reactions 2.27 and 2.28) the aforementioned consideration is in analogy: When molecules X_i and Z_j react, both sources i and j are attributed equal importance for the destruction of one Z molecule and the resulting change $-1Z$ arises from $-\frac{1}{2}Z_i - \frac{1}{2}Z_j$. Starting from one molecule Z_j, this results in $-\frac{1}{2}Z_i + \frac{1}{2}Z_j$ on the left side of reaction 2.27.

Along the lines of equations (2.23) to (2.25), the following differential equations can be derived for the sub-species:

$$\dot{X}_i = E_{X,i} - \tau_{X,i}^{-1} \tag{2.29}$$

$$\dot{Y}_i = E_{Y,i} - \tau_{Y}^{-1} \tag{2.30}$$

$$\dot{Z}_i = P_{Z,i} X_i Y_i - D_{Z,i} X_i Z_i - D_{Z,i} Y_i Z_i, \tag{2.31}$$

with $P_{Z,i}$ (production term of Z_i) and $D_{Z,i}$ (destruction term of Z_i) defined as

$$P_{Z,i}(X_i, Y_i) = P_{XY}\left(X_i Y_i + \sum_{j \neq i} \frac{1}{2} X_i Y_j + \sum_{j \neq i} \frac{1}{2} X_j Y_i\right) \tag{2.32}$$

$$\Rightarrow P_{Z,i}(X_i, Y_i) = P_{XY}\left(X_i Y_i + \sum_{j \neq i} \frac{1}{2} X_i (Y - Y_i) + \sum_{j \neq i} \frac{1}{2} (X - X_i) Y_i\right) \tag{2.33}$$

$$\Rightarrow P_{Z,i}(X_i, Y_i) = \frac{1}{2} P_{XY}(X_i Y + X Y_i), and \tag{2.34}$$

$$D_{Z,i}(X_i, Y_i, Z_i) = D_X\left(X_i Y_i + \sum_{j \neq i} \frac{1}{2} X_i Y_j + \sum_{j \neq i} \frac{1}{2} X_j Y_i\right) \tag{2.35}$$

$$\Rightarrow D_{Z,i}(X_i, Y_i, Z_i) = D_X\left(X_i Z_i + \frac{1}{2} X_i (Z - Z_i) + \frac{1}{2}(X - X_i) Z_i\right) + \tag{2.36}$$

$$D_Y\left(Y_i Z_i + \frac{1}{2} Y_i (Z - Z_i) + \frac{1}{2}(Y - Y_i) Z_i\right) \tag{2.37}$$

$$\Rightarrow D_{Z,i}(X_i, Y_i, Z_i) = \frac{1}{2} D_X (X_i Z + X Z_i) + \frac{1}{2} D_Y (Y_i Z + Y Z_i) \tag{2.38}$$

It can easily be shown that

$$\sum_{i=1}^{n} P_{Z,i}(X_i, Y_i) = P_{XY} XY \tag{2.39}$$

$$\sum_{i=1}^{n} D_{Z,i}(X_i, Y_i, Z_i) = D_X XZ + D_Y YZ \tag{2.40}$$

The tagging methodology explained in this section [Grewe *et al.* 2010] possesses two major characteristics:

1. it is invariant, and
2. it is convergent.

The first point means that for any solutions of equations (2.26) to (2.28), the constraints (2.17) to (2.19) are fulfilled. The second point implies that for any two existing solutions (X_i^1, Y_i^1, Z_i^1) and (X_i^2, Y_i^2, Z_i^2) of equations (2.29) to (2.31) with two different initial conditions, the difference in the solutions exponentially converge to zero (see Appendix A of Grewe *et al.* 2010).

The tagging method required for applications in real chemistry schemes is in principle not different from the described one. To each species, n (number of considered emission sources) tagged species are associated. For each of these n number of tagged species, their respective production and loss terms have to be found. The decomposition of these corresponding production and loss terms into the contributions from individual emission sources is essential to the tagging method. This is a combinatorical problem, which can be solved in analogy to the above mentioned cases for 2 and 3-body reactions [Grewe *et al.* 2010]. However, since the tagging of a whole chemical system is likely to be too computational demanding a mapping of the complex chemical system, including the production and loss terms, a simpler concept of chemical species family might be helpful. Then only these chemical families need to be tagged [Grewe 2004].

2.3.2. Sensitivity analysis (or "Perturbation") approach

Grewe *et al.* 2010 stated that most research studies evaluate the impact of a change in emission from a source on the atmosphere's chemical composition. Such studies analyze the contribution of this emission source to the atmospheric concentration of a species (e.g. O_3) using two simulations, one simulation with all emissions and one simulation with a perturbation of the emission source [Grewe *et al.* 2010].

Mathematically, this sensitivity approach is based on a Taylor approximation of the regarded quantity f as a function of the emissions for a base case, i.e. the case where all emissions from all sources (e_0) are fully implemented:

$$f(e_0 + \alpha e^c) \approx f(e_0) + \alpha e^c f' e_0 \tag{2.41}$$

$$= \tilde{f}(e_0 + \alpha e^c), \tag{2.42}$$

where e^c represents a certain emission category (source) and $\alpha \in [-1,1]$ represents the strength of the perturbation made to that emission source. The case $\alpha = -1$ represents the scenario where all emissions from the respective source are excluded. $f'(e_0)$ (the derivative) is the efficiency of the production of the considered species per emission. Analyzing the contribution of a specific emission source to the concentration of f using this approach implies that all sources experience the same production efficiency, since the derivative f' is evaluated at e_0.

The concentration of f attributed to a certain emission category e^c: δf, is

$$\delta f = \tilde{f}(e_0 + e^c) - \tilde{f}(e_0) \tag{2.43}$$

$$= e^c f'(e_0) \tag{2.44}$$

The derivative f' can be determined using two simulations, one with all the emissions (e_0) and one with a perturbation of an emission category (αe^c):

$$f'(e_0) \approx \frac{f(e_0) - f(e_0 + \alpha e^c)}{e_0 - (e_0 + \alpha e^c)} \tag{2.45}$$

$$= (f(e_0) - f(e_0 + \alpha e^c)) \frac{-1}{\alpha e^c} \tag{2.46}$$

$$= -\frac{\Delta^a f}{\alpha e^c}, \tag{2.47}$$

where $\Delta^a f$ is the difference in two simulations. The smaller α is, the less different is the chemical background in the two simulations, but the more difficult it will be to obtain a statistical robust perturbation of f [Grewe *et al.* 2010]. Within the CCM used for the analyses in this thesis, $\alpha = -0.05$ (see Section 4.2). A small α guarantees that the chemical background is comparable in the simulations thereby ensuring that the estimated contributions from different emission sources are consistently calculated and thereby comparable [Grewe *et al.* 2010].

Substituting equation (2.47) in equation (2.44),

$$\delta f = -\Delta^a f \cdot \frac{1}{\alpha} \tag{2.48}$$

The calculation of the contribution from the particular emission source is therefore mathematically a scaling of the difference between two model simulations in which the corresponding emission source is scaled by the value α^{-1}. However, conceptually α is only used to calculate the derivative f', which is then multiplied by the total emission of the respective source (equation 2.44)[Grewe *et al.* 2010].

Grewe *et al.* 2010 summarized that the perturbation method is in principle not appropriate for source attribution, but is well suited to evaluate the impacts of changes in emission inventories (e.g. future emission policies).

2.3.3. Demonstrating the difference between the results of Tagging & Perturbation methodologies

The tagging method is simply a system which follows reaction pathways and tracks the fate of an emitted species within the chemical system. The perturbation method, on the other hand, estimates the change in the atmospheric composition of chemical species brought by a change in the source(s)' emission(s), through calculating the difference between two different simulations. Both methods have been described in detail in literature [Grewe *et al.* 2010] and in Sections 2.3.1, 2.3.2.

Grewe *et al.* 2012 attempted to re-calculate the contribution of road traffic emissions to northern hemispheric O_3 concentration, which had earlier been estimated by Uherek *et al.* 2010 to be in the range of 2%-12% for the summer season. But that estimation was only obtained through perturbation method and as previously stated several times in literature [Grewe *et al.* 2010], this method is not suitable for calculating the actual contribution of a sector.

So to make a clear comparison of the results from both tagging and perturbation approaches, both these methods were applied in numerical simulations by Grewe *et al.* 2012. Results obtained for the year 1990 are shown in figure 2.4. For both methods, a same set of simulations was employed: A base case with 1990 emissions, and a so-called "zero road" simulation with 100% road traffic emissions turned off.

As depicted on the left side of figure 2.4, the perturbation method only produces the change in net tropospheric O_3 column due to removal of road traffic emissions, without any additional information. On the other hand, the tagging method uses the same simulations to produce the same change in O_3 column between the two simulations, but with essential information about the contribution from other emission sectors. Since the tagging approach keeps track of the "chemical fate" of emissions from different sectors, it allows a true "source apportionment" of the ozone column, as seen on the right side of figure 2.4.

The perturbation method shows a change of 0.6 DU in the O_3 column, the same level seen in the "zero road" case with respect to the base case for the tagging method. This change is small as compared to the 3.5 DU partial ozone column tagged to road traffic. So as simulation is changed from base case to "zero road" case, all the other sectors' emissions increase to partially cover up the gap left by the road traffic sector (for e.g., industry or lightning tags register an increase of 2.5 DU). This compensating increase in the other sectors is simply owing to the non-linearities in the NO_x chemistry (see Section 2.2). Hence as the road traffic emissions are switched off (100% reduction), the total O_3 production due to all sectors combined decreases only slightly. This implies a little less O_3, but ozone production efficiency (defined in section 2.2, where the precursor considered here is NO_x) does increase, which agrees well to what was stated in earlier literature [Lin *et al.* 1988; J. U. Grooß *et al.* 1998].

Overall, the O_3 change amounting to 0.6 DU through the perturbation method was "falsely" attributed to road traffic alone. Therefore it can be stated that the perturbation method here is only capable of estimating a change in total atmospheric O_3 in the event of an alternative emission scenario, but it lacks the capability to estimate compensating effects from other sectors, which may conceal a more detailed interpretation.

Hence, tagging demonstrated that the contribution of road traffic sector to atmospheric concentration of O_3 was substantially underestimated by perturbation method. This was attributed to the fact that gains due to NO_x reductions in one sector were partly being compensated by formation of O_3 from the other sectors still emitting NO_x. Therefore, only the tagging approach allowed for an accurate estimation

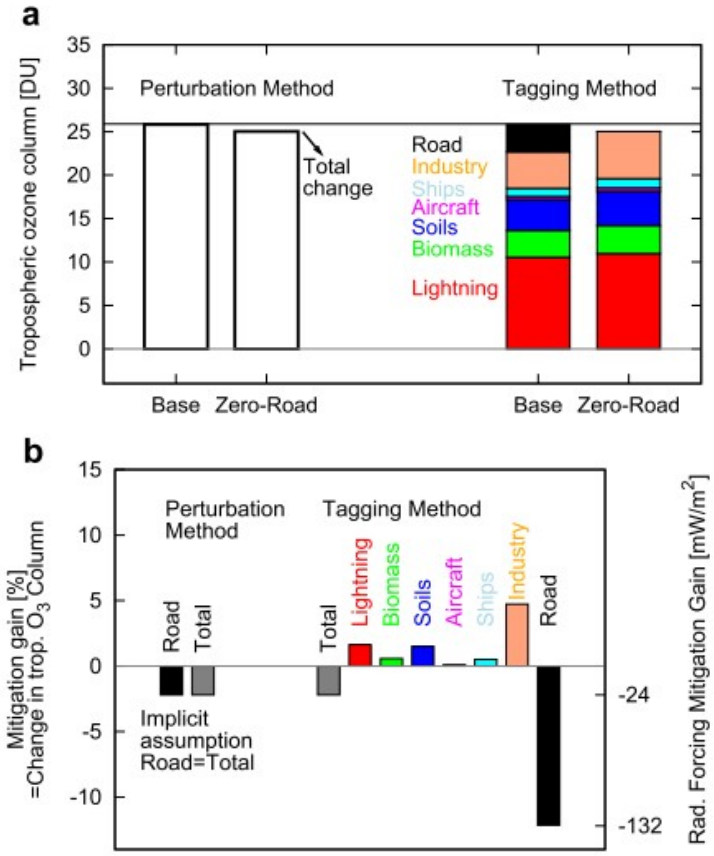

Figure 2.4: Illustration of the difference in results obtained from tagging and perturbation methods for road traffic emissions, for the year 1990. a) Tropospheric O_3 column [DU] due to NO_x emitted by all sources for the base case simulation (first column) and the respective results from a simulation excluding road traffic emissions (second column). The total change, i.e. the difference in both simulations is simply attributed to road traffic by the perturbation method (left). On the other hand, the tagging method (right) provides additional information on the contributions/partial columns from the individual emission sectors. The simulations for both methods are identical, but the tagging method provides much more detailed information. b) Relative changes in tropospheric ozone [%, left axis] and radiative forcing [$mW - m^2$, right axis] between the two simulations. As stated for (a), the tagging method (right) again provides more elaborate information as compared to the perturbation method (left) [Grewe *et al.* 2012].

of separate mitigation gains for any single emission sector from non-linear changes induced by other sectors.

2.4. Previous analysis of aviation's NO_x emissions and subsequent O_3 chemistry

M. O. Köhler *et al.* 2008 evaluated aviation's NO_x emissions and their subsequent impact on atmospheric O_3 column. Furthermore, they analyzed the impact of perturbation to aircraft NO_x emission on O_3. For the perturbations, aircraft NO_x emissions were increased by 5% within a range of designated cruise altitude bands. These perturbations were assumed to represent the introduction of a new aircraft to the existing commercial fleet or changes in air traffic demand.

For their analyses, 3D chemistry transport model p-TOMCAT [F. O'Connor *et al.* 2005; Cook *et al.* 2007] was used, which is an updated version of the earlier TOMCAT model [K. Law *et al.* 1998, 2000; N. Savage *et al.* 2004]. It includes a gas-phase methane-oxidation scheme with simplified $NMHC$ treatment (ethane, propane) on 35 hybrid-pressure levels from the surface to 10 hPa, with a vertical resolution of approximately 700 m in the upper troposphere and lower stratosphere (henceforth named as "UTLS") region. The Earth was modelled with a horizontal grid resolution of 5.6^0 x 5.6^0. Since the p-TOMCAT model does not consider heterogeneous and halogen chemistry in the stratosphere and

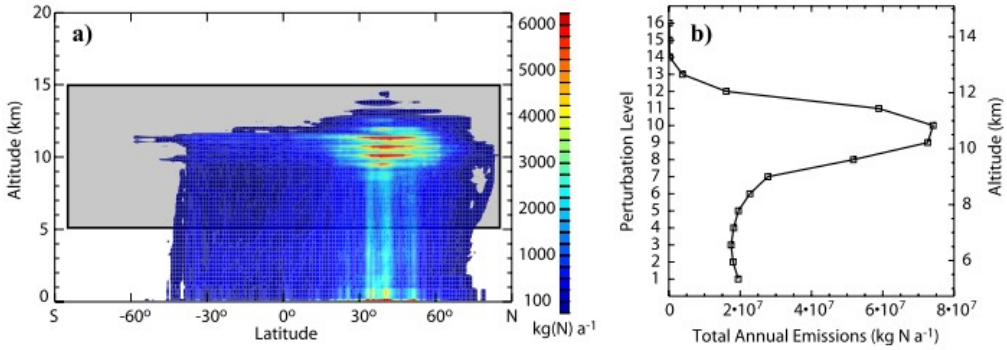

Figure 2.5: (a) AERO2k aircraft NO_x emissions for the year 2002 in $kgN\ a^{-1}$ per 1^0 x 1^0 x 500 ft grid cell. At this vertical resolution the difference between flight levels with high and low air traffic is visible at cruise altitude in the northern mid-latitudes. The grey-shaded box represents the altitude range for the perturbations applied to NO_x emissions. (b) Total annual NO_x emissions on each of the 'perturbation levels' (cruise altitude bands) located inside the grey box of Figure 2.5(a) [M. O. Köhler *et al.* 2008].

its upper boundary is located at 10 hPa (32 km), analyses were also carried out using the SLIMCAT chemistry transport model [Chipperfield 1999] to investigate the impact of aircraft emissions specifically in the stratosphere.

The aircraft NO_x emission data for the year 2002 from the European AERO2k Project [Eyers *et.al.* 2004] was used as the reference with an annual total fuel usage of 176 Tg resulting in emissions of 0.68 TgN. Figure 2.5(a) shows the zonally averaged annual total aircraft emissions from the AERO2k global inventory. The altitude range between 5 km and 15 km (16500–48500 feet), extending over the free troposphere and lower stratosphere, was divided into equal cruise altitude bands of 610 m (2000 feet) thickness, henceforth referred to as 'perturbation levels'. For the analyses, aircraft NO_x emissions were increased on every single perturbation level and the impacts on O_3 were investigated. Figure 2.5(b) shows the annual total emissions on each perturbation level. In order to investigate the impact of perturbation to NO_x emissions on subsequent O_3 chemistry, emissions on perturbation levels 1–11 (5–11.7 km) were locally increased by 5% relative to the reference emissions.

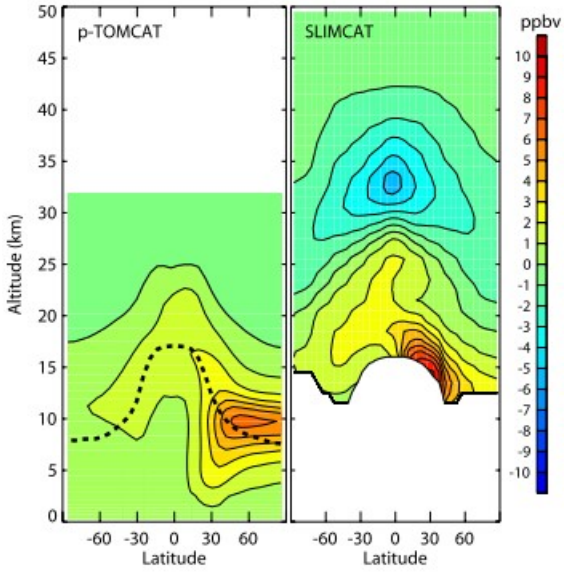

Figure 2.6: Zonal and annual mean O3 changes as calculated by p-TOMCAT (after 2 years) and SLIMCAT (after 7 years). The dashed line indicates the location of the tropopause. SLIMCAT data are shown above the tropopause and above the 335 K isentropic surface only. Changes in mixing ratios are shown with respect to a background atmosphere without aircraft emissions [M. O. Köhler *et al.* 2008].

As shown in figure 2.5, aircraft emissions were found to cover approximately 60% of the globe on perturbation levels 1–11 with a maximum coverage at level 10. This geographical coverage was significantly smaller at altitudes above level 11. The inclusion of AERO2k aircraft NO_x emissions relative to a case without aviation emissions led to a net O_3 increase through an enhancement in O_3 production in turn caused by increased chemical cycling of NO_x both in the troposphere and lower stratosphere. Some O_3 loss occurred at high altitudes due to catalytic destruction. Figure 2.6 depicts the changes in O_3 calculated by p-TOMCAT and SLIMCAT. Mixing ratio of O_3 increased by approximately 6–9 $ppbv$ in the UTLS region, where aircraft emissions had the largest impact. Transport of O_3 to lower altitudes and latitudes led to increased O_3 presence throughout the troposphere with the largest impact in the northern hemisphere.

Rogers *et al.* 2002 showed the SLIMCAT model to be exhibiting an efficient increment of subsonic aircraft emissions within the "tropical pipe", thereby leading to an efficient downward transport in the extra-tropics. M. O. Köhler *et al.* 2008 attributed this argument to the near-tropopause maximum O_3 increase from aircraft NO_x to be located in SLIMCAT at lower latitudes than in the p-TOMCAT model, and to the vertical transport of aircraft NO_x to altitudes above 30 km. Above $\approx$ 25 km altitude, aircraft NO_x emissions contributed to catalytic O_3 destruction, resulting in a small decrease (5 $ppbv$) in stratospheric O_3. In total, aircraft NO_x led to an 8.8 Tg increment in the global O_3 burden. These findings were found to be in reasonable agreement with those of IPCC 1999 and Grewe *et al.* 2002 and with earlier TOMCAT results [M. O. Köhler *et al.* 2004]. However Gauss *et al.* 2006 reported an annual mean O_3 increase in the upper troposphere of up to 4 $ppbv$. This was concluded to be caused by inter-model differences, including the emissions inventory and model formulations such as the chemistry schemes, convective transport schemes, and wet deposition schemes employed.

M. O. Köhler *et al.* 2008 found the monthly aircraft emission rates from June to November to be approximately 10% larger than during the other months, with a maximum in August which contributed to a 'Fall season' peak in the O_3 column change. Furthermore, their results showed that subsonic aircraft flying at cruise altitudes affect O_3 chemistry predominantly in the troposphere and lower stratosphere below 20 km altitude. The O_3 impact above this altitude was relatively small due to large background O_3 mixing ratios and, therefore, the fact that p-TOMCAT is restricted to a model domain below 32 km, did not present itself as a significant disadvantage in the analyses.

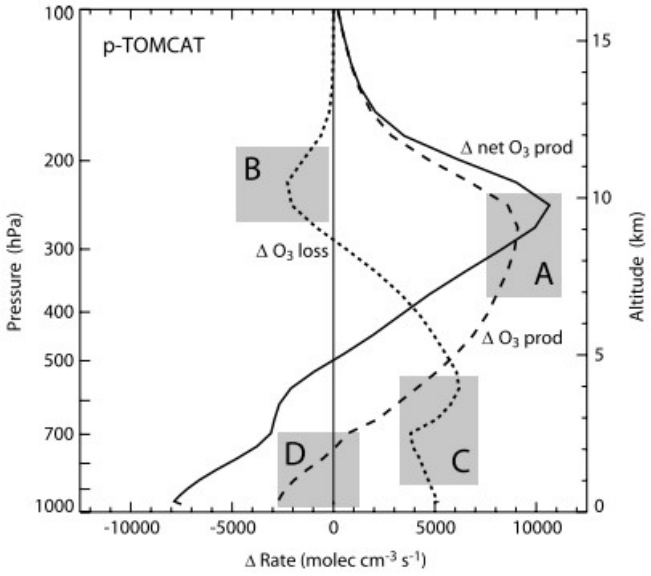

Figure 2.7: Change in O_3 production (dashed line) and loss rates (dotted line) and resulting net O_3 production rate (solid line) due to the inclusion of AERO2k aircraft emissions in p-TOMCAT. The shaded boxes define regions of interest discussed further within the text. Production and loss rates are calculated as zonal and meridional average for July 2002 [M. O. Köhler *et al.* 2008].

Figure 2.7 shows the change in O_3 production and loss rates in July, as calculated by the p-TOMCAT model, due to the inclusion of aircraft emissions. O_3 production peaked in the UTLS region (Box A in figure 2.7) where the largest amounts of NO_x were emitted (See figure 2.5(a)). At the same time loss of O_3 through its reaction with HO_2 (reaction 2.13) was reduced (Box B in figure 2.7) due to an increased reaction of HO_2 with NO (reaction 2.5), further enhancing net O_3 production. A part of the additionally produced O_3 was transported from the upper troposphere to lower altitudes where, in the presence of H_2O, it resulted in increased HO_x formation and therefore increased O_3 loss (Box C in figure 2.7). The increased HO_x levels in proximity to surface NO_x emission sources led to NO_x being increasingly converted in reservoir species, such as HNO_3, thereby leading to a reduction of the gross O_3 production rate at low altitudes (Box D in figure 2.7). M. O. Köhler *et al.* 2008 noted that net O_3 production due to aircraft NO_x emissions occurred only above 5 km altitude and exhibited a maximum at $\approx$ 10 km where the largest amounts of NO_x were emitted by global air traffic (figure 2.5). Therefore the increase in O_3 below 5 km (figure 2.7) was attributed to the transport of O_3 from above, rather than by in-situ production. Moreover, the transport of enhanced O_3 due to aviation from above was deemed responsible for the reduction in the net chemical O_3 production below 5 km by enhancing the conversion from NO_x to HNO_3.

Apart from analyzing the impact of aircraft NO_x emissions on O_3 production and loss rates, M. O. Köhler *et al.* 2008 also studied the impact of perturbation to aircraft NO_x emissions. According to them, such perturbations have an impact on atmospheric chemistry on both local and global scales. Formation of O_3 is affected both at the location of the emissions and further downwind owing to transport of precursors. O_3 and NO_x reservoir species have sufficiently long lifetimes to be transported over significant distances and as such influence the oxidizing capacity of the troposphere globally.

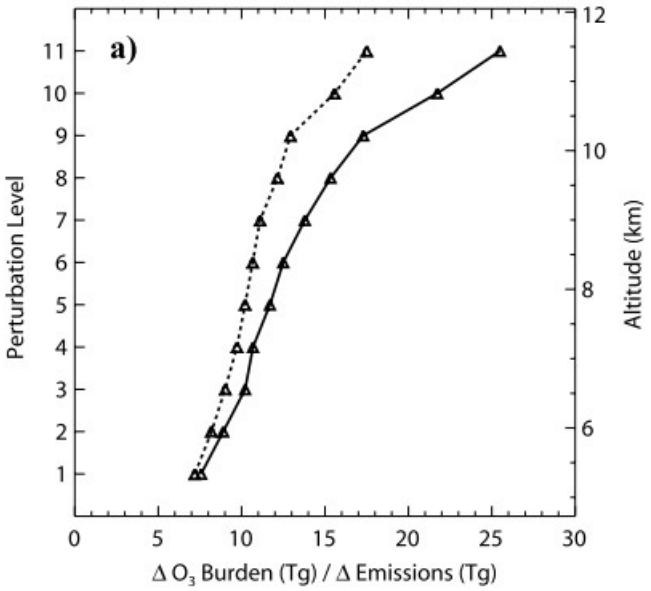

Figure 2.8: Global (solid line) and tropospheric (dotted line) O_3 burden increase in p-TOMCAT due to a 5% NO_x emission increase for each perturbation level, normalized by the global emission increase [M. O. Köhler *et al.* 2008].

As mentioned before, M. O. Köhler *et al.* 2008 found that aircraft NO_x emissions resulted in net chemical O_3 production in the altitude range 5–15 km. In the perturbation levels comprising this altitude range, emissions were increased by 5%. Owing to an already positive net O_3 production rate, an emission increase caused an increase of the global O_3 burden. Figure 2.8 shows the change in global O_3 burden normalized by the emission increase on each perturbation level 1–11 (5–11.7 km). With increasing altitude, the NO_x (NO + NO_2) balance is shifted in favor of NO due to the temperature dependence of the reaction of NO with O_3 [Wild *et al.* 1996; Jaegle *et al.* 1998], reducing the conversion rate of NO_x to HNO_3 and thus increasing the NO_x lifetime with altitude.

M. O. Köhler *et al.* 2008 calculated the O_3 production efficiency (see Section 2.2 for its definition) in January and July from the change in gross O_3 production due to an emission perturbation and from the associated change in loss of NO_x. Their findings approximated the loss of NO_x as being equal to the size of the emission perturbation. In both months (January & July) M. O. Köhler *et al.* 2008 found that the O_3 production efficiency increased with altitude in the troposphere with a particularly sharp increase in the upper troposphere. Correspondingly figure 2.8 shows that the impact on the total O_3 burden increased with the altitude of the applied emission change. Emission changes at higher altitude are much more likely to be transported into the stratosphere and therefore at higher altitudes of the emission change a larger proportion of the stratospheric O_3 burden is perturbed. Therefore, M. O. Köhler *et al.* 2008 concluded that the impact of aircraft NO_x emissions on O_3 depends significantly on cruise altitude, reflecting the increased O_3 production efficiency with altitude.

3

Research questions & their approaches

Investigation of aviation's climate impact is a broad research topic. This thesis therefore analyzes the contribution of aviation to atmospheric mixing ratios of NO_x and O_3 through a particular planned approach in order to answer specific research questions. This thesis provides more clarity regarding the seasonal and zonal patterns of the contribution from global aviation to tropospheric presence of NO_x and O_3. Based on the literature presented in section 2.3, it is clear that comparison of Tagging & Perturbation methods is a good tool to study non-linear atmospheric chemistry. Therefore, the difference between the results of the two aforementioned methodologies is also analyzed using their respective estimates of aviation contribution to tropospheric mixing ratios of NO_x and O_3. The thesis objectives can be achieved by answering a set of research questions mentioned below in Section 3.1.

3.1. Research questions

Within the framework of this thesis, answers to the following research questions are explored:

1. **How does aviation's contribution to tropospheric NO_x and O_3 evolve across seasons? Does aviation O_3 mixing ratio increase linearly across seasons with the increasing aviation contribution to NO_x mixing ratio, & vice versa? If not, then why?**

2. **How does the aviation contribution to the complex NO_x-O_3 tropospheric chemistry differ among different zones of the Earth? Do the tropics exhibit greater accumulation of aviation NO_x and O_3 as compared to the mid-latitudes and polar regions? If so, why? If not, then why?**

3. **By how much do the Perturbation and Tagging methods differ in their estimates of aviation's contribution to tropospheric NO_x and O_3 mixing ratios? Are the Tagging/Perturbation differences in estimation of aviation NO_x and O_3 mixing ratios increasing/decreasing from the tropics towards the poles? Why do these methodological differences arise?**

RESEARCH QUESTION-1

This research question when answered, will present the seasonal changes in the tropospheric chemistry between aviation contribution to atmospheric NO_x mixing ratio and O_3 mixing ratio. The seasonal simulation results for aviation NO_x and O_3 in addition to O_3 precursors such as available background OH and HO_2 are analyzed. Such analyses throw light on the relationship between the aforementioned chemical species and the evolution of the same over different seasons.

RESEARCH QUESTION-2

The second research question concerns the variation in aviation NO_x-O_3 chemistry across different geographical zones to provide a better understanding of the zonal influence on the chemistry. This question explores the geographical factor in the tropospheric O_3 contribution due to aviation NO_x, and in the process looks at the atmospheric distribution of relevant chemical species from the tropics onwards the mid-latitudes and polar regions.

RESEARCH QUESTION-3

The last research question is to investigate the differences between two methodologies (Perturbation and Tagging) to evaluate the NO_x and O_3 mixing ratios due to aviation emissions. The methodological differences' variation across seasons and geographical zones are analyzed. The question seeks to explore the reasoning behind the methodological differences.

3.2. Approach adopted for answering the research questions

The research questions presented in Section 3.1 are answered using the following methodology:

Answering research question-1:
The first question is to be answered by studying the seasonal variation of NO_x and O_3 VMR due to aviation emissions alone. To achieve this goal, climate-chemistry simulation results analysed through Tagging method are evaluated across different seasons. To understand the relationship between the atmospheric presence of aviation NO_x and O_3, the atmospheric availability of other O_3 precursor species, namely OH and HO_2 are studied.

Answering research question-2:
The second question is to be answered by analyzing the variation of aviation NO_x and O_3 VMR across different geographical zones of the Earth. To fulfill this goal, Tagging method results are studied to note the patterns of aviation tropospheric chemistry over tropical latitudes, mid-latitudes and polar regions. Just as in the case of sub-objective 1, atmospheric availability of O_3 precursor chemical species, namely OH and HO_2 are studied to justify the trends of aviation-induced NO_x and O_3.

Answering research question-3:
According to Clappier *et al.* 2017 and many other research studies, Tagging and Perturbation methods attribute different chemical species' contributions respectively to any particular emission source, provided that the chemistry in question is non-linear [Grewe *et al.* 2012; Koo *et al.* 2009] such as that of NO_x-O_3. The final research question thereby deals with the reasoning of the differences observed in Perturbation and Tagging methods' estimations of tropospheric mixing ratios of NO_x and O_3 contributed by global air traffic. These differences in the two methods are analyzed.

4

Climate-chemistry model & simulation setup

Before moving on to apply the theoretical knowledge from Chapter 2 to investigate the contribution of aviation to tropospheric NO_x and O_3, and thereby answer the research questions laid down in Chapter 3, one must understand as to how the climate-chemistry model (CCM) is defined (Section 4.1). Furthermore, the set up of climate-chemistry simulations is to be looked at (Section 4.2), in order to fully understand the simulation results. Last but not the least, the mathematical methodology implemented in this research work is to be understood (Section 4.3) in order to comprehend the results obtained, and then analyze them accordingly in order to derive corresponding conclusions.

4.1. Climate-chemistry model

The objective of this thesis as mentioned in Chapter 1, is to investigate the aviation contribution to tropospheric NO_x and O_3. In order to study the O_3 chemistry in the atmosphere, the CCM in use at DLR's Institute of Atmospheric Physics is used for climate-chemistry simulations. This is the global CCM EMAC (European Centre for Medium-Range Weather Forecasts – Hamburg (ECHAM)/MESSy Atmospheric Chemistry) [Jöckel *et al.* 2010, 2016], which is equipped with the Modular Earth Submodel System (MESSy) interface [Jöckel *et al.* 2010; Jöckel *et al.* 2005]. This interface keeps track of the contribution of source categories (mainly emission sectors) to mixing ratios of various chemical species [Grewe *et al.* 2017]. As emission sectors, the CCM considers road traffic, shipping, air traffic, anthropogenic non-traffic, biogenic, biomass burning and lightning. EMAC uses the general circulation model ECHAM5 [Roeckner *et al.* 2006] as a base model. Within the CCM, the Earth is modelled as a horizontal grid of approximately 2.8^0 x 2.8^0 with 90 hybrid levels characterizing the vertical resolution of the Earth's atmosphere. These hybrid levels correspond to the geographical terrain of the Earth.

Chemistry schemes for gas and aqueous phase chemistry are applied in the CCM as described by Mertens *et al.* 2016. For calculation of chemical kinetics, the MESSy submodel Module Efficiently Calculating the Chemistry of the Atmosphere (MECCA [Sander *et al.* 2019]) is used. The chemical mechanism includes the chemistry of O_3, methane, and odd nitrogen. Alkynes and aromatics are not considered, but alkenes and alkanes are considered up to C_4. The Mainz Isoprene Mechanism [Pöschl *et al.* 2000] is applied for the chemistry of isoprene and some non-methane hydrocarbons. Scavenging of trace gases by clouds and precipitation is calculated by the submodel SCAV (scavenging of traces gases by clouds and precipitation [Tost *et al.* 2006]). Dry deposition is considered according to Kerkweg *et al.* 2006.

In order to implement the Tagging methodology in the CCM, a set of diagnostic tracers for each chemical species or chemical family are embedded. For example, for the family of reactive nitrogen compounds NO_y, a set of tagged tracers NO_y^{ant}, NO_y^{rt}, NO_y^{shp}, NO_y^{air}, NO_y^{bio}, NO_y^{bb} and NO_y^{lig} are added, which describes the NO_y concentration from anthropogenic non-traffic (e.g. industry, households), road traffic, ships, air traffic, biogenic, biomass burning and lightning respectively. The idea is that

these tagged tracers experience the same chemical conversions, sources, and loss processes (such as deposition) as the simulated tracer NO_y [see Section 2.3.1 for the theoretical implementation]. A full partition of the simulated tracer concentration with respect to emission sectors can therefore be achieved. For further details regarding the implementation of Tagging methodology within the CCM, the reader may refer the supplement of Grewe *et al.* 2017.

4.2. Climate-chemistry simulation setup

To limit the role of coupling between chemistry, atmospheric dynamics and meteorology giving rise to natural variability in the climate-chemistry simulation results, simulations performed in "quasi-chemistry transport model" (QCTM) mode are considered (as proposed by Deckert *et al.* 2011 and implemented in Grewe *et al.* 2017, Mertens *et al.* 2020). This simply suppresses the feedback effect from a change in atmospheric chemistry on the meteorology, which in turn would impact the chemistry (& subsequently the atmospheric presence of chemical species) and this cycle would then influence the results to represent scenarios with a significant deviation from reality. Quasi-chemistry transport model simulation mode implies that the emission data from a single year is simulated across a range of several years with their own changing meteorology in order to reduce the impact of natural variability & better estimate the impact of aviation emissions on the NO_x-O_3 chemistry. In this research study, emissions' data from the year 2015 are simulated with the meteorology of July 2012 to December 2017 whereby the last months in 2012 are the spin-up phase and main analyses are done for the 5 years: 2013 to 2017.

In order to study and analyze the contribution of global air traffic to tropospheric NO_x and O_3, 4 seasons are considered as follows:

- SPRING: consisting of the months of March, April & May
- SUMMER: consisting of the months of June, July & August
- FALL: consisting of the months of September, October & November
- WINTER: consisting of the months of December, January & February

The chemical species examined in this thesis work are NO_x, O_3, OH and HO_2. Inspite of CO and $NMHC$ being precursors of O_3, they are not being considered for analysis. This is because among the aircraft engines', NO_x is the major chemical species after CO_2 & H_2O. CO_2 and H_2O are not analyzed owing to the thesis scope not studying CO_2 effects and/or contrails, and as for CO and $NMHC$, they account for only $\approx$ 10% of the emissions. Furthermore, source estimates of $NMHC$ and CO are associated with considerable uncertainty [Brasseur *et al.* 1998]. Due to their short lifetime of weeks to months, the atmospheric distribution of $NMHC$ and CO are highly variable in space and time [Brasseur *et al.* 1998].

The VMR of chemical species formed due to global aviation (& not atmospheric background species such as OH and HO_2) are evaluated using both Tagging and Perturbation approaches. This is done in order to be able to comment on the differences between the aforementioned methodologies in estimating the contribution of air traffic to the tropospheric presence of NO_x and O_3 (just as explained in Section 2.3). Furthermore, in order to analyze aviation's contribution to NO_x and O_3 VMR across different seasons and geographical zones, only the Tagging methodology results are used. This is because previous research (such as Grewe *et al.* 2010, Clappier *et al.* 2017) have repeatedly confirmed that Tagging is the most suitable method to quantify a particular sector's contribution to the atmospheric presence of any chemical species. For the evaluation through Perturbation methodology, data from 2 simulations are considered:

1. SIMULATION (A): one simulation with all emission sources at their 100% emission levels, and
2. SIMULATION (B): the other simulation with just aviation emissions reduced to 95% of their reference level (i.e. emission change α for aviation = -0.05; see Section 2.3.2 for the definition of α).

The aforementioned 95% aviation emission level and the particular emission year 2015 are chosen owing to the data made available by DLR for the project. This thesis project, therefore, does not examine the impact of emission reduction level (α) on results produced by Perturbation methodology.

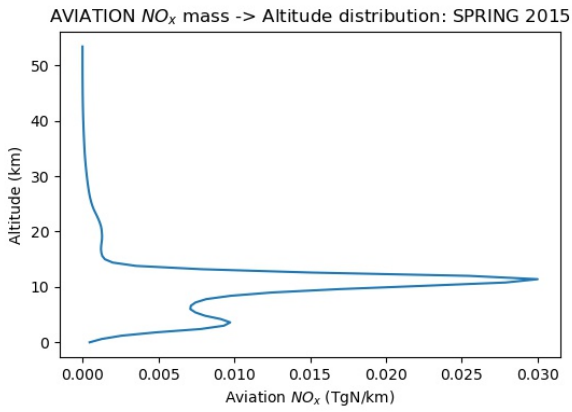

Figure 4.1: Altitude distribution of NO_x mass contributed by aviation, in Spring.

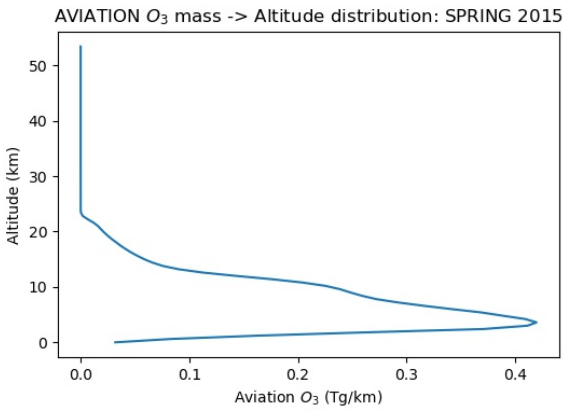

Figure 4.2: Altitude distribution of O_3 mass contributed by aviation, in Spring.

4.3. Methodology

Owing to the fact that the available climate data varies across longitude, latitude & altitude, in order to simplify the analyses all of the data is averaged over one dimension; in this research work, it is the altitude/pressure level. Therefore, all the resulting plots of chemical species discussed as part of this thesis work, are expressed in terms of longitude v/s latitude (unless otherwise specified in the figure captions). The altitude averaging of the climate data is implemented only for those altitudes which are the most significant with respect to global air traffic's contribution to NO_x, i.e. an altitude range encompassing that part of the atmosphere where NO_x due to aviation is mainly found to exist. An instance from the available data of altitude distribution of aviation contribution to NO_x mass is shown in figure 4.1.

Figure 4.1 is representative of the altitude distribution trend of aviation NO_x observed for the entire year (data for other seasons are included in Appendix A). It is clear that the aviation contribution to NO_x is majorly concentrated in the altitude range of 0 to 20 km. This is in agreement with the previous findings (such as those of IPCC 1999; Brasseur *et al.* 1998) that global aviation mainly occurs in this particular altitude range. Furthermore, the subsequent aviation O_3 is also limited within 20 km from the ground surface (in line with the results of D. Lee *et al.* 2010; M. O. Köhler *et al.* 2008), as depicted in figure 4.2. This is also representative of the altitude distribution trend of aviation O_3 observed for the entire year (data for other seasons are included along with that of aviation NO_x in Appendix A). Therefore, this altitude range was chosen for the aforementioned data averaging and all of the further analysis within this thesis work.

For the altitude-averaging, since different altitudes imply different air densities, the VMR of the chemical species cannot be simply summed up to obtain the corresponding average. Therefore, the following steps are implemented:

1. At a given altitude, VMR is converted to MMR as

$$MMR = VMR \cdot \frac{M_{species}}{M_{air}} \tag{4.1}$$

2. Since

$$MMR = \frac{m_{species}}{m_{air}} \tag{4.2}$$

the species MMR is then multiplied with the grid air mass at the given altitude, to get the concerned species' mass at that altitude.

3. This species mass is then summed up across the desired altitude range to obtain the total species mass (= $\sum m_{species}$).

4. This total species mass is then divided by the total air grid mass across the altitudes to get the altitude-averaged species' data in terms of MMR_{avg}.

$$MMR_{avg} = \frac{\sum m_{species}}{\sum m_{air}} \tag{4.3}$$

5. Finally, MMR_{avg} is converted to represent the altitude-averaged data in terms of species VMR_{avg}:

$$VMR_{avg} = MMR_{avg} \cdot \frac{M_{air}}{M_{species}} \tag{4.4}$$

In order to analyze and derive conclusions concerning the differences between the altitude-average data produced through the aforementioned 2 methodologies (Tagging and Perturbation), the Perturbation method's estimations (denoted as $PERT$) of aviation contribution to tropospheric NO_x and O_3 are evaluated as follows:

$$PERT = [sim_a - sim_b] \cdot 20 \tag{4.5}$$

where sim_a and sim_b represent the results obtained from SIMULATION (A) and SIMULATION (B) respectively (Refer to Section 4.2 for the simulations' setups). For the theory used to derive this equation, the reader may refer Section 2.3.2. Equation (4.5) can be easily obtained from equation (2.48) by substituting α = -0.05 (5% reduction in aviation emissions in simulation (B)).

Difference in the results produced by the simulations (A) and (B), provides an estimation of 5% of aviation emissions. In order to study the non-linear chemistry (comparison with Tagging method results), the obtained 5% estimation is to be multiplied by a factor of 20 (to get the results for 100% aviation emissions).

Lastly, it is important to note that all the longitude v/s latitude plots shown in Section 5.2 to analyze the difference between the results of Tagging and Perturbation methodologies, use a percentage difference parameter defined as:

$$\%difference = P = \frac{PERT - TAG}{TAG} * 100, \tag{4.6}$$

where $PERT$ & TAG represent the estimations of the chemical species' data (such as VMR, production & loss rates, etc.) through the Perturbation and Tagging methods respectively.

5

Results and discussions

This chapter presents the results obtained from the climate-chemistry simulations performed using the model, simulation setup and methodology described in Chapter 4. Chemical species: NO_x, O_3, OH and HO_2 were analysed and discussions are presented to help (a) understand the patterns reported for aviation's contribution to tropospheric NO_x and O_3 across different seasons of the year and across several regions of the globe (Section 5.1), in addition to (b) studying the differences between Perturbation and Tagging approaches in evaluating the global air traffic's contribution to NO_x and O_3 presence in the troposphere (Section 5.2).

5.1. Seasonal & Zonal patterns in aviation's contribution to NO_x and O_3

5.1.1. Aviation NO_x

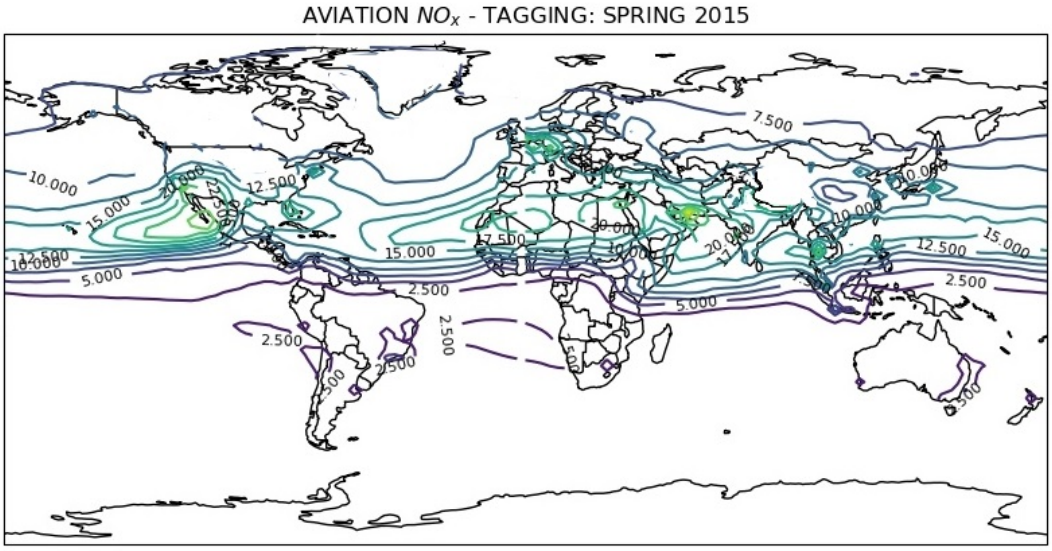

Figure 5.1: VMR of NO_x (units: $pptv$) contributed by global aviation in the Spring season.

Figure 5.1 shows the aviation contribution to NO_x VMR in Spring (for other seasons' plots, refer to figures B.1, B.2 and B.3 in the Appendix B). It is clear from these aforementioned seasonal representations that Western Europe emerged as a region of significant NO_x accumulation due to aviation, with an annual average of 30 $pptv$. Along with the European continent, the USA too witnessed a high presence of aviation NO_x at both its East Coast (close to New York) as well as the West Coast (over California), with the annual average amounting to 29.5 $pptv$. One other local peak was also observed over the

Middle East. A common trend observed across all the seasons is that the Northern mid-latitudes witnessed greater amounts of NO_x contributed by aviation as compared to the tropical regions. This is in line with the observation of Lelieveld and F. J. Dentener 2000, that mid-latitudes & higher latitudes in the Northern Hemisphere see a greater accumulation of NO_x reservoirs, consequentially leading to more NO_x in the corresponding regions.

5.1.2. Background O_3 precursors

Going by the representation of tropospheric O_3 production reaction chain in reactions (2.1) to (2.7), it is clear that increased presence of OH radical is a good indicator of the atmosphere's oxidation capacity [Prinn 2003]. Oxidation capacity is the rate at which the atmosphere self-cleanses, or undergoes removal of organic compounds such as NO_x through their oxidation (refer to reaction 2.5). Therefore, regions with greater VMR of background OH (and also background HO_2 since it is formed due to the reaction cycle of OH; refer to Section 2.1) expect a greater accumulation of O_3 due to aviation, as compared to the regions with relatively lesser VMR of OH and HO_2. Therefore background OH and HO_2 radicals were analyzed in order to comprehend the chemical transformation of aviation-induced NO_x into O_3.

A first look at figure 5.2 depicts the fact that the most significant presence of OH was in the tropics, as compared to mid-latitudes and polar latitudes. This is owing to the presence of abundant sunlight and high moisture [Singh *et al.* 1990]. Although figure 5.2 corresponds to that of Spring, it is similar to the CCM results obtained for the seasons of Summer and Fall (refer to figures B.4 and B.5 in the Appendix B). The Western coast of Africa along with that of South America, emerged as hotspots with an annual average presence of 0.130 $pptv$ OH due to increased photo-chemistry as compared to the polar regions.

An interesting conclusion can be drawn here in regard to the nature of winds observed. Figure B.5 depicts that the South-Eastern trade winds in the Southern Hemisphere registered their greatest intensity in the Fall season, thereby transporting OH precursors (such as O_3: refer to reactions 2.8 and 2.9) westwards off the coasts of both South America and Africa (& hence subsequent peak presence of OH). Although, peaks of background OH presence in the Winter (refer to figure B.6 in Appendix B) were predominantly found in the Southern Hemisphere. This is because the Southern Hemisphere witnesses its hottest time of the year during these months, resulting in increased photo-chemistry (& therefore more OH) as compared to the Northern Hemisphere.

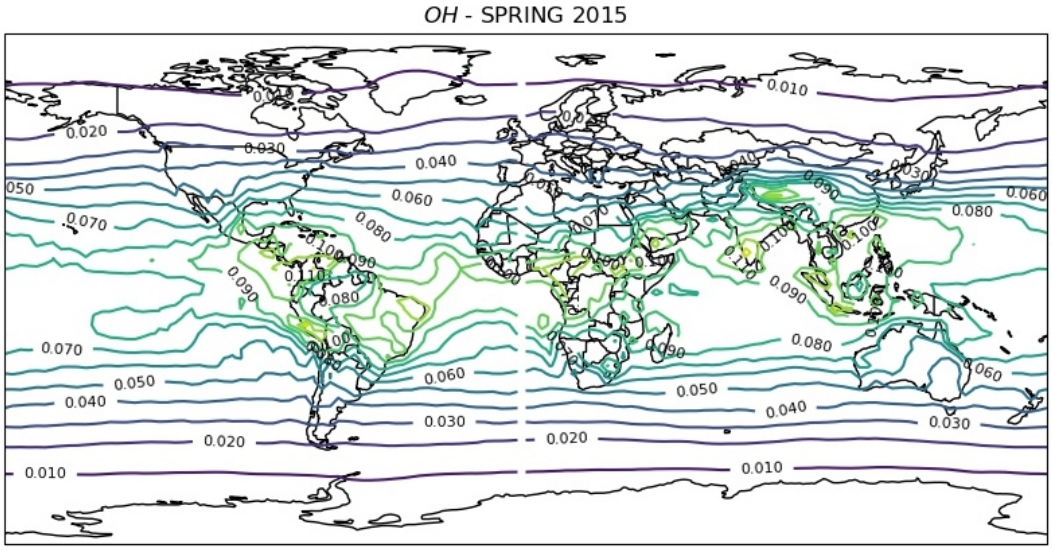

Figure 5.2: Background OH VMR (units: $pptv$) in the troposphere during Spring.

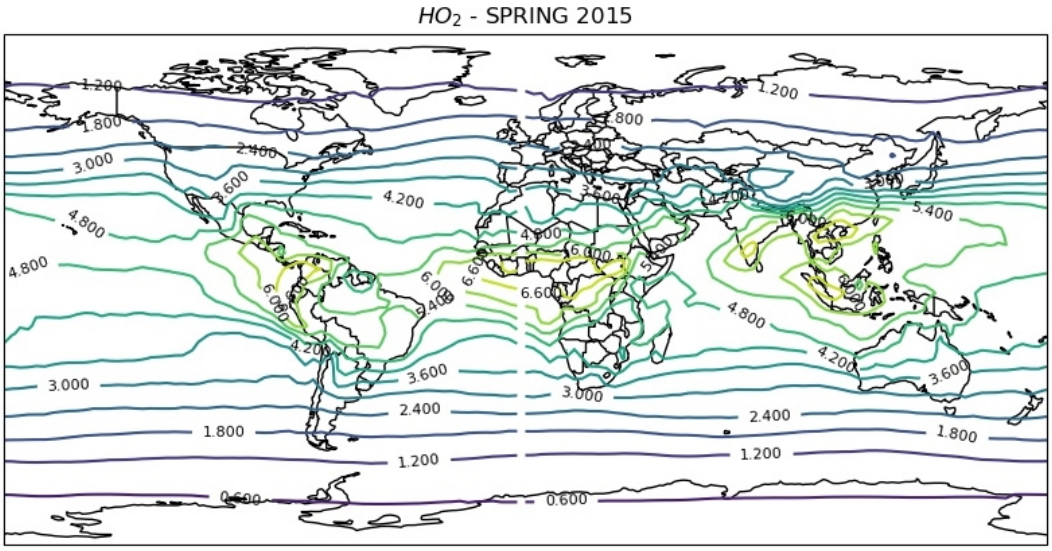

Figure 5.3: Background HO_2 VMR (units: $pptv$) in the troposphere during Spring.

In the case of HO_2 radical (shown in figure 5.3), the Indian subcontinent along with South-East Asia emerged as the key hotspot. Again just as noted for OH radical, figure 5.3 can be used to depict the overall simulated trend witnessed throughout Summer & Fall (refer to figures B.7 and B.8 in Appendix B). Maximum presence of HO_2 in these regions was witnessed at 8 $pptv$ over Northern India in Summer. This can be attributed to the problem of severe air pollution in the region [Guo *et al.* 2017]. Also, the Western coast of Africa (around Nigeria) observed an annual average presence of 6.40 $pptv$ of HO_2 and was a key hotspot.

Since the HO_2 radical is short-lived just like OH, a similar conclusion can be drawn in regard to the effect of South-Eastern trade winds, just as done in the case of OH. Figure B.8 points out that the South-East trade winds attained their greatest intensity in the Fall season, thereby pushing the peak accumulations of HO_2 precursors westwards over the ocean, off the coasts of South America. Here the South American coast observed a high presence of HO_2 at 7.20 $pptv$. Furthermore, another similarity between the seasonal trends of HO_2 and OH is that HO_2 presence is also the highest over the tropical regions (with an annual average of 4.89 $pptv$) as compared to the mid-latitudes and polar regions.

5.1.3. Aviation O_3

Aviation-induced tropospheric O_3 was distributed across the globe in Spring, as per the climate-chemistry simulation results depicted in figure 5.4. The results for the other seasons' O_3 tropospheric presence are attached in figures B.10, B.11 and B.12 in Appendix B. From the aforementioned figures, it can be seen that aviation O_3 predominantly accumulated over tropical and mid-latitude regions. This can be attributed to the corresponding high presence of aviation NO_x over the mid-latitudes (figures 5.1, B.1, B.2 and B.3) and higher oxidation capacity of the atmosphere (more presence of OH and HO_2) in the tropics as compared to the polar regions (figures 5.2, 5.3, B.4, B.5, B.6, B.7, B.8 and B.9).

In the Northern Hemisphere, all throughout the year, a hotspot of aviation O_3 was visible in the form of a continuous belt covering the regions of North-Western China, Middle East & Northern Africa (with an annual average of 1.57 $ppbv$). This is in line with the simulated VMR of NO_x contributed by aviation. As per the figures 5.1, B.1, B.2 and B.3, the highest NO_x from aircraft accumulated over Northern Africa & Middle East. Also the seasonal distribution of HO_2 radical (refer figures 5.3, B.7, B.8 and B.9) showed HO_2 peak contours over Northern India & off the coast of West Africa. In addition to the aforementioned O_3 belt, the Western Coast of USA was a notable region of aviation O_3 presence with an annual average of 1.53 $ppbv$. This is also attributable to the high NO_x VMR due to aviation, as depicted in the simulation results in figures 5.1, B.1, B.2 and B.3.

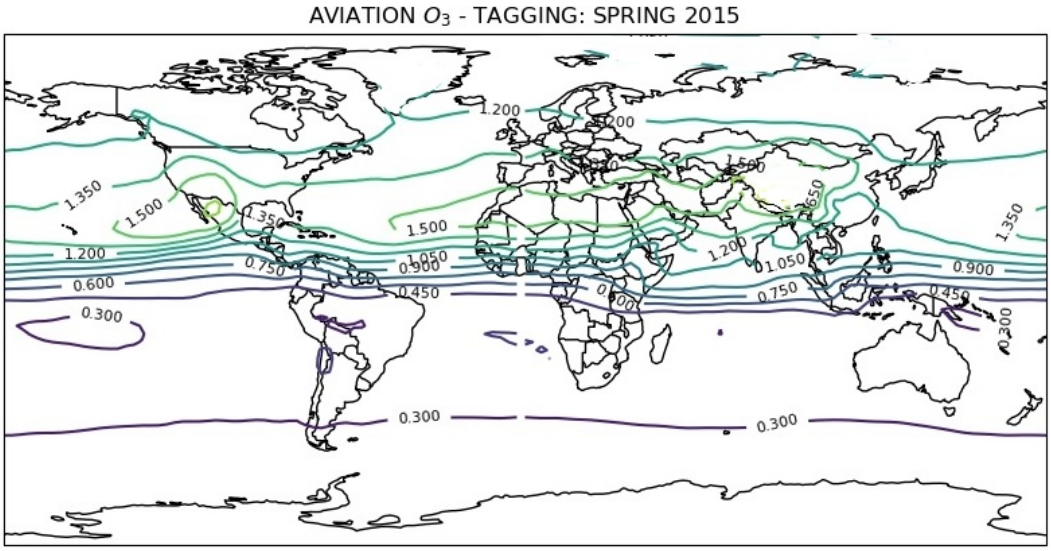

Figure 5.4: Tropospheric O_3 VMR (units: $ppbv$) contributed by global aviation in Spring.

Since the lifetime of O_3 can be of several months, the simulated VMR of atmospheric O_3 due to aviation is more likely to be influenced by transport effects as compared to species such as OH, HO_2 and even NO_x. Hence, the simulated CCM response for aviation O_3 showed a wider region of scope. Also, the simulated aviation O_3 trend is in agreement with the expected weather phenomena, such as the seasonal movement of the Inner Tropical Convergence Zone (ITCZ). Figure B.10 clearly depicts the northward movement of ITCZ from Spring towards Summer, thereby also moving the aviation O_3 contours northwards, before moving back south again for Fall & Winter (see figures B.11 and B.12 respectively).

Depicted below in figure 5.5 is the seasonal distribution of masses of aviation NO_x, aviation O_3 in addition to background presence of OH, HO_2 in the North Hemisphere. In the Northern Hemisphere, aviation NO_x exhibited its highest presence in Summer and Fall at 0.74 TgN and 0.82 TgN respectively. This is in agreement with the observation by M. O. Köhler ***et al.*** 2008 that the aviation emission rates are larger from June to November, as compared to the other months, with a maximum in August. Since NO_x is a primary precursor to O_3, the calculated seasonal values of NO_x mass are also in line with the observation by Mertens ***et al.*** 2020 that O_3 production peaks during the period May-July (Summer) & in October (Fall). It is evident from figure 5.5 that with the aviation NO_x mass increasing from Spring to Summer, the mass of aviation O_3 did not increase proportionately owing to the lesser available atmospheric mass of OH (indicating a lower oxidation capacity) in Summer. This clearly shows the non-linear characteristic of the NO_x-O_3 tropospheric chemistry.
Further, as the NO_x mass contributed by aviation again increased in Fall, the O_3 per unit NO_x this time also went up from 4.7 to 4.85 Tg/TgN due to a higher OH mass available in Fall as compared to Summer. Finally, as the aviation NO_x decreased in Winter, the O_3 per unit NO_x proportionately decreased to 4.62 Tg/TgN. This decrease can also be attributed to the decrease in the background available masses of OH and HO_2 (decreased oxidation capacity of the atmosphere).

As for the scenario in the Southern Hemisphere (refer to figure 5.6), amongst all the seasons, Summer witnessed the least NO_x-O_3 tropospheric chemistry due to aviation. This is clearly visible from the figure 5.6 where the mass of aviation NO_x was only at a mere 0.00075 TgN consequentially leading to the aviation O_3 per unit NO_x amounting to $\approx$ 27 Tg/TgN. This simulated minima in the chemistry can also be seen in the background levels of OH and HO_2 in the troposphere, which were as expected since the Southern Hemisphere is exposed to lesser of the incident solar radiation during the months of Northern Hemisphere's Spring & Summer, thereby leading to reduced photo-chemistry as compared to Fall & Winter.

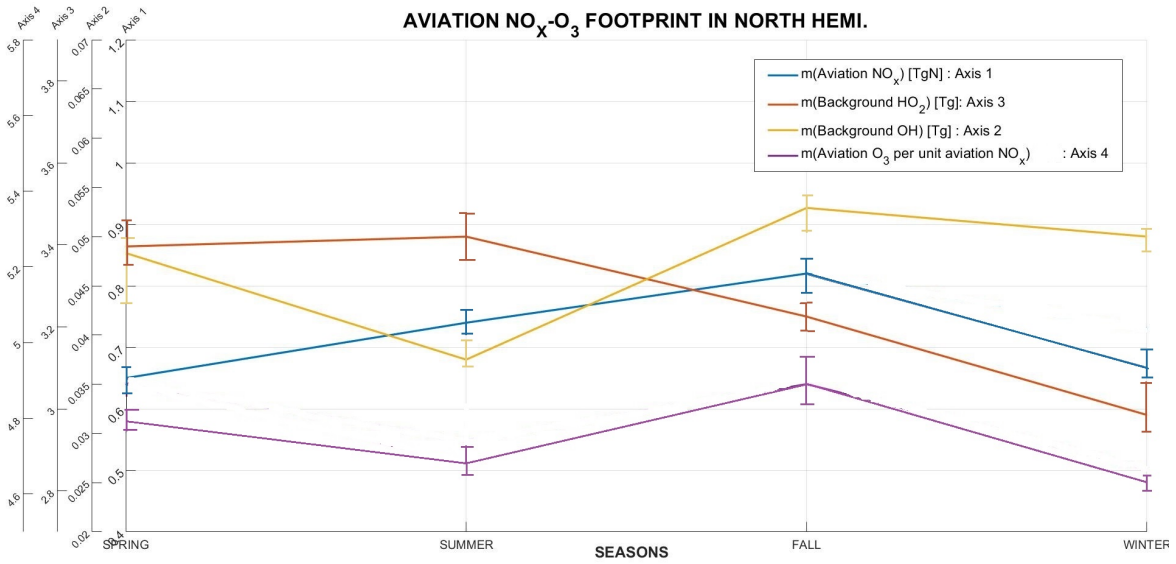

Figure 5.5: Seasonal distribution of aviation NO_x mass (units: TgN) and consequently formed O_3 mass per unit NO_x (units: Tg/TgN), along with masses of background OH (units: Tg) and HO_2 (units: Tg), in the Northern Hemisphere. The vertical lines corresponding to the seasonal values for every chemical species represent 95% confidence interval (see Section 6.1).

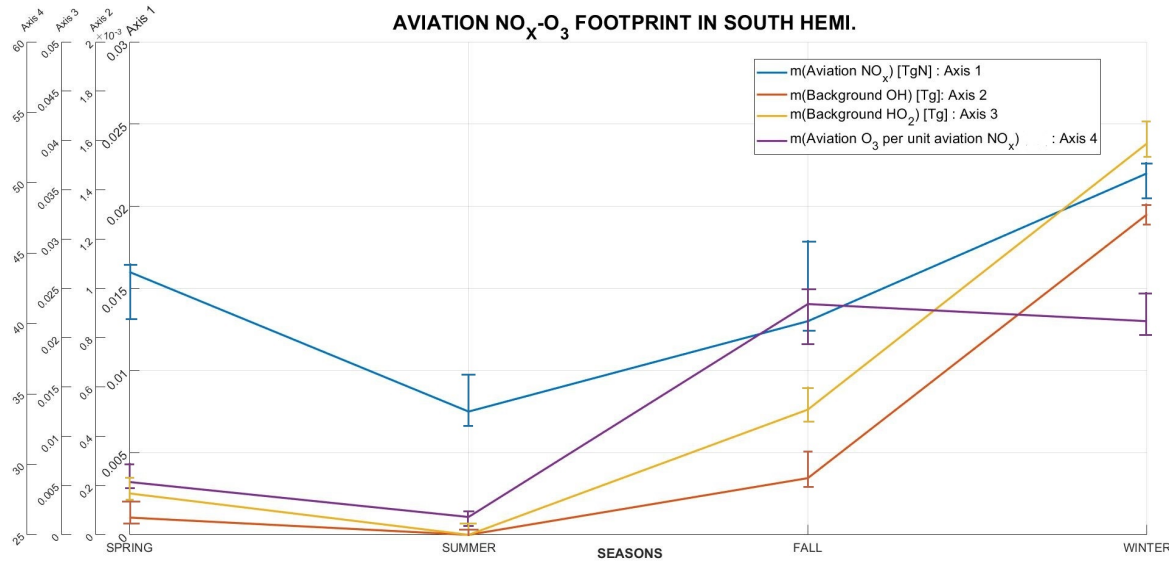

Figure 5.6: Seasonal distribution of aviation NO_x mass (units: TgN) and consequently formed O_3 mass per unit NO_x (units: Tg/TgN), along with masses of background OH (units: Tg) and HO_2 (units: Tg), in the Southern Hemisphere. The vertical lines corresponding to the seasonal values for every chemical species represent 95% confidence interval (see Section 6.1).

In the Fall & Winter, as more of solar energy is incident on the Southern Hemisphere (as compared to Spring & Summer), increased levels of background OH and HO_2 radicals were present in the troposphere. This coupled with an increase in the aviation NO_x after Summer, the aviation O_3 produced per unit corresponding NO_x also rose in these seasons. Unlike the Northern Hemisphere which registered the lowest level of tropospheric chemistry due to aviation emissions in the Winter, its Southern counterpart witnessed its highest NO_x-O_3 chemistry in the same time. It must be noted that the mass values of aviation NO_x & O_3 along with those of background OH and HO_2 were all of a much lesser magnitude in the Southern Hemisphere than in the Northern Hemisphere. This implies that all throughout the year, the Southern Hemisphere always witnessed lesser tropospheric NO_x-O_3 chemistry due to aviation, as compared to its Northern counterpart (also predicted by Dahlmann *et al.* 2011).

5.2. Comparison of Tagging and Perturbation results

Tagging & Perturbation methods as explained by Clappier *et al.* 2017, produce different estimations for the atmospheric presence of a chemical species, in the case where the concerned chemistry is non-linear in nature. Whereas for a linear chemistry environment, the estimates using both the Tagging and Perturbation are expected to be quite similar, if not exactly the same. As per the theory explained in Section 2.2 and shown by J. U. Grooß *et al.* 1998, Cohan *et al.* 2005 and several others, it is certain that the NO_x-O_3 chemistry is non-linear. The calculated differences between Tagging and Perturbation methodologies' estimations of aviation contribution to NO_x and O_3 VMR, are analyzed and discussed below.

5.2.1. Aviation's contribution to tropospheric NO_x

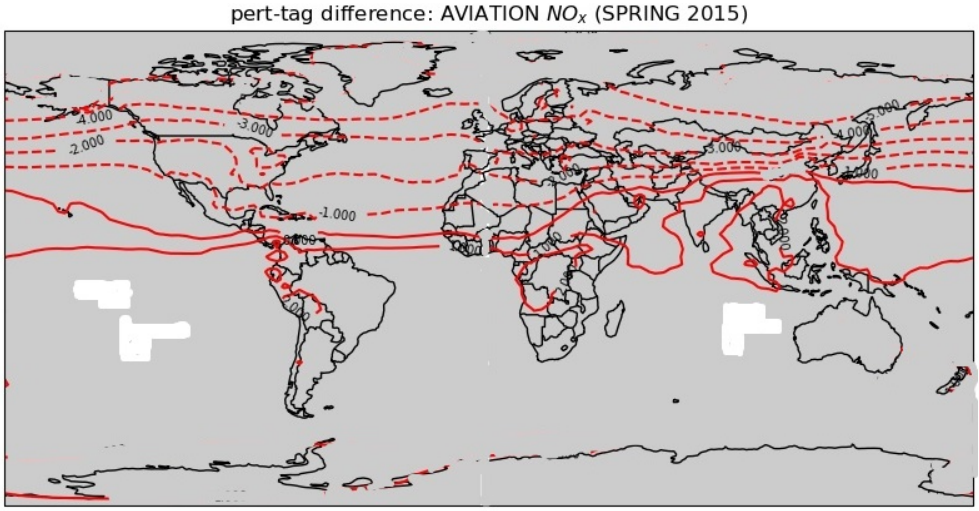

Figure 5.7: Percentage difference between Perturbation & Tagging estimations for the mean tropospheric contribution of aviation to NO_x VMR in the Spring season. Every grid point in the plot is subjected to a statistical 2-tailed t-test with 95% confidence level (see Section 6.1), whereby the grey-shaded areas indicate that the differences between the Tagging & Perturbation estimations are statistically significant and not a coincidence.

As per figure 5.7, the percentage difference between Tagging & Perturbation results of aviation contribution to mean tropospheric NO_x lies within the range of 1% to $\approx$ 4 or 5%. Although figure 5.7 corresponds to the calculations in Spring, it is well representative of a similar trend observed for the other seasons (refer to figures C.1, C.2 and C.3 in Appendix C). Since literature (e.g. Clappier *et al.* 2017) has indicated that Perturbation and Tagging results are almost same (if not exactly same) for linear chemistry, the calculated differences in figure 5.7 indicate an almost linear relationship between the (simulation) input aviation NO_x emissions and the corresponding CCM response (resulting NO_x concentration). This implies that the emitted nitrogen (in the form of NO_x) which gets eventually washed out of the atmosphere [Chameides and Walker 1973] in the form of acid rain (HNO_3) (refer to reaction 2.14), or dry deposition, follows a linear pattern. This can be understood using the simple atmospheric chemical system representation in Section 2.3.1:

$$\dot{X}_i = E_{X,i} - \tau_{X,i}^{-1},$$

where i is aviation (emission source being analyzed) and X is NO_x. As NO_x emission ($E_{X,i}$) increases (for e.g. from 100 Tg to 200 Tg), the associated NO_x loss ($\tau_{X,i}^{-1}$) also increases (for e.g. from 80 Tg to 160 Tg). The resulting NO_x concentration (CCM response) denoted by $\dot{X}_i$ therefore increases from 20 Tg to 40 Tg, thereby following a linear pattern. This is an injecture put forth by the reported differences between Perturbation & Tagging for aviation NO_x (figures 5.7, C.1, C.2 and C.3). From the reported methodological differences in figure 5.7 (& corresponding figures for other seasons in Appendix C), it was concluded that aviation NO_x itself induced only minor non-linearities in the NO_x-O_3 chemistry.

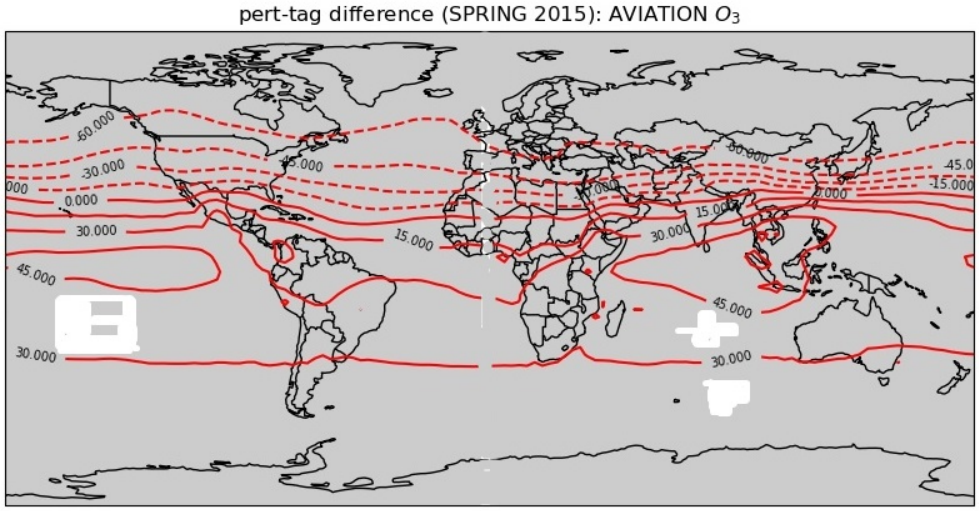

Figure 5.8: Percentage difference between Perturbation & Tagging estimations for the mean tropospheric O_3 VMR due to aviation NO_x emissions, in the Spring season. Every grid point in the plot is subjected to a statistical 2-tailed t-test with 95% confidence level (see Section 6.1), whereby the grey-shaded areas indicate that the differences between the Tagging & Perturbation estimations are statistically significant and not a coincidence.

5.2.2. Aviation's contribution to tropospheric O_3

As for the aviation-induced tropospheric O_3, the calculated differences between the Perturbation & Tagging methods for the Spring season are depicted in figure 5.8 (For the other seasons, refer to figures C.4, C.5 and C.6 in Appendix C). It is clearly observed from these aforementioned figures that Perturbation results differ from the Tagging ones by a margin of 15% to around 60%. This implies that the non-linear behavior observed in the tropospheric NO_x-O_3 chemistry due to aviation emissions, is mainly induced by aviation O_3.

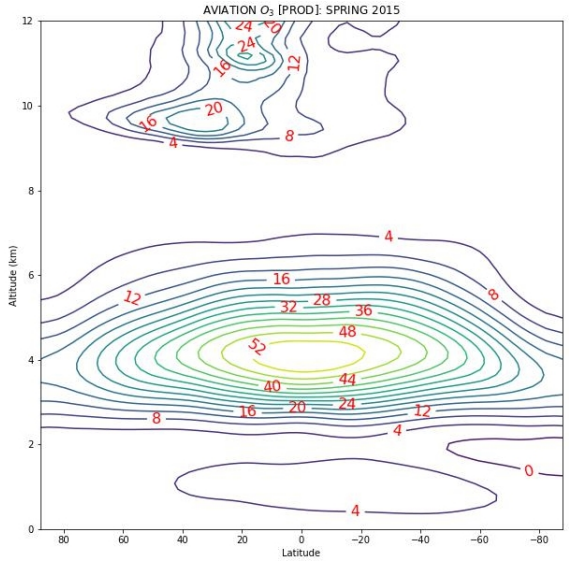

Figure 5.9: Vertical distribution of the O_3 production rate (units: x 10^{-16} $mol/mol/s$) due to aviation emissions, in Spring.

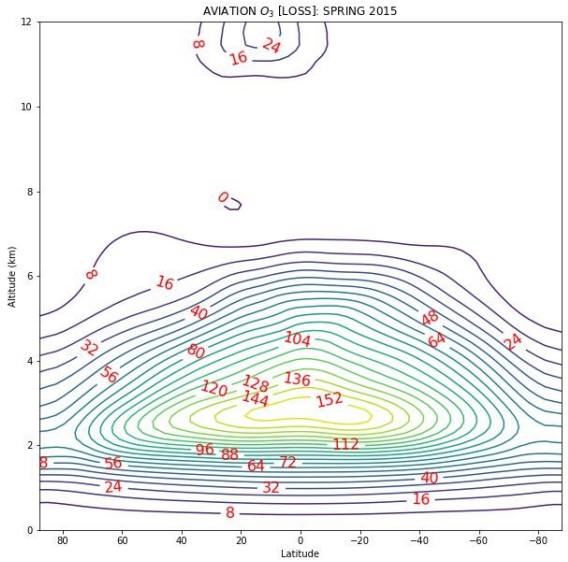

Figure 5.10: Vertical distribution of the O_3 loss rate (units: x 10^{-16} $mol/mol/s$) due to aviation emissions, in Spring.

Figure 5.9 shows the vertical distribution of O_3 production rate due to aviation, in Spring (for other seasons, refer to figures A.19, A.20 and A.21 in Appendix A). All throughout different seasons, the simulation results depicted a significantly high O_3 production rate due to aviation activities closer to the surface (0 to 5 km) (see figure 5.9). This could be attributed to the takeoff & landing operations of

aircraft worldwide. However it is seen that there was also a corresponding peak in the tropospheric O_3 loss due to aviation, in the aforementioned altitude range (see figure 5.10). M. O. Köhler *et al.* 2008 noted that the transport of enhanced O_3 due to aviation from above is responsible for the reduction in the net chemical O_3 production below 5 km by enhancing the conversion from NO_x to HNO_3.

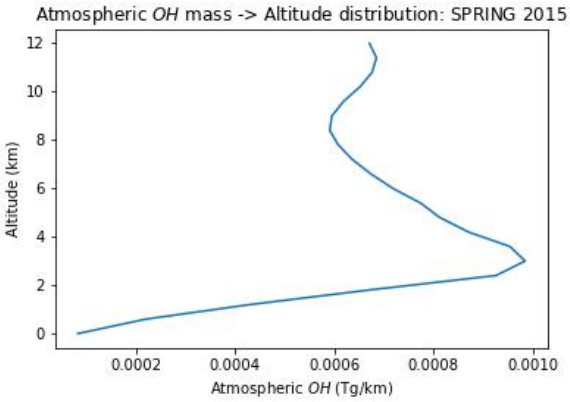

Figure 5.11: Altitude distribution of background OH mass in Spring.

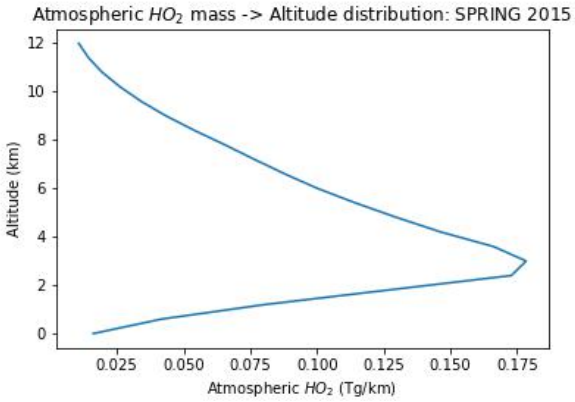

Figure 5.12: Altitude distribution of background HO_2 mass in Spring.

The increased O_3 loss closer to the surface was also traced back to a significantly high background presence of OH and HO_2 in the corresponding altitudes (seen in figures 5.11 and 5.12), since OH and HO_2 are not only precursors to O_3 but also form the main reaction mechanisms for tropospheric O_3 loss (refer to reactions 2.12 and 2.13 in Section 2.1). As a result, significant contribution of aviation activities to net O_3 production in the troposphere only stems from the altitudes closer to the standard cruise altitudes of passenger aircraft (around 9-12 km), as is depicted in figure 5.13. This is in agreement with the observation by M. O. Köhler *et al.* 2008 that net O_3 production due to aircraft NO_x emissions exhibits a maximum at approximately 10 km where the largest amounts of NO_x are emitted by aviation.

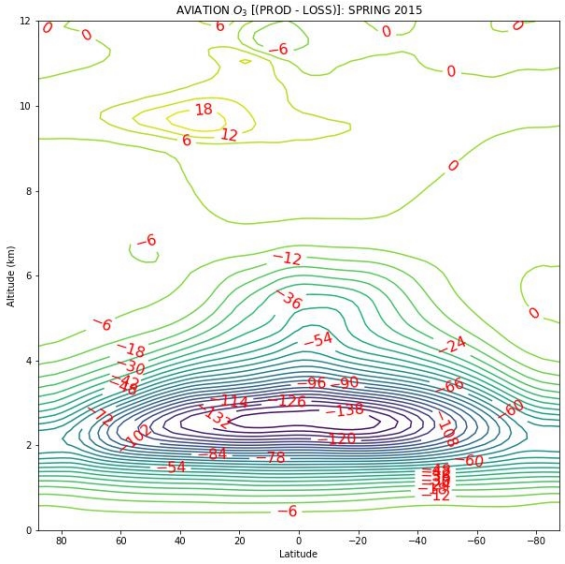

Figure 5.13: Vertical distribution of the net O_3 production rate [= O_3 production rate - O_3 loss rate] (units: x 10^{-16} $mol/mol/s$) due to aviation emissions, in Spring.

Therefore, estimations for aviation O_3 using Perturbation and Tagging methods were analyzed for the altitudes ranging from 8 to 12 km. In figure 5.14, it can be seen that Perturbation significantly underestimated (average $\approx$ 14% lesser than Tagging) O_3 production rate due to aviation, in the Northern

Hemisphere. The corresponding aviation O_3 loss rate for the Northern Hemisphere was however found to be underestimated by Perturbation at an average of only 4.25% (figure 5.15). Hence a significant underestimation of aviation O_3 production rate is why the Northern Hemisphere registered a corresponding underestimation of tropospheric O_3 VMR by Perturbation, as seen in figure 5.8.

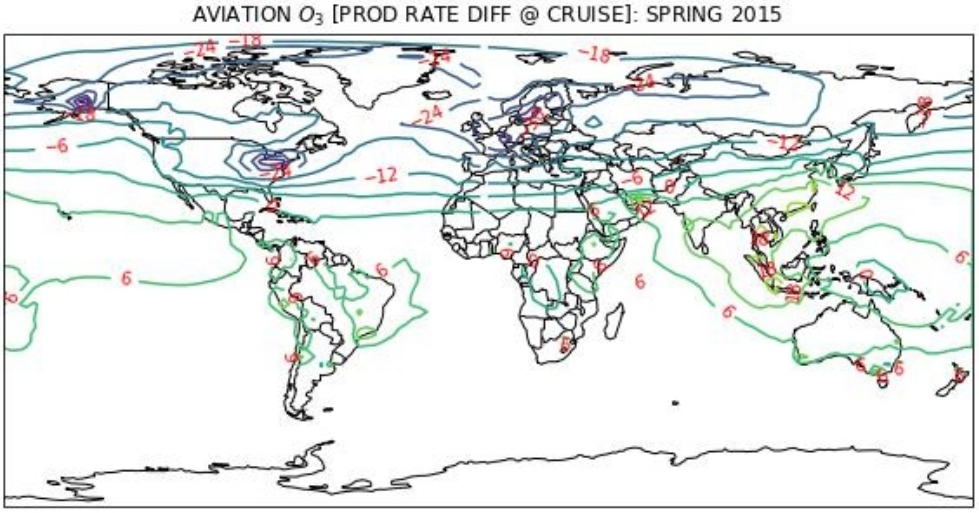

Figure 5.14: Percentage difference between Perturbation and Tagging method estimations for tropospheric O_3 production rate, due to aviation emissions in the cruise altitude range 8 to 12 km, in Spring.

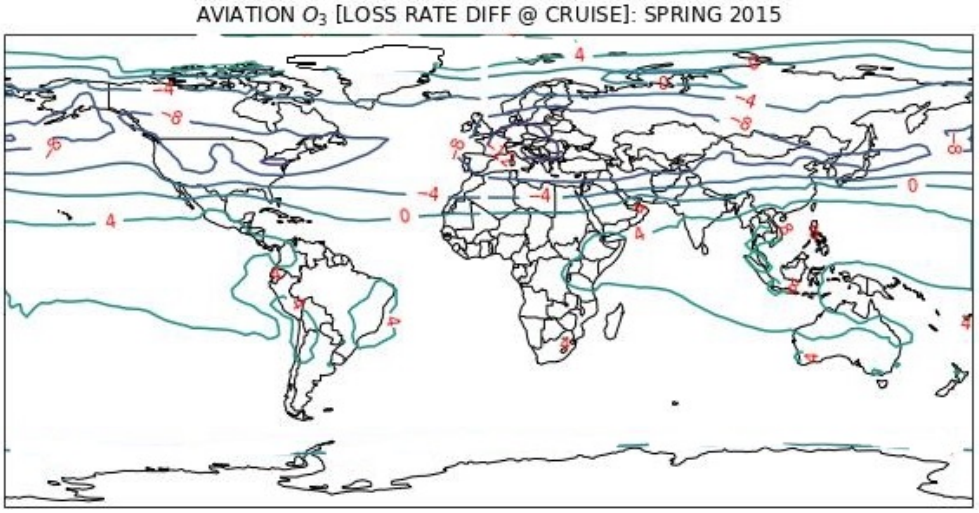

Figure 5.15: Percentage difference between Perturbation and Tagging method estimations for tropospheric O_3 loss rate, due to aviation emissions in the cruise altitude range 8 to 12 km, in Spring.

An underestimation of O_3 production rate implies that the rate of reactions 2.5 to 2.7 (i.e, the rate at which the NO_x is oxidized and eventually transformed to O_3) is underestimated by the corresponding methodology. From equation 2.5, it is clear that HO_2 is needed to oxidize the NO, where HO_2 in turn is involved in a chemical cycle starting with OH (equations 2.1 to 2.4). This implies that an underestimation in the atmospheric rate of oxidation by OH (whereby OH reaction chain eventually forms HO_2 and transforms NO to NO_2 and then to O_3) is the factor responsible for the underestimation of O_3 production rate. Similarly in the case of an overestimation of the O_3 production rate, it effectively translates to the concerned methodology overestimating the atmospheric oxidation capacity. Therefore according to the calculated differences between Perturbation & Tagging results for O_3 production rate in the Northern Hemisphere, it can be concluded that the Perturbation method underestimated the

atmospheric oxidation capacity in the Northern Hemisphere.

As for the Southern Hemisphere the aviation O_3 production rate was overestimated by Perturbation (around 6.32% higher) which dominated the 3.73% overestimation of the aviation O_3 loss rate. This is why aviation O_3 VMR was overestimated by Perturbation method, as can be seen in figure 5.8. Just as in the Northern Hemisphere, these results for the Southern Hemisphere can be extrapolated to conclude that Perturbation method overestimated the reaction rates (2.5) to (2.7). This overestimation in oxidation capacity by the Perturbation method, is what led to a subsequent overestimation of the O_3 production rate and finally the resulting O_3 VMR itself.

Furthermore, figure 5.14 also depicts a gradual northwards increase in the underestimation of aviation O_3 production rate by Perturbation method. This effectively implies that the Perturbation method's underestimation of atmospheric oxidation capacity (with respect to Tagging) becomes more pronounced towards polar latitudes as compared to tropics.

Therefore, the underestimation and/or overestimation of the atmospheric oxidation capacity by the Perturbation method (as compared to Tagging) is the reason behind the trend obtained for methodological differences in the prediction of O_3 production rate (figure 5.14) & eventually O_3 VMR (figure 5.8). Although figures 5.14 and 5.8 correspond to Spring, same argument holds for the other seasons owing to the similar trends in O_3 production rates and O_3 VMR (refer Appendix C).

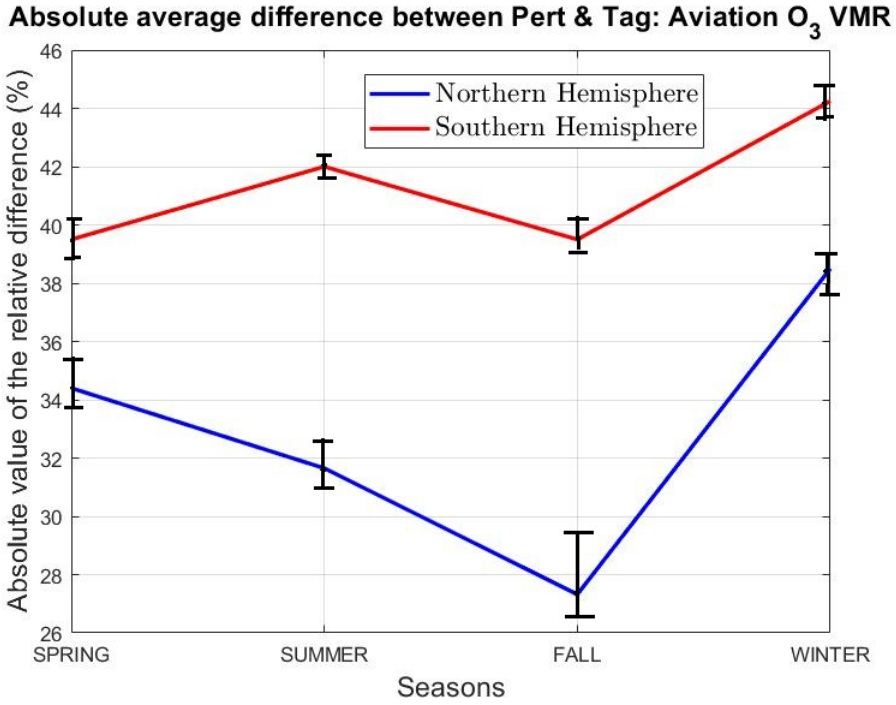

Figure 5.16: Absolute values of the relative differences between Perturbation and Tagging methods' estimations of aviation O_3 VMR across different seasons, for both the Northern & Southern Hemispheres. The vertical lines (colored in black) corresponding to the seasonal values represent 95% confidence interval (see Section 6.1).

Among all the seasons, Winter registered the largest absolute value of the relative differences between Perturbation Tagging estimations for aviation O_3 VMR, as depicted in figure 5.16. This is owing to that Perturbation's estimation of aviation O_3 production rate & loss rate was the most deviant from Tagging results in the Winter (for the rest of the seasons, refer to figures C.7, C.8, C.9 and C.10 in Appendix C). Figure 5.17 depicts upto 40% underestimation in O_3 production rate by Perturbation in the Northern Hemisphere. This implies that among all the seasons, Winter registered the greatest difference in the estimations of atmospheric oxidation capacity produced by Tagging & Perturbation methods.

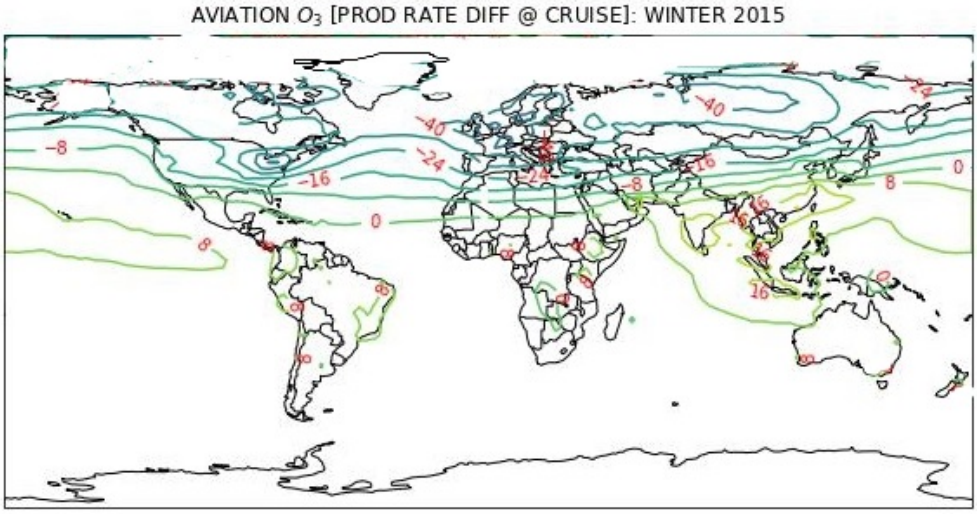

Figure 5.17: Percentage difference between Perturbation and Tagging method estimations for tropospheric O_3 production rate, due to aviation emissions in the cruise altitude range 8 to 12 km, in Winter.

	Spring	Summer	Fall	Winter
North Hemisphere	1.52	1.46	1.38	1.63
South Hemisphere	0.72	0.70	0.72	0.70

Table 5.1: Conversion factor 'x' between Perturbation & Tagging estimates of O_3 VMR, where $PERT \cdot x = TAG$ (this relation is the result of a simple mathematical rearrangement of equation 4.6).

Table 5.1 presents some additional information on the differences between the 2 methodologies. If one was to simply quantify the aforementioned methodological difference by a single parameter, that could be x, where x when multiplied to the Perturbation method's estimate (for aviation-contributed O_3 mixing ratio) gives the corresponding value for Tagging. From the values in table 5.1, x reported for Winter in the Northern Hemisphere is the highest amongst all the seasons owing to the previous observation from figure 5.16 that Winter registered the greatest absolute value of the differences between Perturbation & Tagging estimates for aviation O_3 VMR.

The last essential point of discussion is with respect to the reported inter-hemispherical differences between the Perturbation & Tagging results from the climate-chemistry simulations. Figures 5.8, 5.14 and 5.15 (for rest of the figures, see Appendix C) show an underestimation of the corresponding parameters for aviation O_3 by Perturbation method with respect to Tagging, in the Northern Hemisphere. Whereas for the Southern Hemisphere, it is a case of overestimation of the aviation O_3 presence by Perturbation with respect to Tagging. This is a consequence of the relationship between the tropospheric mixing ratio of O_3 and the corresponding NO_x emission level.

Grewe *et al.* 2010 investigated the NO_x-O_3 relationship and their reported trend is shown in figure 5.18. Figure 5.18(b) depicts the scenario of a linear chemistry where both the Tagging estimate (shown by the dotted line) & Perturbation estimate (shown by the green line) match with each other. But as the NO_x emission (along x-axis) increases and the chemistry considered is non-linear (see figure 5.18(d)), the slope of the green line (which is the Perturbation estimate for O_3) becomes lesser than that of the dotted line (Tagging estimate for O_3). This is the case reported in the Northern Hemisphere results presented earlier in this Section 5.2. Now if one were to move extreme left along the x-axis of figure 5.18(d), i.e., if NO_x emissions were to reduce significantly, the slope of the green line would slightly exceed that of the dotted line. This means that for low NO_x emissions, the Perturbation method's estimate for O_3 would slightly exceed the corresponding estimate obtained through Tagging. As per figure 5.1 and rest of the figures pertaining to NO_x VMR in Appendix B, it is evident that the resulting VMR of NO_x in the Southern Hemisphere is significantly lesser than that in the Northern Hemisphere. This implies that the NO_x emission from global aviation is lower in the Southern Hemisphere than the North,

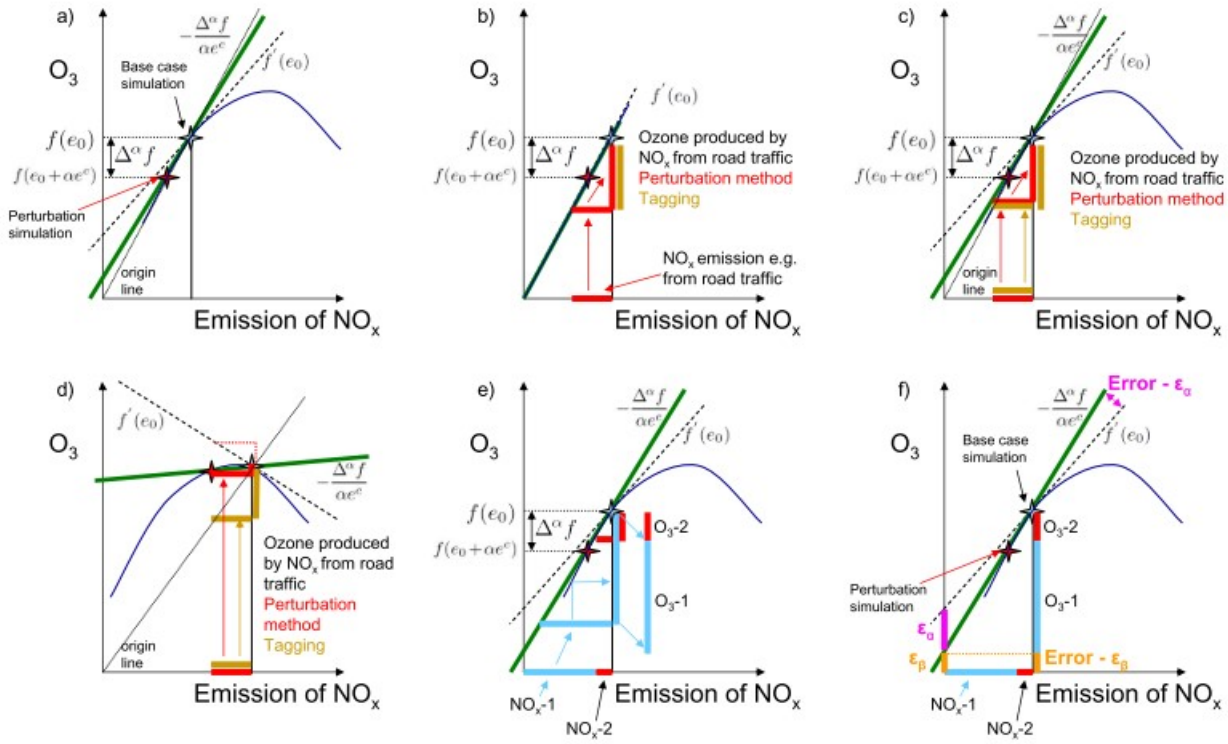

Figure 5.18: Illustration of the perturbation method to derive contributions from emission categories and inter-comparison with the tagging method. The O_3 concentration in arbitrary units is shown as a function of the NO_x emission. Two simulations (base case and a simulation in which the emissions is changed by a factor α; see Section 2.3.2) are indicated with stars. The derivative is added as a tangent for the base case (dashed line). The line through the base case simulation and the origin (origin line) is dotted. The green line shows the estimated derivative, based on the two simulations. (a) General settings and calculation of the derivative. (b) Assumption of linearity in O_3 chemistry for illustration purpose. An arbitrary NO_x emission (horizontal red line) is considered. The vertical red and brown lines indicate the O_3 contributions caused by this NO_x source (sensitivity method in red and tagging in brown) giving identical results. (c) As (b) but for the assumption of a non-linear O_3 chemistry, however in a situation, which is close to the linear case. The green and dotted lines are used to calculate the contributions based on the sensitivity and tagging method, respectively. (d) As (c), but for a situation, which is far from the linear regime. (e) Calculation of the ozone contributions; two emission categories are considered (NO_x-1: light blue, NO_x-2: red) and the ozone contributions O_3-1 and O_3-2 indicated with vertical lines. (f) Error analysis; the two errors ϵ_α (magenta) and ϵ_β (orange), which describe uncertainties associated with the determination of the tangent and the total estimate of all contributions (intersection of y-axis and tangent). The origin line for tagging represents the equality of all emitted NO_x molecules to take part in a reaction, which implies that a subset of NO_x molecules, e.g. from the source category “road traffic”, produces a sub-set of O_3 molecules in a linear relationship (= origin line) for a non-linear chemistry (blue line) [Grewe *et al.* 2010].

which then causes the Perturbation method to slightly overestimate aviation O_3 VMR as compared to the Tagging method. Therefore, it was concluded that in addition to the methodological differences in estimation of the oxidation capacity of the atmosphere, the level of NO_x emission from global aviation is also responsible for the subsequently obtained differences in the estimation of aviation-contributed O_3 mixing ratio using the Perturbation & Tagging methods.

6

Uncertainties in the research

Any kind of research, irrespective of the concerned domain, comes with its own range of uncertainties. This is owing to the fact that any hypothesis, or research goal(s), require certain assumptions to be made before actual work and analysis can commence. These assumptions are generally done to simplify the research methodology and/or the research goals, thereby rendering the respective results with a certain amount of uncertainties. Furthermore, statistical uncertainties might be induced in the concerned mathematical calculations contributing to additional uncertainties. Research results are therefore mostly only a representative of the corresponding scenario in real-life and never 100% accurate. Although the best results can always be ensured with minimal and/or well founded assumptions, among many other factors.

6.1. Uncertainties: Statistical

In order to ensure that the data presented and discussed in Chapter 5 can be usefully interpreted for conclusions regarding aviation's contribution to tropospheric NO_x and O_3 mixing ratios, the calculated data were subjected to a 2-tailed t-test (degrees of freedom = 4) with 95% confidence.

The confidence intervals represented in figures 5.5, 5.6 and 5.16 depict statistical range of uncertainty induced in the corresponding results. As mentioned in Section 4.2, the climate-chemistry simulations were performed for 5 meteorology years (2013 to 2017), therefore the 5-year average data presented for every season in figures 5.5, 5.6 and 5.16 were analyzed for their respective uncertainty ranges to indicate the upper and lower bounds for their variation.

The longitude v/s latitude representations of Perturbation-Tagging relative differences in estimation of NO_x and O_3 VMR (figures 5.7, C.1, C.2, C.3, 5.8, C.4, C.5 and C.6) have also been equipped with information on statistical uncertainty. These Perturbation-Tagging relative differences were also averaged over 5 years (2013 to 2017), hence the grid points representing statistically insignificant data were distinguished from their significant counterparts (refer to the respective figure captions).

6.2. Uncertainties: Atmospheric Chemistry

Since the research done as part of this thesis deals with the study of aviation's contribution to the NO_x and O_3 VMR in the troposphere, one of the fundamental components of this research is the atmospheric chemistry scheme which was assumed or considered in order to analyze the results in Chapter 5. As explained earlier in Section 2.1, the chemistry describing the production of radicals such as RO_2 and HO_2, and the subsequent production of O_3, is pretty complex and was "simplified" to the equation scheme (2.1)-(2.7).

As per Lin *et al.* 1988, the uncertainties induced by the understanding of atmospheric chemistry are a challenge to quantify, but nevertheless must be understood in order to assess aviation's contribution

to tropospheric mixing ratios of NO_x and O_3. Lin *et al.* 1988 noted that both the O_3 production and the loss of NO_x keep on changing with the atmospheric availability of NO_x & the composition and abundances of the other O_3 precursors, such as hydrocarbons. However as per Liu *et al.* 1987, both O_3 production and NO_x loss register quite similar rates and tend to almost cancel each other, thereby reducing the uncertainty in the estimated total regional O_3 production by a significant amount.

The significant uncertainties in the understanding and subsequent treatment of this atmospheric chemistry was examined by Lin *et al.* 1988. This was done by examining the effects on NO_x-O_3 non-linearity due to two major uncertainties in the chemistry, namely, combination reactions of RO_2 with HO_2 (lowest order of which is shown in reaction 6.1) and the night-time loss of NO_x (whereby NO_2 is first converted to NO_3, then to N_2O_5; refer to reactions 6.3 and 6.4).

$$HO_2 + RO_2 \rightarrow ROOH + O_2 \tag{6.1}$$

In their "baseline runs" of model, combination reactions of RO_2 with HO_2 were included. These reactions were expected to cause a significant change in concentrations of HO_2 and RO_2 radicals (both being precursors of O_3) and hence the O_3 production. However, reaction rates and products formed out of these recombination reactions were quite uncertain, therefore a standard reaction of HO_2 with CH_3O_2 was considered for reaction 6.1, wherein the standard reaction rate values for all the re-combinations of RO_2, HO_2 were obtained from DeMore *et al.* 1983 and Atkinson and Lloyd 1984. As for the reaction products, CH_3OOH was primarily assumed as the surrogate.

	Baseline Run	excl. reactions of RO_2 + HO_2	incl. $PAN - NO_x$ exchange
For NO_x = 0.1 ppbv			
O_3 production	1.89 x10^{11}	2.40 x 10^{11}	2.29 x 10^{11}
O_3 loss	1.21 x10^{11}	1.32 x 10^{11}	1.61 x 10^{11}
O_3 net production	6.79 x 10^{10}	1.08 x 10^{11}	6.78 x 10^{10}
NO_x loss	2.87 x 10^{9}	2.88 x 10^{9}	2.86 x 10^{9}
OH	4.63 x 10^{6}	4.42 x 10^{6}	4.63 x 10^{6}
HO_2	6.13 x 10^{8}	7.20 x 10^{8}	6.13 x 10^{8}
RO_2 + HO_2	1.37 x 10^{9}	1.93 x 10^{9}	1.37 x 10^{9}
For NO_x = 1 ppbv			
O_3 production	1.59 x 10^{12}	1.71 x 10^{12}	2.14 x 10^{12}
O_3 loss	2.71 x 10^{11}	2.94 x 10^{11}	8.36 x 10^{11}
O_3 net production	1.32 x 10^{12}	1.42 x 10^{12}	1.30 x 10^{12}
NO_x loss	5.72 x 10^{10}	5.95 x 10^{10}	5.72 x 10^{10}
OH	8.06 x 10^{6}	8.24 x 10^{6}	8.06 x 10^{6}
HO_2	8.96 x 10^{8}	9.85 x 10^{8}	8.93 x 10^{8}
RO_2 + HO_2	1.55 x 10^{9}	1.74 x 10^{9}	1.54 x 10^{9}
For NO_x = 10 ppbv			
O_3 production	9.67 x 10^{12}	1.01 x 10^{13}	2.02 x 10^{13}
O_3 loss	1.87 x 10^{12}	2.00 x 10^{12}	1.28 x 10^{13}
O_3 net production	7.83 x 10^{12}	8.07 x 10^{12}	7.41 x 10^{12}
NO_x loss	6.89 x 10^{11}	7.12 x 10^{11}	6.91 x 10^{11}
OH	8.22 x 10^{6}	8.46 x 10^{6}	8.24 x 10^{6}
HO_2	1.34 x 10^{9}	1.44 x 10^{9}	1.33 x 10^{9}
RO_2 + HO_2	2.45 x 10^{9}	2.62 x 10^{9}	2.41 x 10^{9}

Table 6.1: Comparison for 24-hour accumulated O_3 Production, O_3 Loss, NO_x loss, along with concentrations of OH, HO_2, and RO_2 + HO_2 for several NO_x levels, for 3 kind of runs: Baseline, one excluding recombination reactions of RO_2+HO_2 and one including $PAN - NO_x$ exchange; Production & loss terms are expressed in units of $cm^{-3}s^{-1}$ [Lin *et al.* 1988].

To clearly examine the effect of these combination reactions on the NO_x-O_3 chemistry, Lin *et al.* 1988 ran their model excluding the combination reactions of HO_2 and RO_2, the corresponding results of which have been shown in Table 6.1. In addition to the recombination reactions, Lin *et al.* 1988 investigated the impact of 'PAN-NO_x exchange' reactions on the species' concentrations and production, loss magnitudes. A possible reaction pathway exists where NO_x can get converted to inactive forms, such as peroxyl nitrate (PAN), that do not produce O_3 directly. PAN is produced through the reaction:

$$CH_3COO_2 + NO_2 + M \rightarrow PAN + M \tag{6.2}$$

At room temperature the reverse reaction is efficient enough to ensure that PAN and NO_2 are in equilibrium. PAN may serve as a temporary storage and a carrier of NO_x into the more remote troposphere [Crutzen 1979; Singh *et al.* 1985].

It is clear from a close examination of the shown results that not accounting for HO_2-RO_2 reactions increased the total concentrations of peroxy radicals, by a greater quantity at low atmospheric NO_x levels. At these levels, the combination reactions compete with reactions of the peroxy radicals and NO_x in converting the radicals [Carter *et al.* 1979]. The net-O_3 production (photo-chemical O_3 production minus loss of O_3) was observed to increase noticeably only for NO_x levels $\leq$ 1 ppbv when the RO_2 + HO_2 combination reactions were removed, as opposed to only a slight change for $NO_x \geq$ 10 ppbv. Therefore, it was concluded by Lin *et al.* 1988 that accounting for the combination reactions of HO_2 + RO_2 in the CCM reduced the non-linearity in the O_3 production due to NO_x.

In addition to the recombination reactions of RO_2 + HO_2 , significant uncertainty arises in the atmospheric chemistry due to the night-time chemistry that NO_x undergoes:

$$NO_2 + O_3 \rightarrow NO_3 + O_2 \tag{6.3}$$
$$NO_2 + NO_3 + M \rightarrow N_2O_5 + M, \tag{6.4}$$

which is then followed by the thermal decomposition of N_2O_5 as:

$$N_2O_5 + M \rightarrow NO_2 + NO_3 + M \tag{6.5}$$

Monitoring of NO_3 concentrations at night have indicated in the past that there might be additional significant loss of NO_x owing to more reactions involving NO_3 or N_2O_5 [Platt *et al.* 1984; Noxon 1983]:

$$NO_3 + X \rightarrow Products \tag{6.6}$$
$$N_2O_5 + Y \rightarrow Products, \tag{6.7}$$

where X and Y represent unspecified reactants and may be anything within the umbrella containing propene, acetaldehyde, aerosols, clouds, and dew droplets [Ehhalt and Drummond 1982; Platt *et al.* 1984]. Clearly, inclusion of the NO_x night-time chemistry would only serve to augment the loss of NO_x. But doing so would also lead to O_3 destruction through reactions 6.3 and 6.4, thereby decreasing the net O_3 production.

NO_x (ppbv)	Composn. A	Composn. B	Composn. C
0.1 (with night-time NO_x loss)	12.73	13.52	14.93
1 (with night-time NO_x loss)	11.50	12.70	15.72
10 (with night-time NO_x loss)	2.29	2.49	2.57
0.1 (without night-time NO_x loss)	22.21	23.66	26.99
1 (without night-time NO_x loss)	20.08	23.12	33.46
10 (without night-time NO_x loss)	9.12	11.41	16.22

Table 6.2: 24-hour averaged O_3 Production Efficiency (mol/mol) calculated with and without additional loss of NO_x during night-time for 3 different kinds of atmospheric NMHC compositions (refer to Section 2.2 for their definitions) at various NO_x Levels [Lin *et al.* 1988].

Table 6.2 depicts the difference in O_3 production efficiency for 3 atmospheric models with different background $NMHC$ compositions (refer to Section 2.2 for the definition of these $NMHC$ compositions). Here the definition of O_3 production efficiency has been used of the one provided by Liu *et al.* 1987 as being the number of O_3 molecules produced for each molecule of NO_x consumed. Appreciable reductions were registered in this efficiency after accounting for the night-time chemistry of NO_x leading to its increased loss.

Among several effects of NO_x emissions, there are also a couple of more short-term ones involving the direct formation of nitrate aerosol and indirect enhancement of sulfate aerosol. These effects have been studied in a few modelling studies already and contribute large uncertainties of their own to the atmospheric NO_x chemistry [Righi *et al.* 2013; Pitari *et al.* 2017; Unger 2011]. Therefore, from all the above explained theory in this section, it is clear that significant uncertainties can be induced in the aviation NO_x-O_3 research from the way atmospheric chemistry is understood and implemented in the climate-chemistry simulations.

7

Conclusion

In the modern world, aviation has emerged as one of the most important global economic activities, responsible for transporting bulk of cargo and passengers across several continents. As pointed out in Chapter 1, both CO_2 and non-CO_2 emissions from aircraft lead to significant changes in the Earth's climate system. The combined effect of both aviation CO_2 and sum of non-CO_2 contributions is the warming of Earth's surface [D. S. Lee *et al.* 2021; IPCC 1999]. These contributions to climate change from aviation involve a wide range of atmospheric physical processes, including plume dynamics, chemical transformations, micro physics, radiation, and transport [D. S. Lee *et al.* 2021]. All of these processes when analyzed together, assists in the calculation of changes in the concentrations of greenhouse gases caused by global air traffic, which is quite a complex challenge for atmospheric modeling systems. Given the fact that aviation depends significantly on burning fossil fuels, along with all of its essential CO_2 and non-CO_2 effects, and the continuous growth of air traffic [D. S. Lee *et al.* 2021], it is vital to have as much clear of an understanding as possible with respect to aviation's emissions and their eventual consequences on the present-day climate forcing, and by extension Earth's climate in general for the upcoming years.

NO_x emissions from aviation through atmospheric chemistry (as described in Section 2.1) lead to an increase in the global O_3 concentration while also causing a decrease in the concentration of CH_4 [D. S. Lee *et al.* 2021]. Earlier studies evaluated the short-term O_3 increase effect along with the long-term CH_4 reduction, thereby yielding positive RF (warming effect) and negative RF (cooling effect), respectively [Sausen *et al.* 2005]. D. S. Lee *et al.* 2009 extended this study of Sausen *et al.* 2005 to examine the 'net NO_x' effect by combining the aforementioned two components. Since the research done by D. S. Lee *et al.* 2009, understanding of the atmospheric chemistry has improved and better modeling capabilities have emerged, along with additional RF terms in response to NO_x emissions, namely a longer-term decrease in O_3 (better known as 'primary mode ozone') and a reduction in H_2O in the stratosphere [D. S. Lee *et al.* 2021]. Both of these effects yield negative RF, or cooling effects [Holmes *et al.* 2011; Myhre *et al.* 2011].

NO_x emissions (NO + NO_2), therefore have a dual role with respect to radiative forcing and climate change. Several studies have highlighted the significance of tropospheric O_3 as a climate gas [e.g. W. C. Wang *et al.* 1980; Lacis *et al.* 1990; Hauglustaine *et al.* 1994a,b]. O_3 is a strong oxidant and has significant consequences on air quality [e.g. World Health Organization 2003; Monks *et al.* 2015]. Large concentrations of O_3 in the atmosphere impact the vegetation and cause the crop yield rates to decrease [e.g. Fowler *et al.* 2009; Mauzerall and X. Wang 2001]. Furthermore, O_3 is radiatively active and thus contributes to global warming [e.g. Stevenson *et al.* 2006]. Therefore, this thesis focused on analysis of aviation's contribution to tropospheric NO_x and the corresponding tropospheric O_3 contribution.

In order to answer the research questions laid down in Chapter 3, two major aspects were studied in this thesis:

1. Seasonal & Zonal patterns of aviation's contribution to atmospheric mixing ratios of NO_x and O_3, and
2. Comparison of the 2 methodologies ('PERTURBATION' & 'TAGGING') in their estimations of aviation's contribution to tropospheric NO_x and O_3 mixing ratios

The climate-chemistry simulation analyses results presented in Chapter 5 put forth interesting insights into the impact of global air traffic on the tropospheric presence of two species essential for evaluating climate change: NO_x and O_3. From the perspective of global aviation emitting nitrogen oxides into the atmosphere, it was seen that throughout all the seasons, Western Europe and the USA (both its Eastern & Western coastal regions) emerged as regions with the most significant accumulation of NO_x (annual average = 30 $pptv$).

In order to facilitate the chemical transformation of aviation-accumulated NO_x to corresponding O_3, the oxidation capacity of the atmosphere was analyzed by studying two vital O_3 precursors: OH and HO_2 radicals, for their tropospheric availability across seasons and zones. As predicted by previous research studies, OH radicals were found to be the most abundant over the tropical regions, implying increased photo-chemistry in those regions as compared to the polar regions. Following along the lines of the former, the HO_2 radicals too depicted a similar significant presence closer to the tropical regions, implying a higher oxidation capacity in the tropics as compared to polar latitudes. Accordingly, the Western coasts of South America and Africa along with the Indian subcontinent were identified as hotspots for these O_3 precursors.

Keeping in line with the aforementioned observations, the tropospheric mixing ratio of O_3 induced by global aviation, was predominantly found to be accumulated over tropical regions and mid-latitudes. A peak O_3 belt presence (with an annual average = 1.57 $ppbv$) was registered over North-Western China, Middle East & Africa. The Western Coast of USA was another notable aviation O_3 hotspot. A comparison study of the seasons in the Northern Hemisphere revealed that Summer & Fall were the ones with the highest contribution of aviation to the mass of atmospheric NO_x. Whereas for the Southern Hemisphere, Summer was found to be the season witnessing lowest contribution from aviation to atmospheric mixing ratios of NO_x, leading to an equivalent minima in the corresponding O_3 per unit NO_x. But another important reason was the lower incident solar energy implying lesser photo-chemistry (lesser mixing ratios of OH and HO_2), leading to lower oxidation capacity of the Southern Hemisphere's atmosphere in Summer as compared to Fall & Winter. Therefore, it was concluded that a chemical transformation of aviation-induced NO_x into O_3 is a function of the atmospheric availability of OH and HO_2 radicals. In other words, the atmospheric background mixing ratios of OH and HO_2 are the controlling factors behind aviation's contribution to the effective O_3 mixing ratio.

The second part of the thesis was focused on analyzing the differences between Perturbation & Tagging methodologies, from the perspective of aviation's contribution to atmospheric mixing ratios of NO_x and O_3. A comparison of both the methods' estimates for aviation-induced NO_x mixing ratio revealed only minor differences with a maximum level of 5%. Since literature suggested that Tagging & Perturbation results are similar for linear chemistry, the calculated results implied that aviation NO_x emission & resulting mixing ratio in the atmosphere followed a linear relationship. Further, it was concluded that NO_x contributed only marginally to the non-linear characteristic of aviation NO_x-O_3 chemistry.

As for the aviation O_3 mixing ratios, significant differences ranging from 15% to around 60% were calculated between Perturbation & Tagging's results. These differences were traced back to the estimates for O_3 production and loss rates, provided by Perturbation method. It turned out that Perturbation method significantly underestimated (average = 14%) aviation's O_3 production rate in the Northern Hemisphere, while overestimating the corresponding values in the Southern Hemisphere. A similar pattern was calculated for aviation's O_3 loss rate, but the magnitudes of differences were far lesser than those for the production rates. This thereby rendered the differences in aviation O_3 production rate as the deciding factor of the methodological differences. Also the differences in O_3 production rate kept on increasing towards mid-latitudes and polar regions for the Northern Hemisphere, thus justifying the corresponding calculated trend for O_3 VMR. A seasonal comparison pointed out that the differences between Perturbation and Tagging methods' estimations for tropospheric O_3 rose to its highest levels in Winter.

Differences in O_3 production rate could be extrapolated to the conclusion that the oxidation capacity of the atmosphere (i.e, the rate at which the atmosphere cleanses itself of the NO_x emissions from aviation, using the available OH and HO_2 radicals) is what effectively induced differences between Perturbation & Tagging results. Furthermore, literature showed that Perturbation and Tagging's estimates of tropospheric O_3 presence are dependent on the NO_x emission level, whereby a low NO_x emission translates into the Perturbation method slightly overestimating the O_3 mixing ratio, and vice versa. In conclusion, differences in the two methods' estimations of the atmospheric oxidation capacity, and the NO_x emission level of global aviation were found to be the reasons behind the reported differences in the results of the 2 methods when evaluating aviation's contribution to tropospheric O_3 mixing ratios.

With more insights offered into the seasonal and zonal patterns in aviation's contribution to tropospheric NO_x and O_3, along with the understanding of differences between Tagging and Perturbation methods in evaluating the aforementioned contributions, researchers can more accurately gauge the corresponding radiative forcing effects. With radiative forcing terms from aviation being updated to their most accurate representations, a better estimate can be made with respect to the warming of the Earth's surface globally. In case a significant change is recorded in the temperature response, there is a massive potential for changes to be made to existing climate change plans globally, which have been formulated based on 'current best' understanding of atmospheric chemistry and climate science.

Climate change plans, the fundamentals of which lie in the understanding of atmospheric chemistry, affect and shape the lives of billions across the world through their far-reaching social measures. These plans also possess the power to change global perspectives towards several key issues in the domain of climate change. Hence even the smallest of understandings in the source (sector) contributions to species such as NO_x and O_3 can go a long way in changing the perspective of the world towards a sector as important as aviation.

A

Aviation NO_x-O_3 chemistry species' behavior across altitude

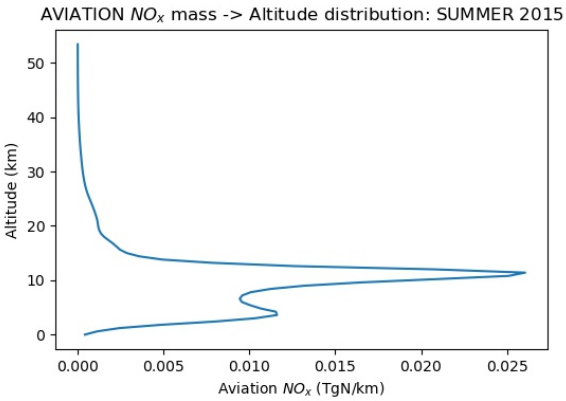

Figure A.1: Altitude distribution of aviation contribution to NO_x mass in Summer

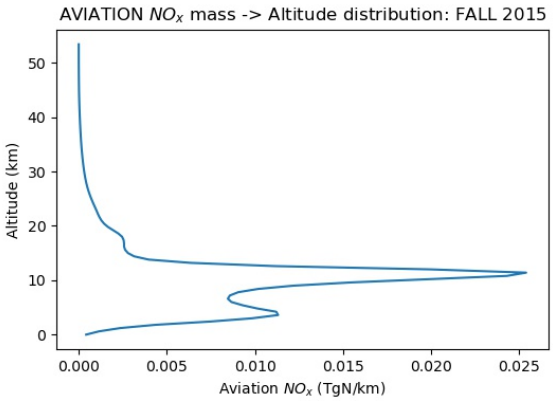

Figure A.2: Altitude distribution of aviation contribution to NO_x mass in Fall

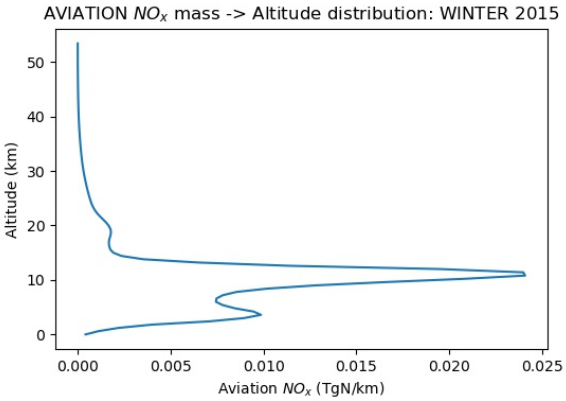

Figure A.3: Altitude distribution of aviation contribution to NO_x mass in Winter

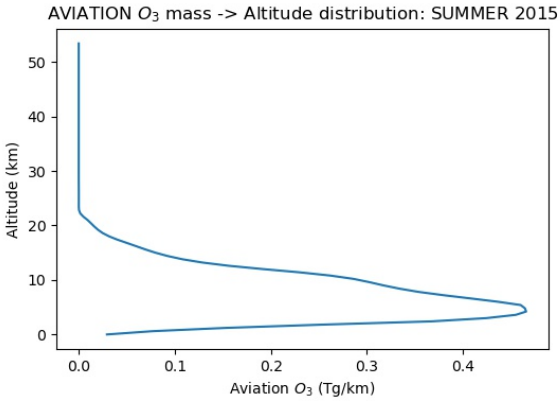

Figure A.4: Altitude distribution of O_3 mass due to aviation, in Summer

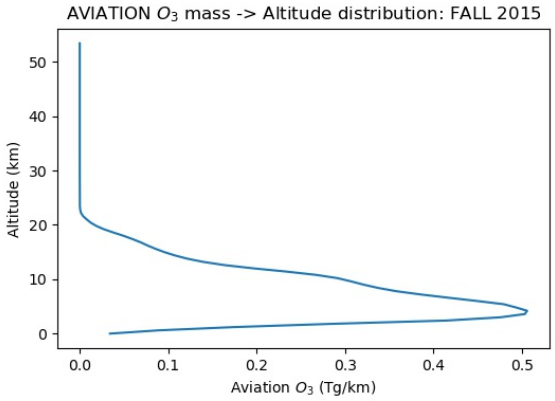

Figure A.5: Altitude distribution of O_3 mass due to aviation, in Fall

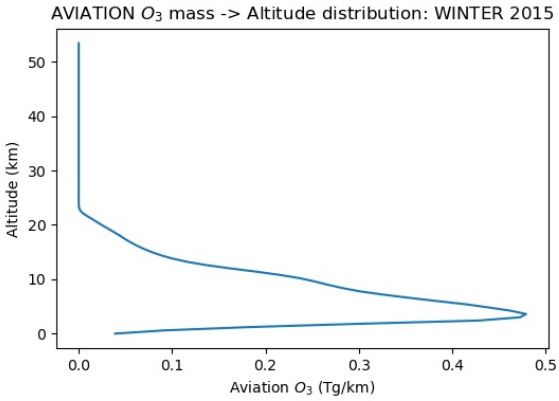

Figure A.6: Altitude distribution of O_3 mass due to aviation, in Winter

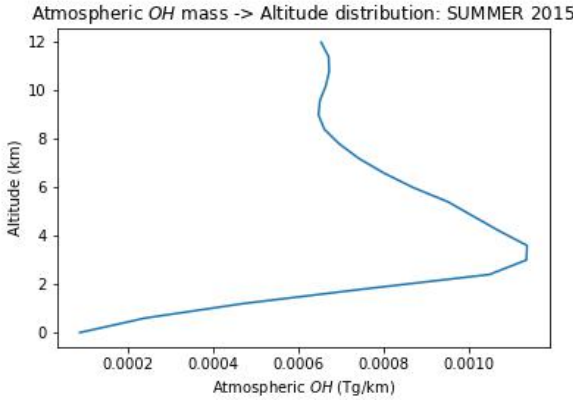

Figure A.7: Altitude distribution of background OH mass in Summer

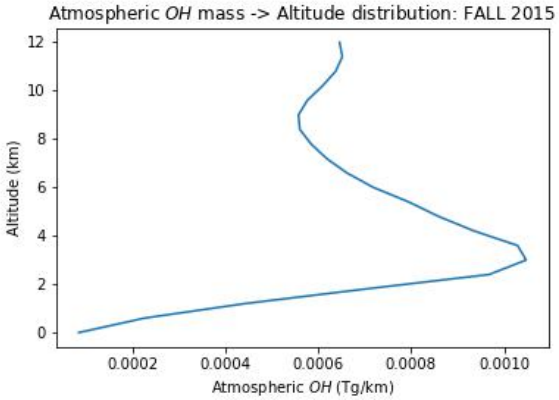

Figure A.8: Altitude distribution of background OH mass in Fall

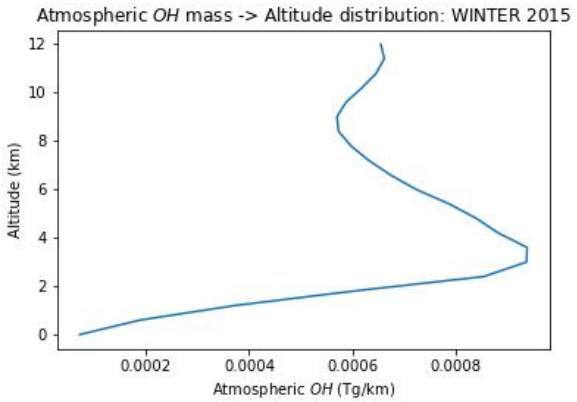

Figure A.9: Altitude distribution of background OH mass in Winter

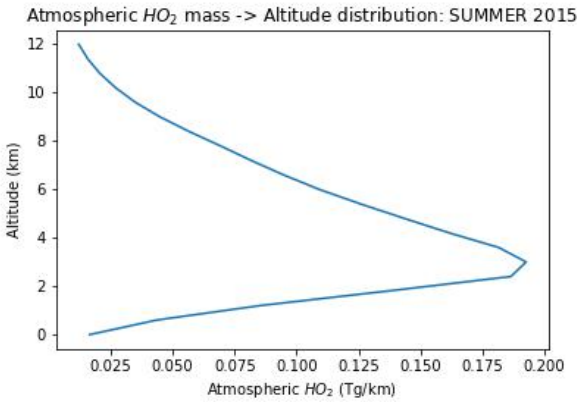

Figure A.10: Altitude distribution of background HO_2 mass in Summer

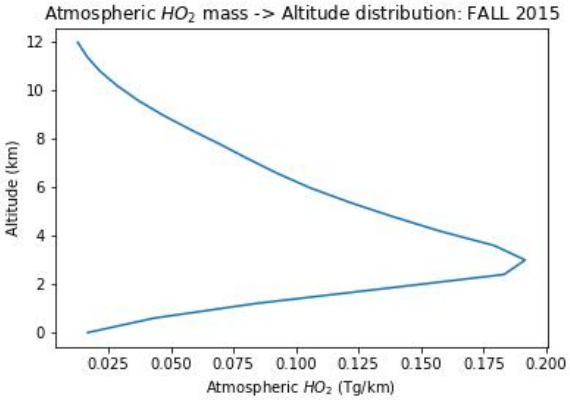

Figure A.11: Altitude distribution of background HO_2 mass in Fall

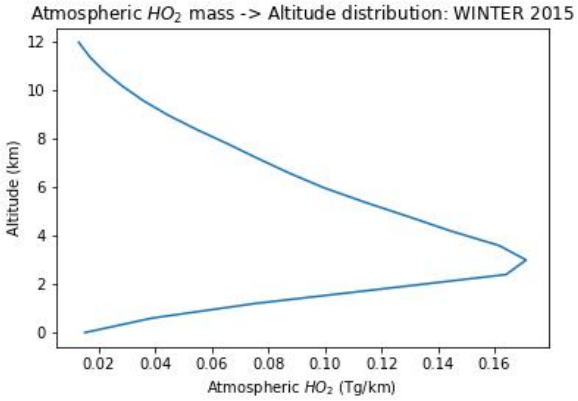

Figure A.12: Altitude distribution of background HO_2 mass in Winter

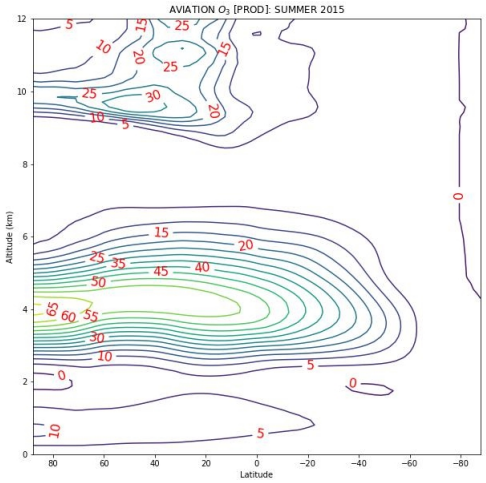

Figure A.13: Vertical distribution of the O_3 production rate (units: x 10^{-16} $mol/mol/s$) due to aviation, in Summer

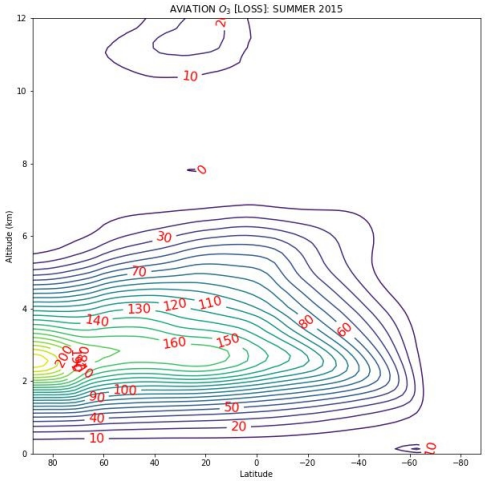

Figure A.14: Vertical distribution of the O_3 loss rate (units: x 10^{-16} $mol/mol/s$) due to aviation, in Summer

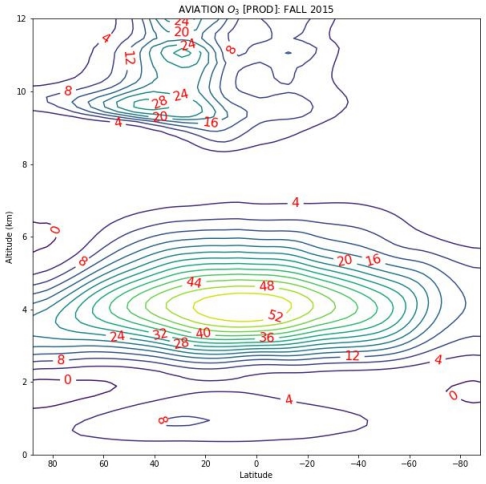

Figure A.15: Vertical distribution of the O_3 production rate (units: x 10^{-16} $mol/mol/s$) due to aviation, in Fall

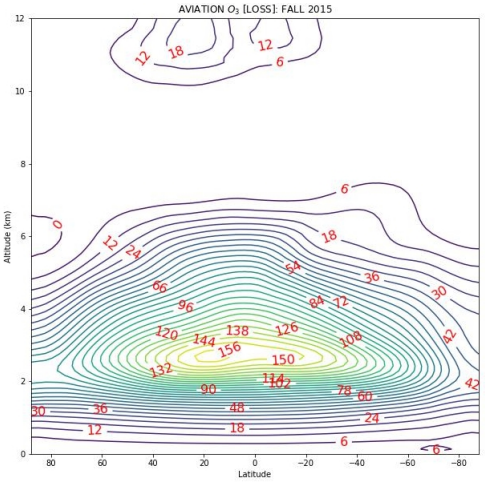

Figure A.16: Vertical distribution of the O_3 loss rate (units: x 10^{-16} $mol/mol/s$) due to aviation, in Fall

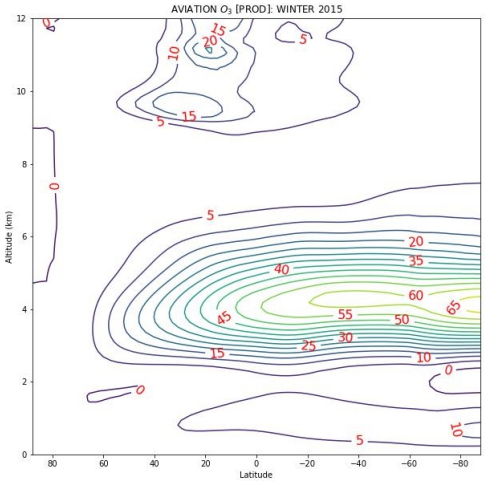

Figure A.17: Vertical distribution of the O_3 production rate (units: x 10^{-16} $mol/mol/s$) due to aviation, in Winter

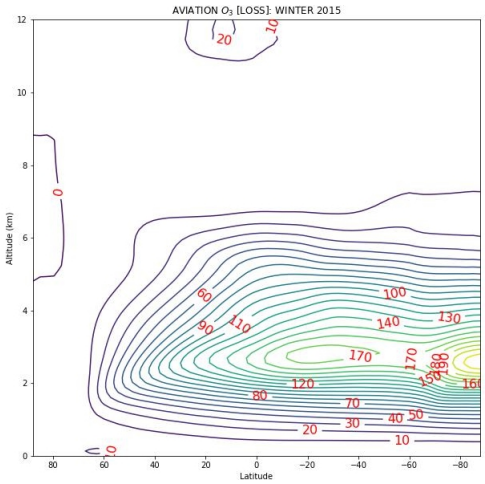

Figure A.18: Vertical distribution of the O_3 loss rate (units: x 10^{-16} $mol/mol/s$) due to aviation, in Winter

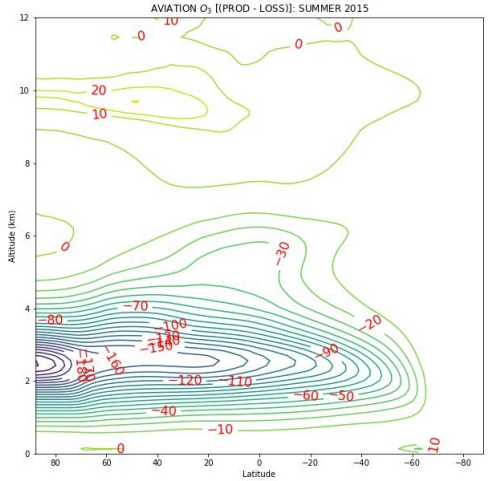

Figure A.19: Vertical distribution of the net O_3 production rate [= O_3 production rate - O_3 loss rate] (units: x 10^{-16} $mol/mol/s$) due to aviation, in Summer

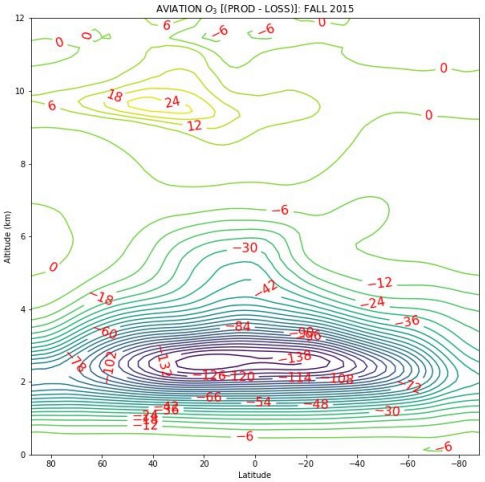

Figure A.20: Vertical distribution of the net O_3 production rate [= O_3 production rate - O_3 loss rate] (units: x 10^{-16} $mol/mol/s$) due to aviation, in Fall

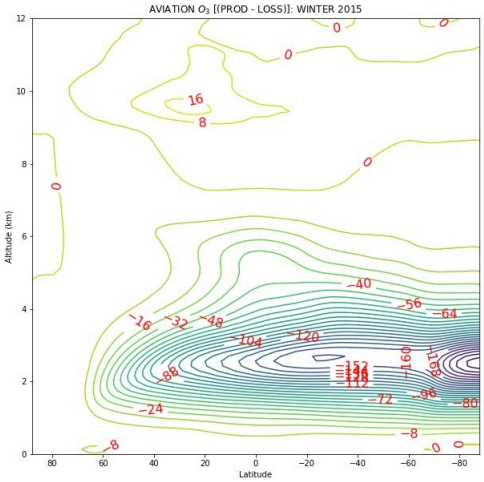

Figure A.21: Vertical distribution of the net O_3 production rate [= O_3 production rate - O_3 loss rate] (units: x 10^{-16} $mol/mol/s$)due to aviation, in Winter

B

Seasonal & Zonal behavior of the tropospheric chemical species

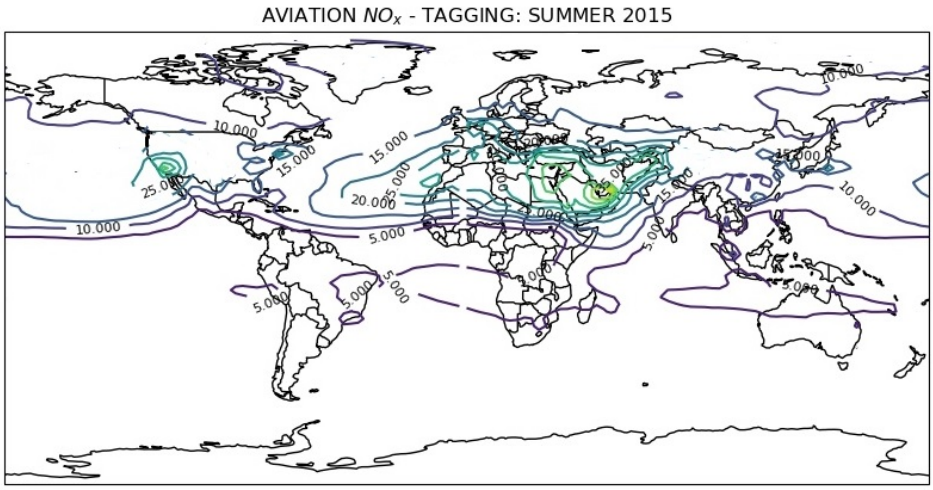

Figure B.1: Atmospheric VMR (units: $pptv$) of aviation NO_x in Summer

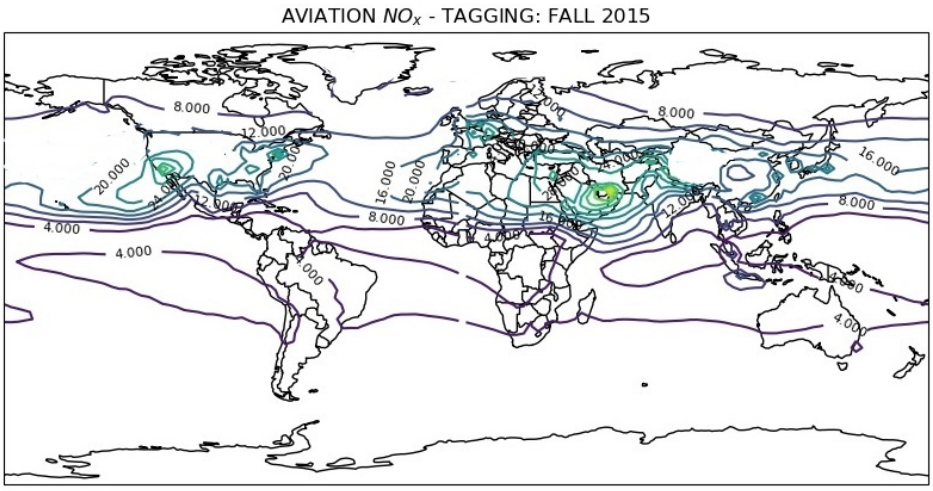

Figure B.2: Atmospheric VMR (units: $pptv$) of aviation NO_x in Fall

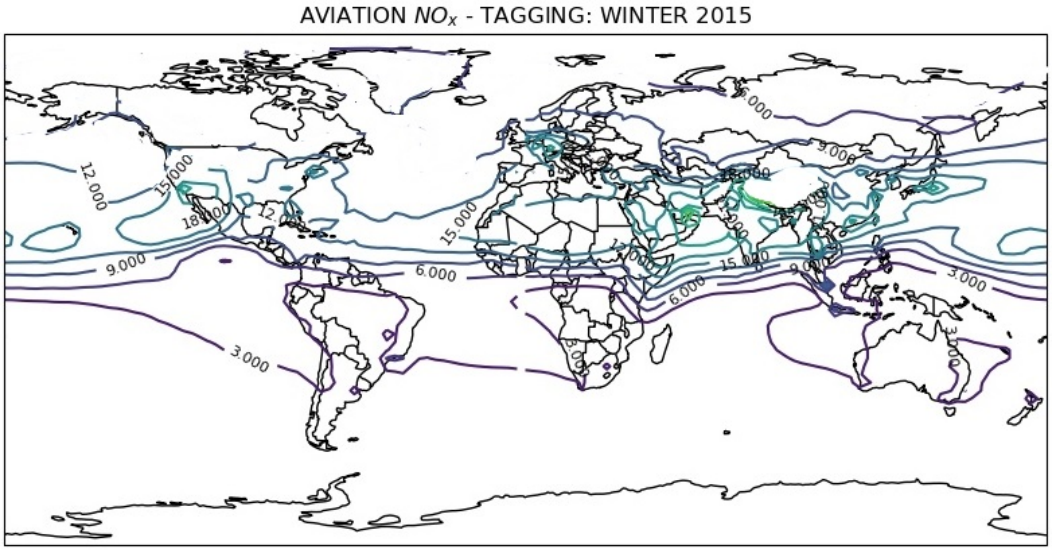

Figure B.3: Atmospheric VMR (units: $pptv$) of aviation NO_x in Winter

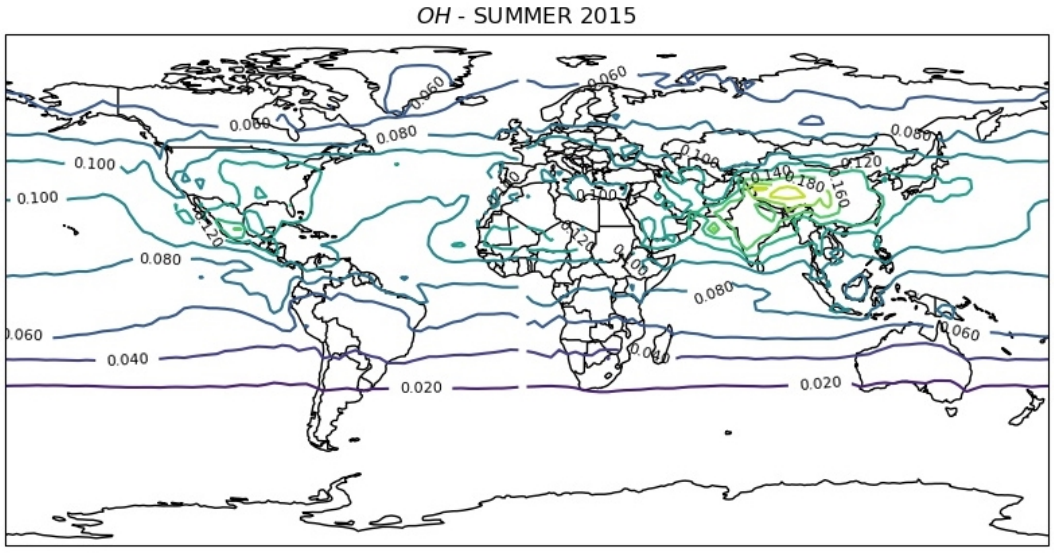

Figure B.4: VMR (units: $pptv$) of background atmospheric OH in Summer

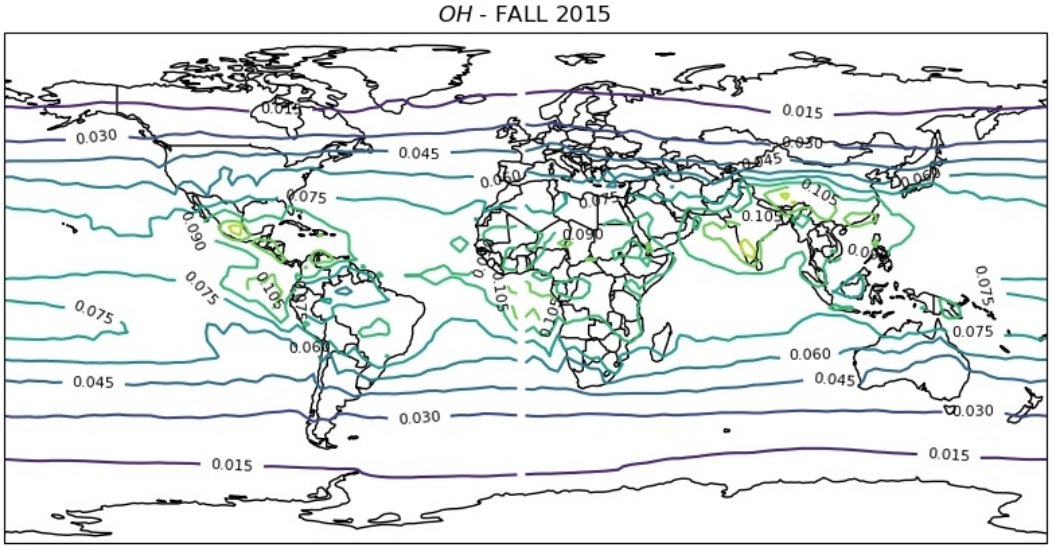

Figure B.5: VMR (units: $pptv$) of background atmospheric OH in Fall

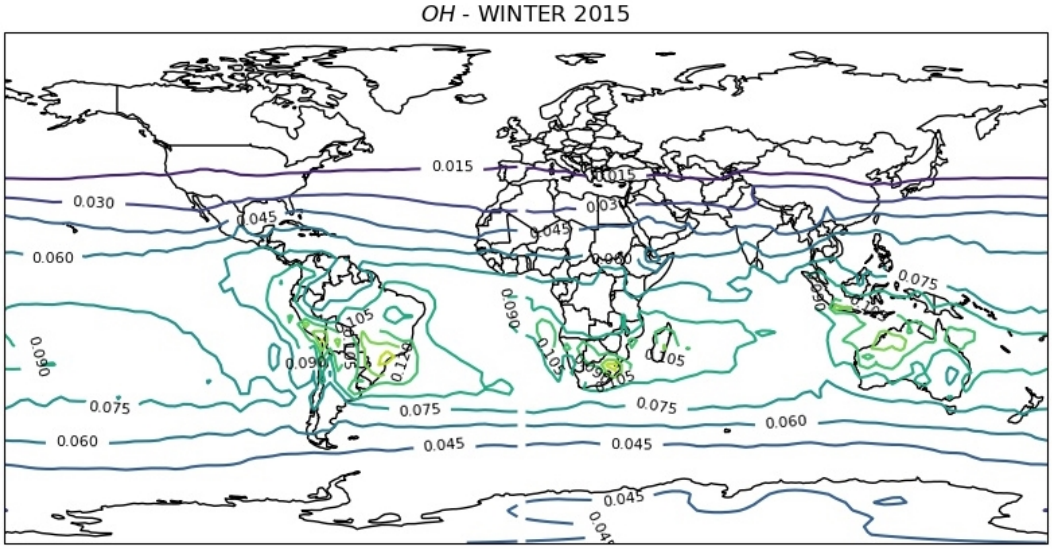

Figure B.6: VMR (units: $pptv$) of background atmospheric OH in Winter

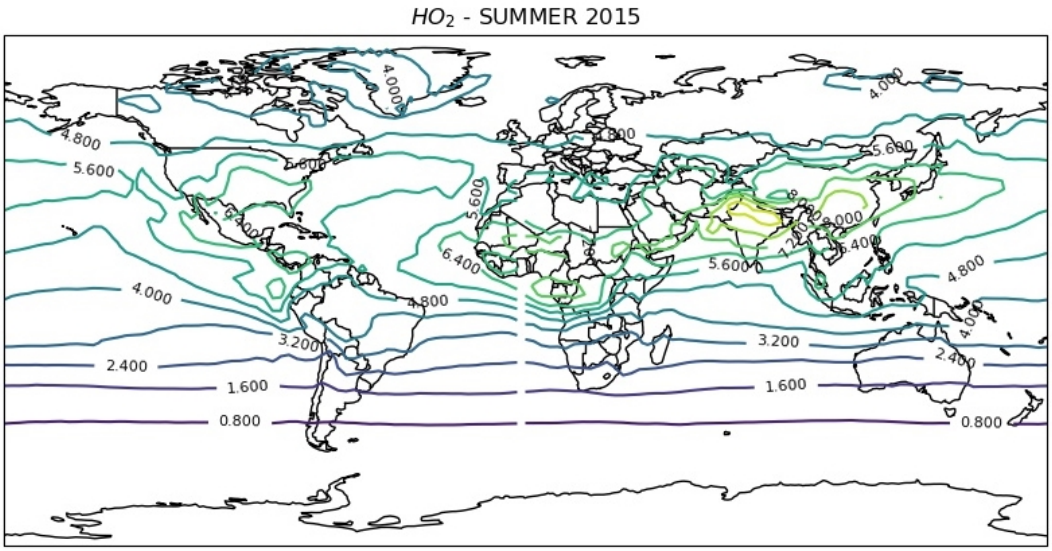

Figure B.7: VMR (units: $pptv$) of background atmospheric HO_2 in Summer

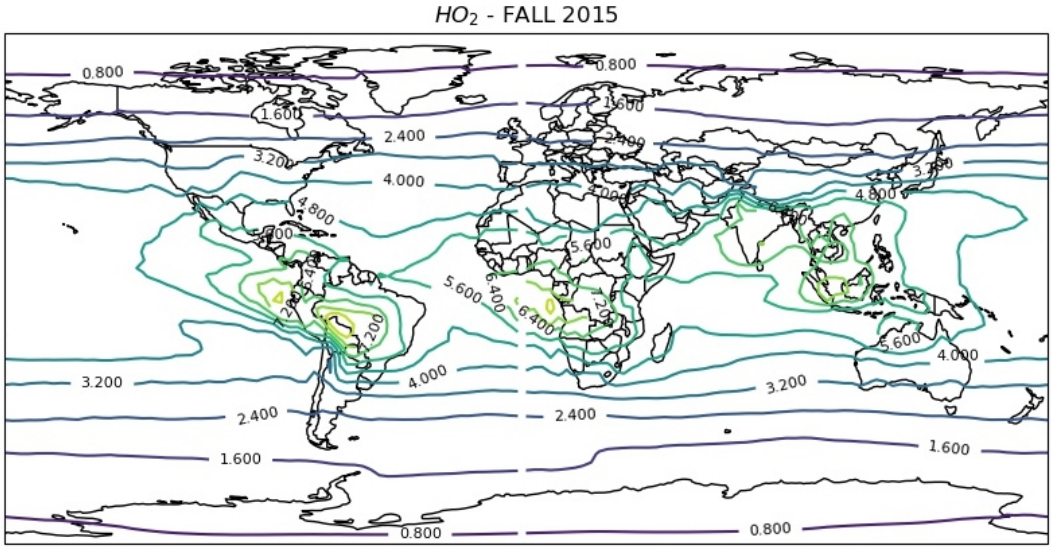

Figure B.8: VMR (units: $pptv$) of background atmospheric HO_2 in Fall

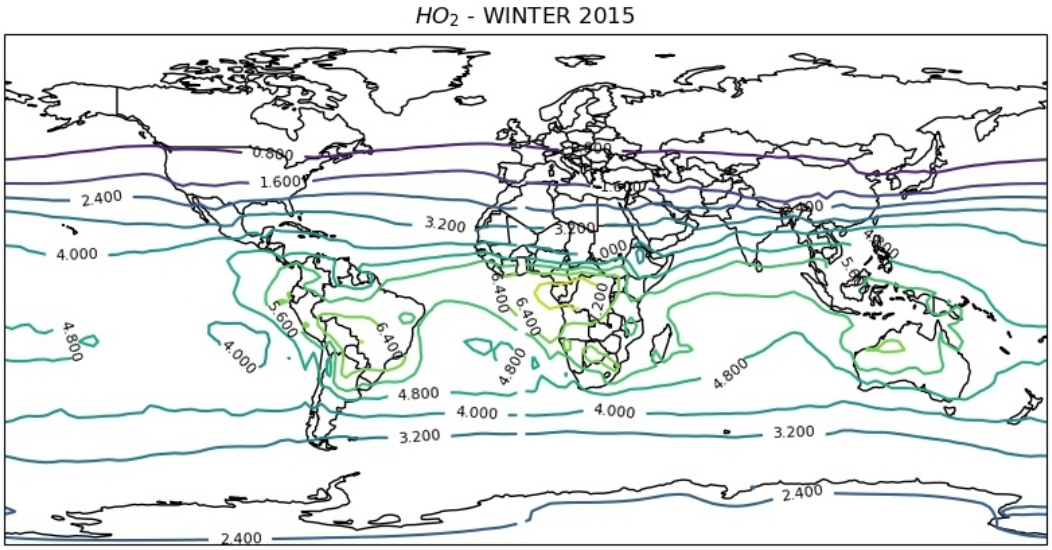

Figure B.9: VMR (units: $pptv$) of background atmospheric HO_2 in Winter

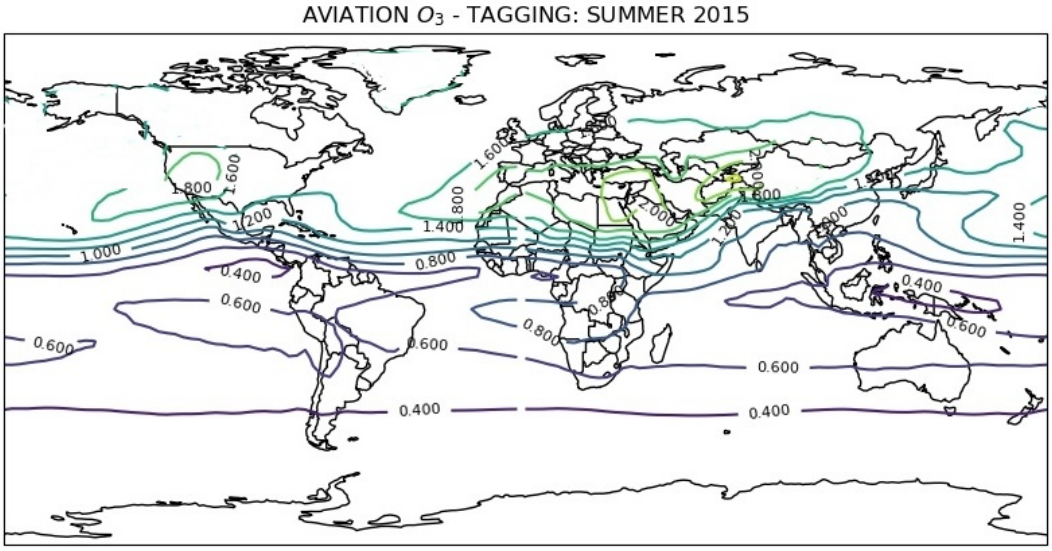

Figure B.10: Atmospheric VMR (units: $ppbv$) of aviation O_3 in Summer

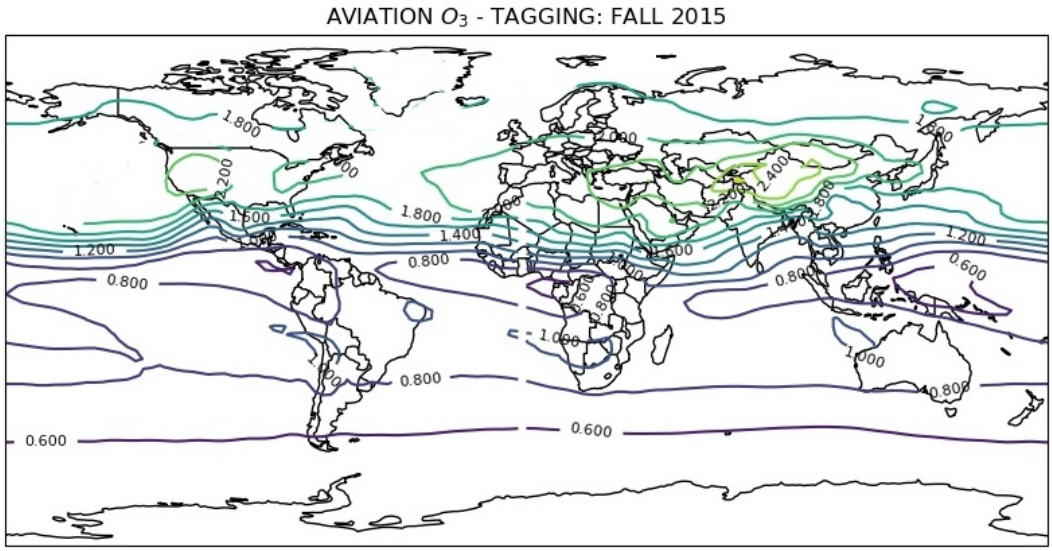

Figure B.11: Atmospheric VMR (units: $ppbv$) of aviation O_3 in Fall

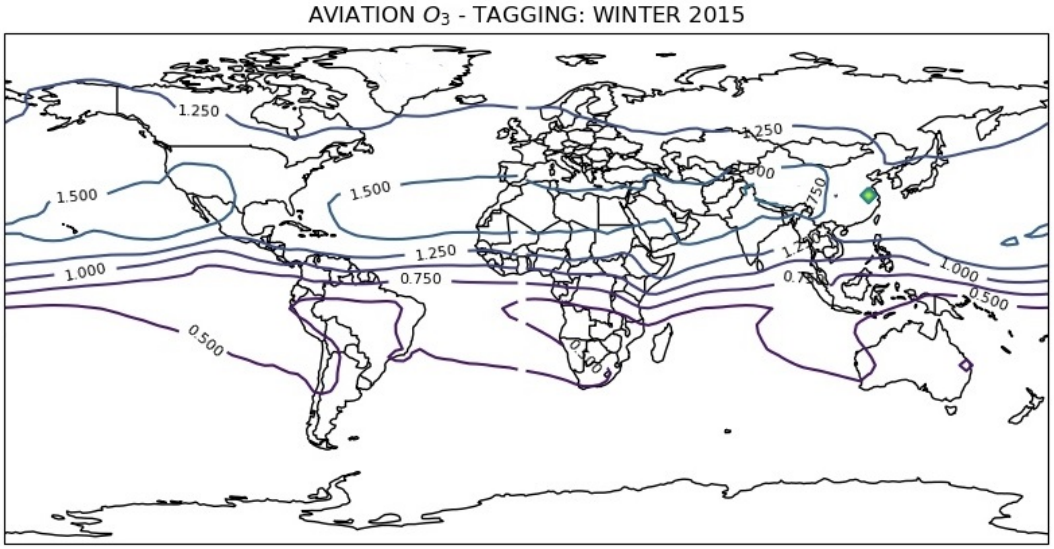

Figure B.12: Atmospheric VMR (units: $ppbv$) of aviation O_3 in Winter

C

Perturbation-Tagging differences of aviation's contribution to NO_x and O_3

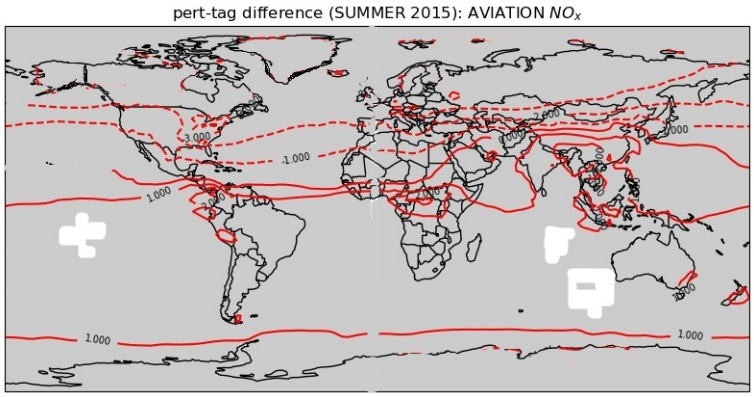

Figure C.1: Percentage difference between Perturbation & Tagging estimations for the mean tropospheric contribution of aviation to NO_x VMR in the Summer season. Every grid point in the plot is subjected to a statistical 2-tailed t-test with 95% confidence level, whereby the grey-shaded areas indicate that the differences between the Tagging & Perturbation estimations are statistically significant and not a coincidence.

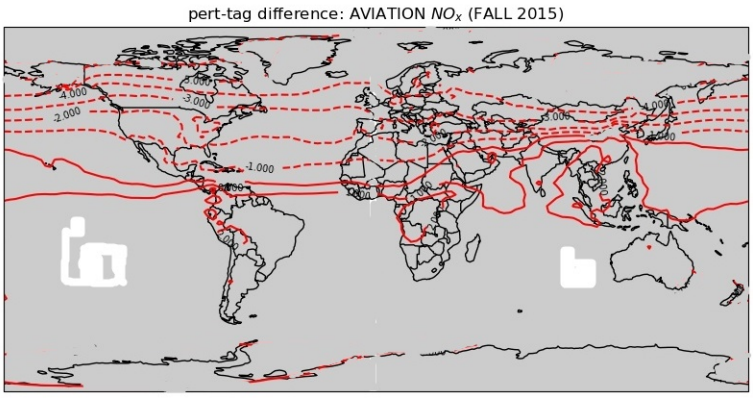

Figure C.2: Percentage difference between Perturbation & Tagging estimations for the mean tropospheric contribution of aviation to NO_x VMR in the Fall season. Every grid point in the plot is subjected to a statistical 2-tailed t-test with 95% confidence level, whereby the grey-shaded areas indicate that the differences between the Tagging & Perturbation estimations are statistically significant and not a coincidence.

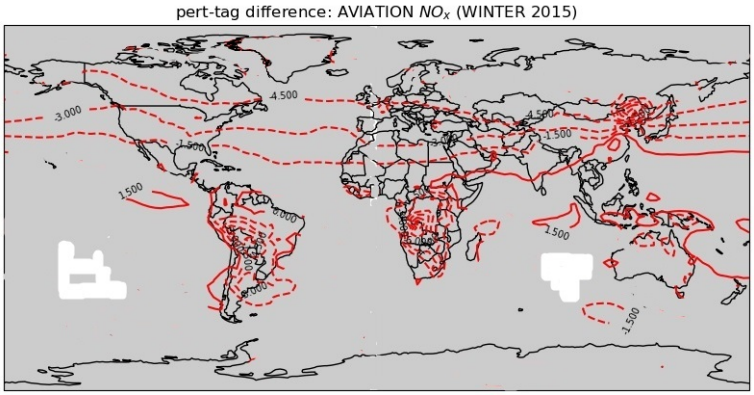

Figure C.3: Percentage difference between Perturbation & Tagging estimations for the mean tropospheric contribution of aviation to NO_x VMR in the Winter season. Every grid point in the plot is subjected to a statistical 2-tailed t-test with 95% confidence level, whereby the grey-shaded areas indicate that the differences between the Tagging & Perturbation estimations are statistically significant and not a coincidence.

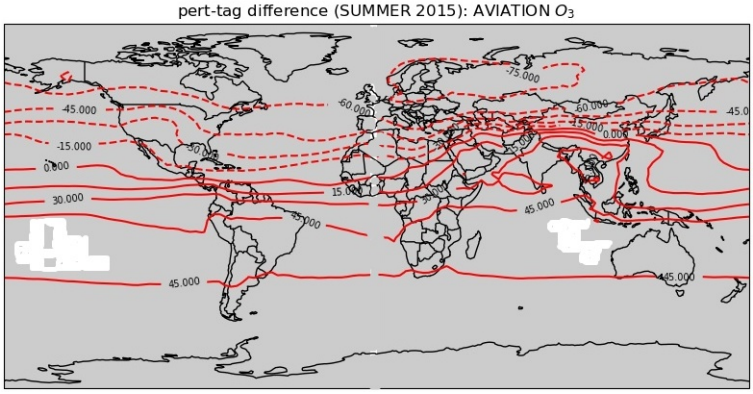

Figure C.4: A representation of the percentage difference between Perturbation & Tagging estimations for the mean tropospheric O_3 VMR due to aviation NO_x, in the Spring season. Every grid point in the plot is subjected to a statistical 2-tailed t-test with 95% confidence level, whereby the grey-shaded areas indicate that the differences between the Tagging & Perturbation estimations are statistically significant and not a coincidence.

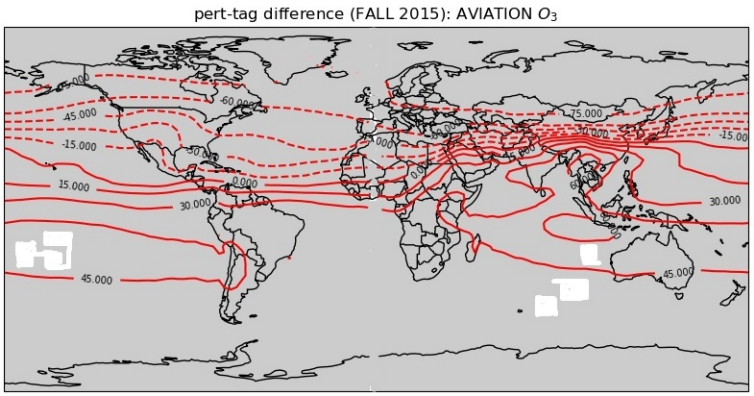

Figure C.5: A representation of the percentage difference between Perturbation & Tagging estimations for the mean tropospheric O_3 VMR due to aviation NO_x, in the Spring season. Every grid point in the plot is subjected to a statistical 2-tailed t-test with 95% confidence level, whereby the grey-shaded areas indicate that the differences between the Tagging & Perturbation estimations are statistically significant and not a coincidence.

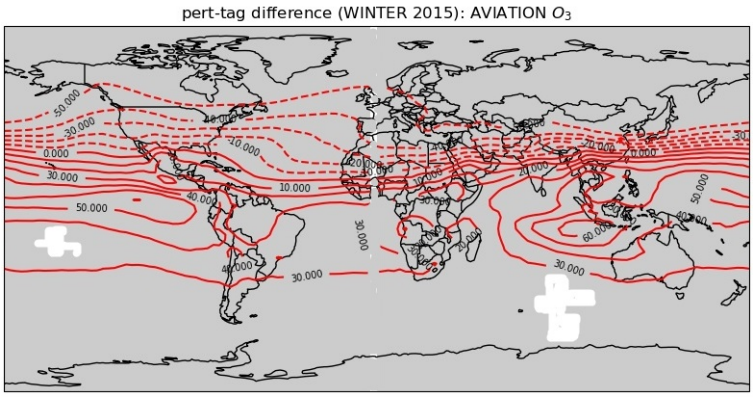

Figure C.6: A representation of the percentage difference between Perturbation & Tagging estimations for the mean tropospheric O_3 VMR due to aviation NO_x, in the Spring season. Every grid point in the plot is subjected to a statistical 2-tailed t-test with 95% confidence level, whereby the grey-shaded areas indicate that the differences between the Tagging & Perturbation estimations are statistically significant and not a coincidence.

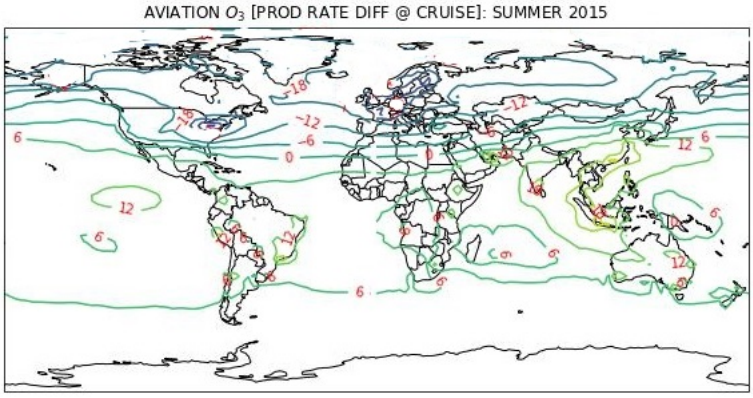

Figure C.7: Percentage difference between Perturbation and Tagging method estimations for tropospheric O_3 production rate, due to aviation in the cruise altitude range 8 to 12 km, in Summer.

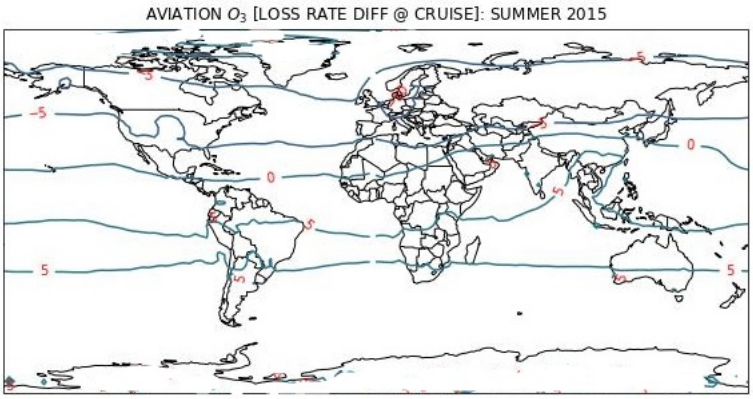

Figure C.8: Percentage difference between Perturbation and Tagging method estimations for tropospheric O_3 loss rate, due to aviation in the cruise altitude range 8 to 12 km, in Summer.

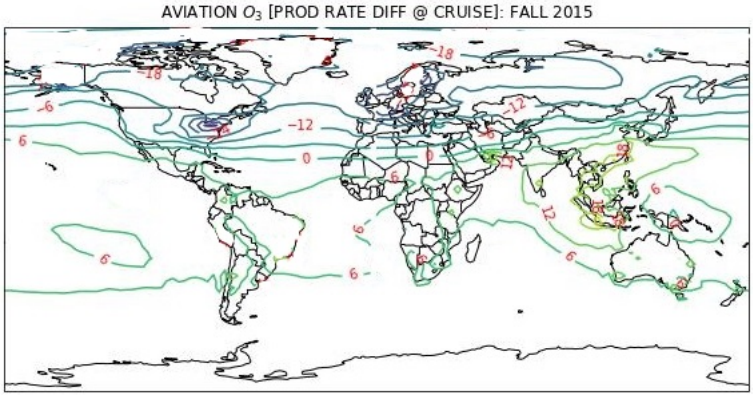

Figure C.9: Percentage difference between Perturbation and Tagging method estimations for tropospheric O_3 production rate, due to aviation in the cruise altitude range 8 to 12 km, in Fall.

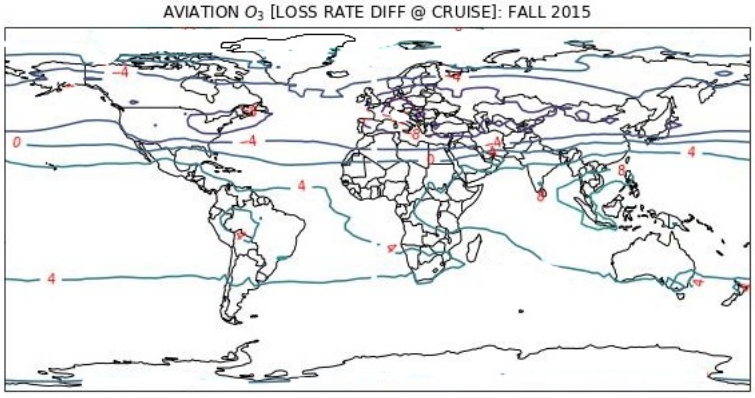

Figure C.10: Percentage difference between Perturbation and Tagging method estimations for tropospheric O_3 loss rate, due to aviation in the cruise altitude range 8 to 12 km, in Fall.

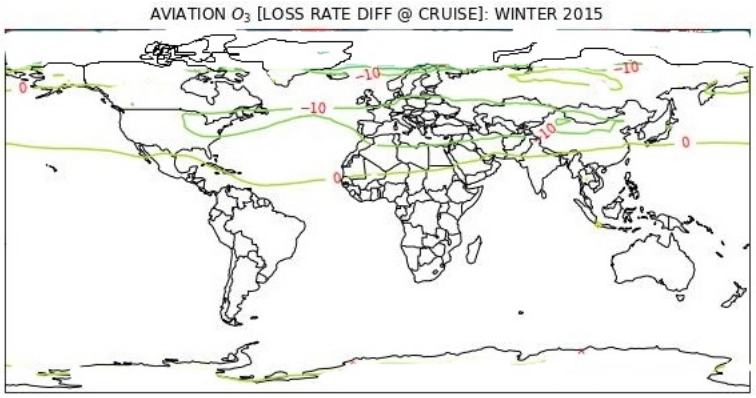

Figure C.11: Percentage difference between Perturbation and Tagging method estimations for tropospheric O_3 loss rate, due to aviation in the cruise altitude range 8 to 12 km, in Winter.

References

[1] D. S. Lee *et al.*, "The contribution of global aviation to anthropogenic climate forcing for 2000 to 2018," *Atmospheric Environment*, vol. 244, no. July 2020, 2021, ISSN: 18732844.

[2] IPCC, *Aviation and the global atmosphere: a special report of the Intergovernmental Panel on Climate Change*. Cambridge University Press, 1999.

[3] M. Prather, R. Sausen, A. Grossman, J. Haywood, D. Rind, and B. Subbaraya, "Potential climate change from aviation," *Aviation and the Global Atmosphere. A Special Report of IPCC Working Groups I and III*, J. Penner, D. Lister, D. Griggs, D. Dokken, and M. McFarland, Eds., pp. 185–215, 1999, LIDO-Berichtsjahr=1999,

[4] D. S. Lee *et al.*, "Aviation and global climate change in the 21st century," *Atmospheric Environment*, vol. 43, no. 22-23, pp. 3520–3537, 2009, ISSN: 13522310.

[5] G. P. Brasseur *et al.*, "European scientific assessment of the atmospheric effects of aircraft emissions," *Atmospheric Environment*, vol. 32, no. 13, pp. 2329–2418, 1998, ISSN: 13522310.

[6] R. Sausen *et al.*, "Aviation radiative forcing in 2000: An update on ipcc (1999)," *Meteorologische Zeitschrift*, vol. 14, no. 4, pp. 555–561, 2005.

[7] S. C. Liu *et al.*, "Ozone production in the rural troposphere and the implications for regional and global ozone distributions," *Journal of Geophysical Research*, vol. 92, no. D4, p. 4191, 1987.

[8] X. Lin, M. Trainer, and S. C. Liu, "On the non-linearity of the tropospheric ozone production," *Journal of Geophysical Research*, vol. 93, no. D12, pp. 879–888, 1988, ISSN: 01480227.

[9] J. U. Grooß, C. Brühl, and T. Peter, "Impact of aircraft emissions on tropospheric and stratospheric ozone. Part I: Chemistry and 2-D model results," *Atmospheric Environment*, vol. 32, no. 18, pp. 3173–3184, 1998, ISSN: 13522310.

[10] K. Dahlmann, V. Grewe, M. Ponater, and S. Matthes, "Quantifying the contributions of individual NO_x sources to the trend in ozone radiative forcing," *Atmospheric Environment*, vol. 45, no. 17, pp. 2860–2868, 2011, ISSN: 13522310.

[11] V. Grewe, K. Dahlmann, S. Matthes, and W. Steinbrecht, "Attributing ozone to NO_x emissions: Implications for climate mitigation measures," *Atmospheric Environment*, vol. 59, no. x, pp. 102–107, 2012, ISSN: 13522310.

[12] B. Koo, G. M. Wilson, R. E. Morris, A. M. Dunker, and G. Yarwood, "Comparison of source apportionment and sensitivity analysis in a particulate matter air quality model," *Environmental Science and Technology*, vol. 43, no. 17, pp. 6669–6675, 2009, ISSN: 0013936X.

[13] D. Lee *et al.*, "Transport impacts on atmosphere and climate: Aviation," *Atmospheric Environment*, vol. 44, no. 37, pp. 4678–4734, 2010, Transport Impacts on Atmosphere and Climate: The ATTICA Assessment Report, ISSN: 1352-2310.

[14] M. O. Köhler *et al.*, "Impact of perturbations to nitrogen oxide emissions from global aviation," *Journal of Geophysical Research Atmospheres*, vol. 113, no. 11, pp. 1–15, 2008, ISSN: 01480227.

[15] M. Lenner, "Nitrogen dioxide in exhaust emissions from motor vehicles," *Atmospheric Environment (1967)*, vol. 21, no. 1, pp. 37–43, 1987, ISSN: 0004-6981.

[16] J. H. Seinfeld, "Urban air pollution: State of the science," *Science*, vol. 243, no. 4892, pp. 745–752, 1989.

[17] B. J. Finlayson-Pitts and J. N. Pitts, "Tropospheric air pollution: Ozone, airborne toxics, polycyclic aromatic hydrocarbons, and particles," *Science*, vol. 276, no. 5315, pp. 1045–1051, 1997.

[18] E. Uherek *et al.*, "Transport impacts on atmosphere and climate: Land transport," *Atmospheric Environment*, vol. 44, no. 37, pp. 4772–4816, 2010, Transport Impacts on Atmosphere and Climate: The ATTICA Assessment Report, ISSN: 1352-2310.

[19] D. H. Ehhalt and J. W. Drummond, "The tropospheric cycle of NO_x," in *Chemistry of the Unpolluted and Polluted Troposphere*, H. W. Georgii and W. Jaeschke, Eds., Dordrecht: Springer Netherlands, 1982, pp. 219–251, ISBN: 978-94-009-7918-5.

[20] U. F. Platt, A. M. Winer, H. W. Biermann, R. Atkinson, and J. N. Pitts, "Measurement of nitrate radical concentrations in continental air," *Environmental science & technology*, vol. 18, no. 5, pp. 365–369, 1984.

[21] J. Noxon, "NO_3 And NO_2 in the mid-pacific troposphere," *Journal of Geophysical Research: Oceans*, vol. 88, no. C15, pp. 11 017–11 021, 1983.

[22] M. Dodge, "Combined use of modeling techniques and smog chamber data to derive ozone-precursor relationships," in *International conference on photochemical oxidant pollution and its control: Proceedings*, US Environmental Protection Agency, Environmental Sciences Research …, vol. 2, 1977, pp. 881–889.

[23] M. C. Dodge, "Effect of selected parameters on predictions of a photochemical model," Environmental Protection Agency, Research Triangle Park, NC (USA …, Tech. Rep., 1977.

[24] V. Grewe, "A generalized tagging method," *Geoscientific Model Development*, vol. 6, no. 1, pp. 247–253, 2013, ISSN: 19919603.

[25] A. Clappier, C. A. Belis, D. Pernigotti, and P. Thunis, "Source apportionment and sensitivity analysis: Two methodologies with two different purposes," *Geoscientific Model Development*, vol. 10, no. 11, pp. 4245–4256, 2017, ISSN: 19919603.

[26] C. L. Blanchard, "Methods for attributing ambient air pollutants to emission sources," *Annual Review of Energy and the Environment*, vol. 24, no. 1, pp. 329–365, 1999.

[27] G. Yarwood, R. E. Morris, and G. M. Wilson, "Particulate matter source apportionment technology (psat) in the camx photochemical grid model," in *Air Pollution Modeling and Its Application XVII*, C. Borrego and A.-L. Norman, Eds., Boston, MA: Springer US, 2007, pp. 478–492.

[28] V. Grewe, E. Tsati, and P. Hoor, "On the attribution of contributions of atmospheric trace gases to emissions in atmospheric model applications," *Geoscientific Model Development*, vol. 3, no. 2, pp. 487–499, 2010, ISSN: 1991959X.

[29] V. Grewe, "A diagnostic for ozone contributions of various NO_x emissions in multi-decadal chemistry-climate model simulations," *Atmospheric Chemistry and Physics*, vol. 4, no. 3, pp. 729–736, 2004.

[30] F. O'Connor *et al.*, "Comparison and visualisation of high-resolution transport modelling with aircraft measurements," *Atmospheric Science Letters*, vol. 6, no. 3, pp. 164–170, 2005.

[31] P. A. Cook *et al.*, "Forest fire plumes over the north atlantic: P-tomcat model simulations with aircraft and satellite measurements from the itop/icartt campaign," *Journal of Geophysical Research: Atmospheres*, vol. 112, no. D10, 2007.

[32] K. Law *et al.*, "Evaluation of modeled O_3 using measurement of ozone by airbus in-service aircraft (mozaic) data," *Journal of Geophysical Research: Atmospheres*, vol. 103, no. D19, pp. 25 721–25 737, 1998.

[33] K. Law *et al.*, "Comparison between global chemistry transport model results and measurement of ozone and water vapor by airbus in-service aircraft (mozaic) data," *Journal of Geophysical Research: Atmospheres*, vol. 105, no. D1, pp. 1503–1525, 2000.

[34] N. Savage, K. S. Law, J. Pyle, A. Richter, H. Nüß, and J. Burrows, "Using gome NO_2 satellite data to examine regional differences in tomcat model performance," *Atmospheric Chemistry and Physics*, vol. 4, no. 7, pp. 1895–1912, 2004.

[35] M. Chipperfield, "Multi-annual simulations with a three-dimensional chemical transport model," *Journal of Geophysical Research: Atmospheres*, vol. 104, no. D1, pp. 1781–1805, 1999.

[36] H. Rogers, H. Teyssedre, G. Pitari, V. Grewe, P. van Velthoven, and J. Sundet, "Model intercomparison of the transport of aircraft-like emissions from sub-and supersonic aircraft," *Meteorologische Zeitschrift*, pp. 151–159, 2002.

[37] V. Grewe, M. Dameris, C. Fichter, and R. Sausen, "Impact of aircraft NO_x emissions. part 1: Interactively coupled climate-chemistry simulations and sensitivities to climate-chemistry feedback, lightning and model resolution," *Meteorologische Zeitschrift*, vol. 11, no. 3, pp. 177–186, 2002.

[38] M. O. Köhler, H. L. Rogers, and J. A. Pyle, “Modelling the impact of subsonic aircraft emissions on ozone: Future changes and the impact of cruise altitude perturbations,” in *Proceedings of the European Conference on Aviation, Atmosphere and Climate (AAC), Friedrichshafen, Germany*, vol. 30, 2004, pp. 173–177.

[39] M. Gauss, I. Isaksen, D. Lee, and O. Søvde, “Impact of aircraft NO_x emissions on the atmosphere–tradeoffs to reduce the impact,” *Atmospheric Chemistry and Physics*, vol. 6, no. 6, pp. 1529–1548, 2006.

[40] O. Wild, K. S. Law, D. S. McKenna, B. J. Bandy, S. A. Penkett, and J. A. Pyle, “Photo-chemical trajectory modeling studies of the north atlantic region during august 1993,” *Journal of Geophysical Research: Atmospheres*, vol. 101, no. D22, pp. 29 269–29 288, 1996.

[41] L. Jaegle *et al.*, “Sources and chemistry of NO_x in the upper troposphere over the united states,” 1998.

[42] P. Jöckel *et al.*, “Development cycle 2 of the modular earth submodel system (messy2),” *Geoscientific Model Development*, vol. 3, no. 2, pp. 717–752, 2010.

[43] P. Jöckel *et al.*, “Earth system chemistry integrated modelling (escimo) with the modular earth submodel system (messy) version 2.51,” *Geoscientific Model Development*, vol. 9, no. 3, pp. 1153–1200, 2016.

[44] P. Jöckel, R. Sander, A. Kerkweg, H. Tost, and J. Lelieveld, “The modular earth submodel system (messy)-a new approach towards earth system modeling,” *Atmospheric Chemistry and Physics*, vol. 5, no. 2, pp. 433–444, 2005.

[45] V. Grewe, E. Tsati, M. Mertens, C. Frömming, and P. Jöckel, “Contribution of emissions to concentrations: The TAGGING 1.0 submodel based on the Modular Earth Submodel System (MESSy 2.52),” *Geoscientific Model Development*, vol. 10, no. 7, pp. 2615–2633, 2017, ISSN: 19919603.

[46] E. Roeckner *et al.*, “Sensitivity of simulated climate to horizontal and vertical resolution in the echam5 atmosphere model,” *Journal of Climate*, vol. 19, no. 16, pp. 3771–3791, 2006.

[47] M. Mertens, A. Kerkweg, P. Jöckel, H. Tost, and C. Hofmann, “The 1-way on-line coupled model system meco (n)–part 4: Chemical evaluation (based on messy v2. 52),” *Geoscientific Model Development*, vol. 9, no. 10, pp. 3545–3567, 2016.

[48] R. Sander *et al.*, “The community atmospheric chemistry box model caaba/mecca-4.0,” *Geoscientific model development*, vol. 12, no. 4, pp. 1365–1385, 2019.

[49] U. Pöschl, R. von Kuhlmann, N. Poisson, and P. J. Crutzen, “Development and intercomparison of condensed isoprene oxidation mechanisms for global atmospheric modeling,” *Journal of Atmospheric Chemistry*, vol. 37, no. 1, pp. 29–52, 2000.

[50] H. Tost, P. Jöckel, A. Kerkweg, R. Sander, and J. Lelieveld, “A new comprehensive scavenging submodel for global atmospheric chemistry modelling,” *Atmospheric Chemistry and Physics*, vol. 6, no. 3, pp. 565–574, 2006.

[51] A. Kerkweg, J. Buchholz, L. Ganzeveld, A. Pozzer, H. Tost, and P. Jöckel, “An implementation of the dry removal processes dry deposition and sedimentation in the modular earth submodel system (messy),” *Atmospheric Chemistry and Physics*, vol. 6, no. 12, pp. 4617–4632, 2006.

[52] R. Deckert, P. Jöckel, V. Grewe, K.-D. Gottschaldt, and P. Hoor, “A quasi chemistry-transport model mode for emac,” *Geoscientific Model Development*, vol. 4, no. 1, pp. 195–206, 2011.

[53] M. Mertens, A. Kerkweg, V. Grewe, P. Jöckel, and R. Sausen, “Attributing ozone and its precursors to land transport emissions in Europe and Germany,” *Atmospheric Chemistry and Physics*, vol. 20, no. 13, pp. 7843–7873, 2020, ISSN: 16807324.

[54] J. Lelieveld and F. J. Dentener, “What controls tropospheric ozone?” *Journal of Geophysical Research Atmospheres*, vol. 105, no. D3, pp. 3531–3551, 2000, ISSN: 01480227.

[55] R. G. Prinn, “The cleansing capacity of the atmosphere,” *Annual Review of Environment and Resources*, vol. 28, p. 29, 2003.

[56] H. B. Singh *et al.*, “Atmospheric peroxyacetyl nitrate measurements over the Brazilian Amazon Basin during the wet season: relationships with nitrogen oxides and ozone,” *Journal of Geophysical Research*, vol. 95, no. D10, 1990, ISSN: 01480227.

[57] H. Guo *et al.*, “Source apportionment of pm2.5 in north india using source-oriented air quality models,” *Environmental Pollution*, vol. 231, pp. 426–436, 2017, ISSN: 0269-7491.

[58] D. S. Cohan, A. Hakami, Y. Hu, and A. G. Russell, “Nonlinear response of ozone to emissions: Source apportionment and sensitivity analysis,” *Environmental Science and Technology*, vol. 39, no. 17, pp. 6739–6748, 2005, ISSN: 0013936X.

[59] W. Chameides and J. C. G. Walker, “A photochemical theory of tropospheric ozone,” *Journal of Geophysical Research*, vol. 78, no. 36, pp. 8751–8760, 1973, ISSN: 0148-0227.

[60] W. DeMore *et al.*, “Chemical kinetics and photo-chemical data for use in stratospheric modeling,” *Evaluation*, vol. 6, no. 210, pp. 83–62, 1983.

[61] R. Atkinson and A. C. Lloyd, “Evaluation of kinetic and mechanistic data for modeling of photochemical smog,” *Journal of physical and chemical reference data*, vol. 13, no. 2, pp. 315–444, 1984.

[62] P. J. Crutzen, “The role of NO and NO_2 in the chemistry of the troposphere and stratosphere,” *Annual review of earth and planetary sciences*, vol. 7, no. 1, pp. 443–472, 1979.

[63] H. B. Singh *et al.*, “Relationship between peroxyacetyl nitrate and nitrogen oxides in the clean troposphere,” *Nature*, vol. 318, no. 6044, pp. 347–349, Nov. 1985, ISSN: 1476-4687.

[64] W. P. Carter, A. C. Lloyd, J. L. Sprung, and J. N. Pitts Jr, “Computer modeling of smog chamber data: Progress in validation of a detailed mechanism for the photo-oxidation of propene and n-butane in photo-chemical smog,” *International Journal of Chemical Kinetics*, vol. 11, no. 1, pp. 45–101, 1979.

[65] M. Righi, J. Hendricks, and R. Sausen, “The global impact of the transport sectors on atmospheric aerosol: Simulations for year 2000 emissions,” *Atmospheric Chemistry and Physics*, vol. 13, no. 19, pp. 9939–9970, 2013.

[66] G. Pitari, I. Cionni, G. Di Genova, O. A. Søvde, and L. Lim, “Radiative forcing from aircraft emissions of NO_x: Model calculations with CH_4 surface flux boundary condition,” *Meteorologische Zeitschrift*, vol. 26, no. 6, pp. 663–687, 2017.

[67] N. Unger, “Global climate impact of civil aviation for standard and desulfurized jet fuel,” *Geophysical research letters*, vol. 38, no. 20, 2011.

[68] C. D. Holmes, Q. Tang, and M. J. Prather, “Uncertainties in climate assessment for the case of aviation NO,” *Proceedings of the National Academy of Sciences*, vol. 108, no. 27, pp. 10 997–11 002, 2011.

[69] G. Myhre *et al.*, “Radiative forcing due to changes in ozone and methane caused by the transport sector,” *Atmospheric Environment*, vol. 45, no. 2, pp. 387–394, 2011.

[70] W. C. Wang, J. P. Pinto, and Y. L. Yung, “Climatic effects due to halogenated compounds in the earth’s atmosphere,” *Journal of Atmospheric Sciences*, vol. 37, no. 2, pp. 333–338, 1980.

[71] A. A. Lacis, D. J. Wuebbles, and J. A. Logan, “Radiative forcing of climate by changes in the vertical distribution of ozone,” *Journal of Geophysical Research: Atmospheres*, vol. 95, no. D7, pp. 9971–9981, 1990.

[72] D. Hauglustaine, C. Granier, G. Brasseur, and G. Megie, “The importance of atmospheric chemistry in the calculation of radiative forcing on the climate system,” *Journal of Geophysical Research: Atmospheres*, vol. 99, no. D1, pp. 1173–1186, 1994.

[73] D. Hauglustaine, C. Granier, G. Brasseur, and G. Mégie, “Impact of present aircraft emissions of nitrogen oxides on tropospheric ozone and climate forcing,” *Geophysical research letters*, vol. 21, no. 18, pp. 2031–2034, 1994.

[74] World Health Organization, “Health aspects of air pollution with particulate matter, ozone and nitrogen dioxide: Report on a who working group, bonn, germany 13-15 january 2003,” Copenhagen: WHO Regional Office for Europe, Tech. Rep., 2003.

[75] P. S. Monks *et al.*, “Tropospheric ozone and its precursors from the urban to the global scale from air quality to short-lived climate forcer,” *Atmospheric Chemistry and Physics*, vol. 15, no. 15, pp. 8889–8973, 2015.

[76] D. Fowler *et al.*, “Atmospheric composition change: Ecosystems–atmosphere interactions,” *Atmospheric Environment*, vol. 43, no. 33, pp. 5193–5267, 2009.

[77] D. L. Mauzerall and X. Wang, “Protecting agricultural crops from the effects of tropospheric ozone exposure: Reconciling science and standard setting in the united states, europe, and asia,” *Annual Review of energy and the environment*, vol. 26, no. 1, pp. 237–268, 2001.

[78] D. Stevenson *et al.*, “Multi-model ensemble simulations of present-day and near-future tropospheric ozone,” *Journal of Geophysical Research: Atmospheres*, vol. 111, no. D8, 2006.